Enhancing barrier and shielding properties of multilayered flexible packaging with carbon-based composites

by

José Carlos FERREIRA JÚNIOR

Ph.D. THESIS PRESENTED TO ÉCOLE DE TECHNOLOGIE SUPÉRIEURE
AND FEDERAL UNIVERSITY OF SANTA CATARINA (CO-TUTORSHIP)
IN PARTIAL FULFILLMENT OF THE REQUIREMENTS FOR THE
DEGREE OF DOCTOR OF PHILOSOFY
Ph.D.

MONTREAL, NOVEMBER 3, 2023

ÉCOLE DE TECHNOLOGIE SUPÉRIEURE
UNIVERSITÉ DU QUÉBEC

BOARD OF EXAMINERS

THIS THESIS HAS BEEN EVALUATED

BY THE FOLLOWING BOARD OF EXAMINERS

Mrs. Nicole Raymonde Demarquette, Thesis Supervisor
Department of Mechanical Engineering at École de technologie supérieure

Mr. Abdellah Ajji, Thesis Co-supervisor
Department of Chemical Engineering at Polytechnique Montréal

Mr. Guilherme Mariz de Oliveira Barra, Thesis Co-supervisor
Department of Mechanical Engineering at Federal university of Santa Catarina (Brazil)

Mr. Ricardo Izquierdo, President of the Board of Examiners
Department of Electrical Engineering at École de technologie supérieure

Mr. Éric David, Member of the jury
Department of Mechanical Engineering at École de technologie supérieure

Mrs. Cláudia Merlini, External Evaluator
Department of Mechanical Engineering at Federal university of Santa Catarina (Brazil)

THIS THESIS WAS PRENSENTED AND DEFENDED

IN THE PRESENCE OF A BOARD OF EXAMINERS AND PUBLIC

ON SEPTEMBER 14, 2023

AT ÉCOLE DE TECHNOLOGIE SUPÉRIEURE

ACKNOWLEDGMENTS

First, I thank my family and wife for everything they have done and do for me, for all the care, love, and support, believing when not even I could. And in the loving memory of my dear father. You are deeply missed.

I would like to thank my advisors and co-advisors, Professor Nicole R. Demarquette, Guilherme Mariz de Oliveira Barra, and Abdellah Ajji, for their guidance and trust in me. Merci beaucoup, muito obrigado! A sincere thank you to Professor Lucas Hof and Professor Patrick Lee. Thank you all for providing me with the resources and support necessary to complete this work.

I am grateful for the members of the jury Professor Ricardo Izquierdo, Professor Éric David and Professor Cláudia Merlini for agreeing to evaluate this work during defense.

A big thank you to everybody in the many labs I have been part of at the Federal University of Santa Catarina, in the École de Technologie Supérieure, Polytechnique Montréal, and briefly at the University of Toronto. A special thank you goes to Daria, Debora, Cherif, JX, Emna, Ennouri and Scheyla; this work could not be done without you.

The staff at the École de Technologie Supérieure, Polytechnique Montréal, and Federal University of Santa Catarina, Claire, Mathieu, Nabil, Radu, Richard, and Rogério, Simon I appreciate your excellent work!

I am grateful to FAPESC, CAPES, NanoXplore and Mitacs for the financial support.

Amélioration des propriétés de barrière et de blindage des emballages flexibles multicouches avec des composites à base de carbone

José Carlos FERREIRA JUNIOR

RÉSUMÉ

Les solutions actuelles d'emballage flexible multicouche pour protéger les dispositifs électroniques sensibles souffrent d'une faible réutilisation et recyclabilité. Cela entraîne une aggravation des déchets, une dégradation lente, des émissions et la contamination des sols et des océans, entre autres problèmes. Le manque de recyclabilité est dû à leur structure complexe. Pour fournir des propriétés de barrière et de blindage, des matériaux hétérogènes, c'est-à-dire l'aluminium et le polymère, sont joints avec des couches adhésives. Le recyclage de ce type de structure nécessite des approches énergivores et longues. Dans ce contexte, nous avons proposé de remanier la structure multicouche pour créer une solution plus durable en utilisant des composites à base de carbone. Notre approche vise à être compatible avec l'utilisation industrielle et est basée sur des matériaux largement disponibles à l'échelle industrielle : une matrice de polyéthylène haute densité (PE-HD) avec des propriétés clés fournies par deux charges à base de carbone: les plaquettes de graphène (G) pour une barrière contre la perméabilité et les nanotubes de carbone multi parois (CNT) pour une conductivité électrique augmentée. Méthodologiquement, nous avons pris trois étapes pour atteindre le composite proposé : premièrement, nous avons étudié les effets de barrière et de conductivité électrique de G en utilisant la coextrusion dans un processus de fabrication à l'échelle semi-industrielle pour produire une structure à 8 couches. Des concentrations inférieures à 0,5 % en poids, G a amélioré l'effet barrière d'environ 42 % pour l'oxygène et l'eau dans des échantillons avec des surfaces plus lisses. Cependant, aucune augmentation de la conductivité électrique n'a été trouvée à 1 % en poids. De plus, la conception en couches - en particulier, le placement sélectif de la charge dans les couches choisies - s'est avérée être un outil important pour obtenir des propriétés améliorées. Deuxièmement, nous nous sommes concentrés sur l'amélioration des propriétés électriques nécessaires pour obtenir des propriétés de blindage en étudiant des films PE-HD/CNT monocouche avec G comme charge secondaire, aboutissant à un composite hybride. Une transition d'un composite isolant à un composite plus conducteur a été obtenue à 6,49 % en poids CNT. Une synergie a été trouvée pour les composites hybrides avec des rapports CNT:G 99:1 à une concentration fixe de 9 % en poids, mais était fortement dépendante des conditions de refroidissement de l'échantillon. À la même teneur en charge, aucune amélioration des propriétés barrière n'a été trouvée. Troisièmement et enfin, en utilisant une technique de coextrusion avec un élément multiplicateur, nous avons produit des films multicouches avec 129 couches PE-HD/CNT, PE-HD/G et HDPE/CNT/G avec des compositions allant jusqu'à 4,5 % en poids et comparé leurs propriétés barrière et blindage aux films monocouches. Les structures multicouches ont présenté une barrière globale améliorée à l'eau et à l'oxygène. Augmentation du blindage, allant de 13 % à 110 % selon le type de structure, et les propriétés d'absorption micro-ondes. Les améliorations ont été attribuées au placement sélectif du remplissage et aux propriétés diélectriques accrues des films multicouches. Bien que nous n'ayons pas pu atteindre les valeurs commerciales recommandées pour le blindage (10 dB) des dispositifs sensibles avec des films flexibles épaisseur 100 μm,

notre enquête a démontré le potentiel d'atteindre des propriétés combinées dans un film composite flexible pour les applications d'emballage en ajustant la méthode de traitement et la conception en couches.

Mots-clés: Emballage multicouche flexible, composite, charges à base de carbone, perméabilité, blindage

Enhancing barrier and shielding properties of multilayered flexible packaging with carbon-based composites

JOSÉ CARLOS FERREIRA JUNIOR

ABSTRACT

Current multilayered flexible packaging solutions for protecting sensitive electronic devices suffer from low reuse and recyclability. It leads to increasing amounts of waste, slow degradation, emissions, and contamination of soil and oceans, among other issues. The lack of recyclability is due to their complex structure. To provide barrier and shielding properties, dissimilar materials, i.e., aluminum and polymer, are joined with adhesive layers. The recycling of this type of structure requires energy and time-consuming approaches. In this context, we proposed redesigning the multilayered structure to create a more sustainable solution using carbon-based composites. Our approach aims to be compatible with industrial use and is based on widely available materials at the industrial scale: a high-density polyethylene (HDPE) matrix with key properties provided by two carbon-based fillers: graphene platelets (G) for a barrier against permeability and multiwalled carbon nanotubes (CNT) for increased electrical conductivity. Methodologically, we took three steps to achieve the proposed composite: First, we investigated the barrier and electrical conductivity effects of G using coextrusion in a semi-industrial scale fabrication process to produce an 8-layer structure. Concentrations lower than 0.5 wt.%, G improved the barrier effect by around 42% for oxygen and water in samples with smoother surfaces. However, no increase in electrical conductivity was found at 1 wt.%. Additionally, layer design - specifically, selective placement of filler in chosen layers - proved to be an important tool for achieving enhanced properties. Second, we focused on improving the electrical properties necessary for achieving shielding properties by investigating single-layer HDPE/CNT films with G as a secondary filler, resulting in a hybrid composite. A transition from an insulative to a more conductive composite was achieved at 6.49 wt.% CNT. Synergism was found for hybrid composites with 99:1 CNT:G ratios at a fixed concentration of 9 wt.% but was highly dependent on the cooling conditions of the sample. At the same filler content, no improvement in barrier properties was found. Third and finally, using a coextrusion technique with a multiplying element, we produced multilayered films with 129 layers of HDPE/CNT, HDPE/G, and HDPE/CNT/G with compositions up to 4.5 wt.% and compared their barrier and shielding properties to single-layer films. The multilayered structures exhibited an overall improved barrier to water and oxygen. Increased shielding, ranging from 13% to 110% depending on the structure type, and microwave absorption performance properties. The improvements were ascribed to the selective filler placement and increased dielectric properties of the multilayered films. Although we were unable to achieve the commercial values recommended for shielding (10 dB) of sensitive devices with flexible 100 μm thick films, our investigation demonstrated the potential to achieve combined properties in a composite flexible film for packaging applications by adjusting the processing method and layer design.

Keywords: flexible multilayer packaging, composite, carbon-based fillers, permeability, shielding

TABLE OF CONTENTS

Page

LIST OF TABLES

LIST OF FIGURES

Page

LIST OF ABREVIATIONS

AFM	Atomic force microscopy
AR	Aspect ratio
BDS	Broadband dielectric spectroscopy
CB	Carbon black
CE	Circular economy
CNT	Carbon nanotubes
DSC	Differential scanning calorimetry
E	Young's modulus
EC	Electrical conductivity
EMI	Electromagnetic interference
EPT	Electrical percolation threshold
ESD	Electrostatic discharges
EVA	Ethylene vinyl acetate
EVOH	Ethylene-vinyl alcohol copolymer
G	Industrial-grade graphene
GBM	Graphene-based materials
GHG	Greenhouse gases
GNP	Graphene nanoplatelets
HDPE	High-density polyethylene
IPCC	Intergovernmental Panel on Climate Change
LDPE	Low-density polyethylene

MB	Masterbatch
MD	Machine direction
MWCNT	Multi-walled carbon nanotubes
N	Nipped
NN	Non-nipped
OM	Optical microscopy
PA	Polyamide
PAN	Polyacrylonitrile
PC	Polycarbonate
PET	Polyethylene terephthalate
PLA	Polylactide
PMMA	Polymethyl methacrylate
PS	Polystyrene
RH	Relative humidity
RL	Reflection loss
SE	Shielding effectiveness
SEM	Scanning electron microscopy
SR	Surface roughness
SWCNT	Single-walled carbon nanotubes
TD	Transverse direction
TEM	Transmission electron microscopy
TPU	Thermoplastic polyurethane
VNA	Vector network analyzer

LIST OF SYMBOLS

A	Absorption coefficient or surface area
D	Diffusion coefficient
D	Filler thickness
D50	Particle size below which 50% of the sample lies
D90	Particle size below which 90% of the sample lies
E_L	Longitudinal Young's modulus
E_c	Composite Young's modulus
E_f	Filler Young's modulus
E_m	Matrix Young's modulus
F	Geometric factor
L	Filler length
L	Thickness
P	Permeability coefficient or permeability of the polymer composite
P_0	Permeability of the unfilled polymer
Q	Mass of permeant
R	Reflection coefficient
S	Scattering parameter or solubility coefficient
SE_A	Shielding by absorption
SE_{MR}	Shielding by multiple internal reflections
SE_R	Shielding by reflection
T	Transmission coefficient
V_{fc}	Volume fraction of the filler at the percolation threshold

V_f	Volume fraction of filler
Z_0	Characteristic impedance of free space
Z_{in}	Input impedance at the interface of free space and material
F	Frequency
f	Herman's orientation function
t	Critical exponent
t	Thickness
tan δ	Dielectric loss tangent
ΔH^0_m	Enthalpy of fusion
ΔH_m	Experimental heat of fusion
α	Flake aspect ratio
ε’	Real part of permittivity
ε’’	Imaginary part of permittivity
θ	Angle between the diffusion direction and the normal vector of the filler particle
ρ	Volume resistivity
σ	Volumetric conductivity
σ_T	Total electrical conductivity
σ_c	Composite’s electrical conductivity
φ_s	Particle volume fraction in the composite
Δp	Permeant partial pressure difference across the film

INTRODUCTION

What is the environmental price of multilayered flexible packaging? Human activity is the primary cause of climate change, which can have significant impacts on both human and natural systems. According to the most recent report of the Intergovernmental Panel on Climate Change (IPCC), climate change poses a significant threat to human and natural systems, including food production, human health, and biodiversity (Rawshan Ara Begum et al., 2022). This translates to reduced crop yield, extreme weather events for almost half of the world population in the form of storms, droughts, and floods, as well as species losses (Rawshan Ara Begum et al., 2022). The main contributor to the rise in global temperature is the continued emission of greenhouse gases (GHG), particularly carbon dioxide (CO_2) and methane, whose increasing concentrations result in an energy imbalance due to their interaction with infrared radiation. Compared to 1990, there was an estimated 54% increase in GHG emissions in 2019, with CO_2 emissions from fossil fuels and industry contributing the most. Therefore, it is crucial to reduce GHG emissions to mitigate the impacts of climate change.

As part of the collective effort to significantly reduce GHG emissions to a net-zero target and thus reduce their impacts, it is important to identify the share of emissions of each sector. According to the IPCC (2022), these sectors are energy (34%), industry (24%), land use (22%), transport (15%), and buildings (6%) (IPCC, 2022; Rawshan Ara Begum et al., 2022). However, when accounting for the energy needed for each sector, industry becomes the largest contributor with 34% of the emissions (Dhakal et al., 2022; IPCC, 2022). The sector's industrial GHG emissions are mainly due to the production of basic materials such as steel, cement, and plastic, which make up 62% of the total (Bashmakov et al., 2022). A major issue is that this sector's production of basic materials such as plastic leads to GHG emissions and a considerable amount of waste. The current use of plastics is rather inefficient, with most plastics ending up as waste. Approximately 8.3×10^{12} kg of plastic was produced until 2015; in the 65-year window of the study, only around 30% of that amount was still in use (Geyer, Jambeck, & Law, 2017). Unsustainably, most plastics (6.3×10^{12} kg) end up as waste, with only 9% being recycled and the remaining 91% being discarded as waste in landfills (79%) or

incinerated (12%) (Geyer et al., 2017). Plastics in landfills can represent 5-25% wt.% of the deposited waste (Canopoli, Fidalgo, Coulon, & Wagland, 2018), potentially leading to several negative consequences, including slow degradation, methane emissions, contamination of soil and groundwater through chemical leaching, or ending up in the ocean when mismanaged (Gómez & Michel, 2013; Jambeck et al., 2015; Okunola A., 2019). Therefore, addressing this challenge requires the adoption and development of more efficient ways of industrial production and material use through its life cycle to support sustainable development.

The circular economy (CE) model has been proposed as a way to promote sustainable development and move away from the current wasteful industrial linear system of "take-make-waste" (Van Buren, Demmers, Van der Heijden, & Witlox, 2016). Despite many possible definitions, it simply proposes that materials be reduced, reused, recycled, and recovered from production to consumption (Kirchherr, Reike, & Hekkert, 2017). The end goal of CE is to decouple economic growth from negative impacts caused to the environment and the intensive resource use (Ghisellini, Cialani, & Ulgiati, 2016). Presently, emissions are aggravated with economic development as increases the demand for materials and industrial products; this increases the emissions of the industrial sector, an already major emitter (Bashmakov et al., 2022). Although the industrial sector is not considered the main actor in the implementation of CE, a role that is attributed to governments through the promotion of regulations and taxation incentives (Govindan & Hasanagic, 2018), the sector still has improvements to be made, especially in plastic's recycling. Recycling would help to reduce the dependence on primary production.

Among the challenges faced in transitioning towards a circular economy (CE) model in the plastic industry is the issue of recyclability, hampered by products lacking designs that support their reuse as feedstock materials. This is aggravated when taking into consideration that most plastics are used for packaging, which are typically single-use only and have the shortest life span among all categories of plastics (Geyer et al., 2017). This results in an increased amount of waste and negative consequences. To better understand how to improve the recyclability

and reduce the barriers to reusing packaging materials in the context of CE, it is essential to examine the role of packaging, its structure, and possible improvements.

The main role of plastic packaging is to provide protection for an item, either during transportation or storage. Plastic packaging is commonly based on commodity polymers of non-renewable sources such as polyethylene and polypropylene, which provide a low-cost, lightweight solution due to their low density and low processing temperature when compared to metals or glass (Selke & Culter, 2015). Multilayered flexible packaging is currently the toughest problem to solve when it comes to recycling to its industry. This is due to its layered structure, which increases its landfilling or incineration (Kaiser, Schmid, & Schlummer, 2017; C. T. de M. Soares, Ek, Östmark, Gällstedt, & Karlsson, 2022). This type of packaging is composed of different layers for a total thickness of a film of less than 250 μm as opposed to rigid packaging, which can handle external loads during use but at greater thicknesses (Beswick & Dunn, 2002; Morris, 2017a). Each layer provides specific functions that are unattainable with single-layer packaging. These functions include sealability, printability, barrier, and light barrier properties (Kaiser et al., 2017; Morris, 2017a), to name a few. These functions are obtained by combining different layers of polymers and/or other materials such as aluminum or paper (Morris, 2017a). A common method to bind those dissimilar layers together is by using an adhesive layer. However, combined with the different materials, they form a significant barrier to effective recycling. The use of single materials or compatible blends as found in single-layer packaging is preferred for achieving effective recycling (Horodytska, Valdés, & Fullana, 2018). In comparison, recycling multilayer structures involves time- and energy-intensive steps including layer delamination or selective layer dissolution to separate their core materials (Cervantes-Reyes et al., 2015; Horodytska et al., 2018; Kaiser et al., 2017). Alternatively, a more sustainable solution is to design multilayered packaging for recyclability (C. T. de M. Soares et al., 2022). This can be achieved by reducing the complexity of multilayered structures rather than using the current layer design that hinders the separation of layers to their key components.

In this work, we propose to redesign multilayered flexible packaging used to protect sensitive electronic devices towards a more sustainable solution. This type of packaging is a suitable candidate for redesign because it has the potential to avoid the use of adhesive and metallic layers and is not subject to the same regulatory constraints as food packaging materials (Kaiser et al., 2017). Herein, the proposed redesign aims to be the most compatible for industrial use and is based in the most recent developments and potential of polymer and carbon-based composites. Widely available materials at the industrial scale were employed, namely a polyethylene matrix with properties of interest provided by two carbon-based fillers: graphene platelets for reduction of permeability and multiwalled carbon nanotubes for increased electrical conductivity. Additionally, coextrusion processes, which are at the base of the multilayered packing industry, were used as the main fabrication techniques. Methodologically, three steps were taken successively: ensuring the reduction of permeability with graphene platelets using a semi-industrial scale fabrication process; evaluating the electrical conductivity and barrier efficiency performance by combining both fillers in a single layer; and evaluating the feasibility of a multilayered composite with a simpler design aiming to attain both properties: increased barrier effects for both permeability and increased electrical conductivity. All those steps were deemed necessary to obtain a more sustainable multilayered packing solution. The next chapter will discuss the most relevant topics in more depth, presenting the necessary properties of flexible packaging, its current drawbacks, and possible solutions within the literature.

CHAPTER 1

LITERATURE REVIEW

In this chapter, we present the current performance requirements and drawbacks of multilayered flexible packaging to protect sensitive electronic devices. A literature review is presented on the use of carbonaceous-based composites as a potential alternative for flexible packaging. This is done through two main topics: firstly, the importance of specific morphologies for gas permeability, electrical conductivity, and shielding, supported by a theoretical background, with a focus on polyolefins due to their importance in flexible packaging. Secondly, we address the fabrication techniques necessary to achieve multilayered structures at an industrial scale.

1.1 Flexible packaging to protect sensitive electronic devices: Structure, requirements and inherent drawbacks

Flexible packaging is the current method used to protect electronic devices from potentially damaging effects, for example, moisture, electrostatic discharge events, or electromagnetic interference (EMI). A flexible packaging is typically fabricated by coextrusion processes with a multilayered structure of functional layers to a total thickness less than 250 μm (Wagner & Marks, 2016). It is based on thin polyolefins films which allow for a product with light weight, lower cost and shapable, saving space and with fast production rate (Beswick & Dunn, 2002; Demirci & Ngadi, 2012; Wagner & Marks, 2016). This type of packaging by conforming to its contents (Bajpai, 2019, p. 4) ensures safe transport, handling and the proper performance of the electronic devices. Figure 1.1 a) shows an example of commercially available flexible packaging protecting an electronic device, while Figure 1.1 b) illustrates its possible multilayered packaging structure achieved by joining polyester, polyethylene, and aluminum-based layers with adhesive layers in between them. This structure results in an integrated packaging with moisture barrier, electrostatic dissipation, and electromagnetic shielding properties. The requirements for each of these properties and the current limitations are briefly addressed below.

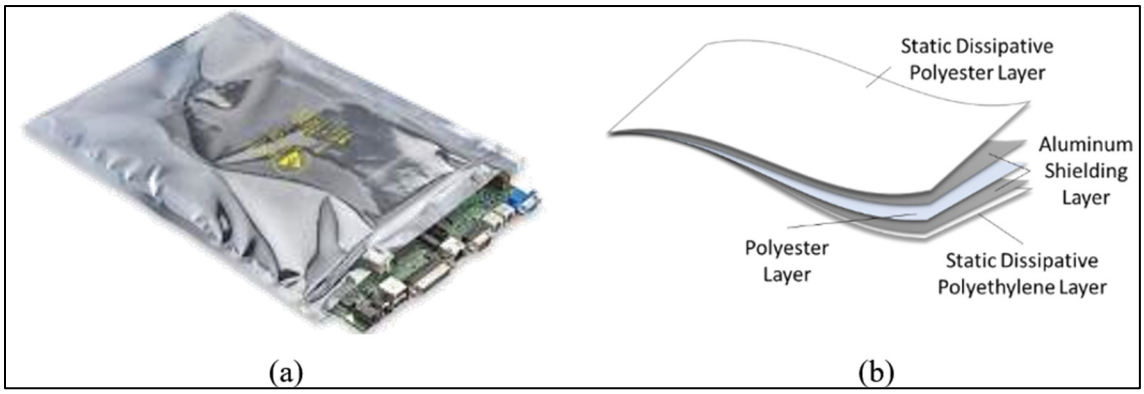

Figure 1.1 (a) An electronic device protected by a flexible packaging ensuring protecting during transport, against moisture, electrostatic discharges and electromagnetic interference. Taken from Samtec (2017). (b) A multilayer structure of a commercial packaging solution to protect electronics

Water present in the environment can cause damage to electronics because it can facilitate electrochemical corrosion and surface electrical leakage of the electronic devices (Greenhouse, Lowry, & Romenesko, 2012). One method to reduce the effects of moisture and other permeating species is to reduce its permeation rate by using barrier layers or coatings based on organic materials such as high-density polyethylene (HDPE), a high barrier polymer against moisture, or inorganic materials such as aluminum, a high barrier against both moisture and oxygen. To illustrate the barrier effect Figure 1.2 shows the permeation values for moisture vapour and oxygen for a variety of packaging materials under the same conditions, aluminium foil showing the lowest value.

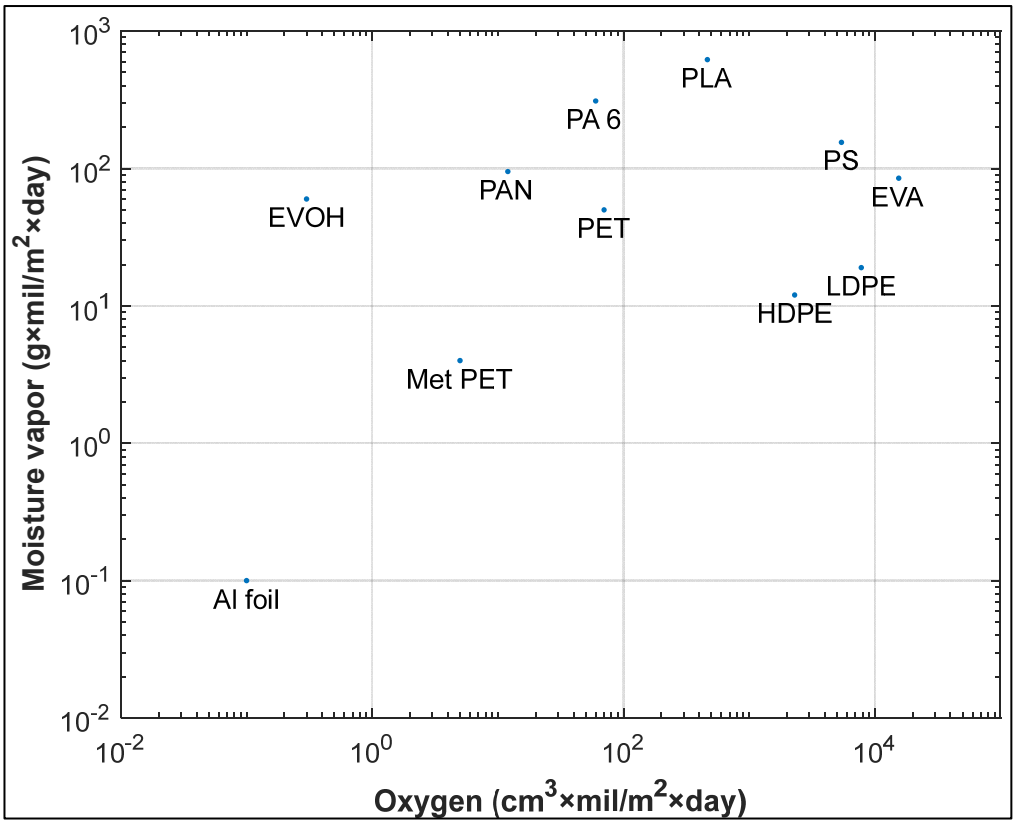

Figure 1.2 Values of moisture vapor transmission rate at 38ºC, 90% Relative humidity (RH) and oxygen permeation at 23ºC, 0% RH of different packaging materials. Where abbreviations stand for, Aluminum (Al); ethylene vinyl acetate (EVA); high-density polyethylene (HDPE); low-density polyethylene (LDPE); Polyacrylonitrile (PAN); Metalized (Met); polyamide (PA); polyethylene terephthalate (PET); polylactide (PLA); polystyrene (PS); ethylene-vinyl alcohol copolymer (EVOH). Adapted from Decker & Henry (2002, p. 35) and Morris (2017c, p. 273)

The aluminum foil is integrated to the multilayered structure made with an adhesive by extrusion coating, lamination or coextrusion processes (Morris, 2017c). Although an aluminum layer offers a higher barrier to permeation, in real service, it can inadvertently allow increased permeation through the packaging due to structural defects such as scratches, pinholes, or corrosion (Weiss, 1991). These defects can occur at various stages - fabrication, distribution, or end use - due to the metallic layer's inability to withstand the associated stresses, as for example (Decker & Henry, 2002; Trost, 1995a). Flexing tests on metallized films demonstrate the referred inability as an increase in moisture permeability by approximately two orders of magnitude due to the formation of pinholes after testing (Parkar, 2005). Figure 1.3 a)

exemplifies a pinhole defect in an aluminum foil that occurred during its manufacturing process, and Figure 1.3 b) illustrates the increased diffusion of permeating species through a pinhole defect in a packaging material.

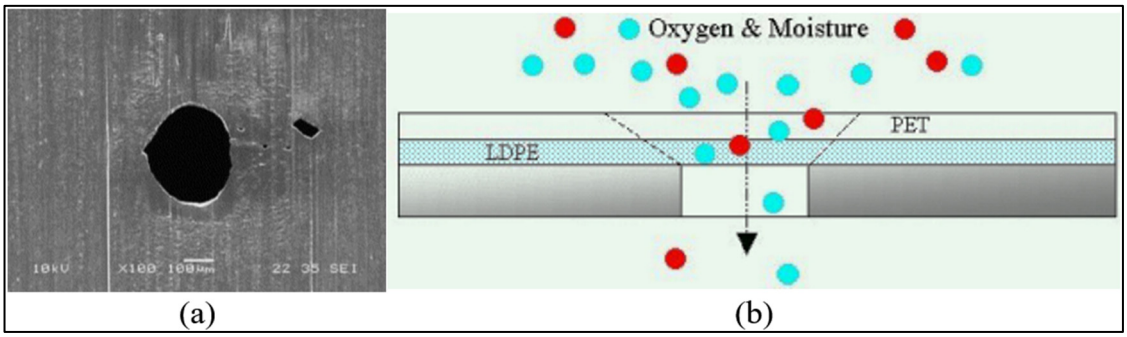

Figure 1.3 (a) Pinholes caused in an aluminum foil during its lamination process observed under a scanning electrical microscope (SEM). Taken from Keles & Dundar (2007, p. 132) and (b) Representation of oxygen and moisture diffusion through a pinhole in a PET/ LDPE/ Foil packaging material. Taken from Murray (2005, p. 2)

Another important disadvantage is that both the packaging metallic layers and the protected electronic devices are more susceptible to corrosion due to the antistatic additives and their hygroscopic nature that provide protection against electrostatic discharges (ESD) for the packaging material (Trost, 1995b). Antistatic additives or agents are compounds that are added to the plastic packaging material to decrease charge accumulation by temporarily creating a more conductive pathway through water adsorption, as polymers are typically electrically insulating materials. Examples of additives include amides containing hydroxyl groups, tertiary amines, and quaternary ammonium salts (Markarian, 2008; Trost, 1995b). The accumulation of static electricity on the packaging happens due to the triboelectricity effect generated at the surfaces of the packaging by friction during transportation or by improper handling (Trost, 1995b). And as electronic devices get smaller and faster, their susceptibility to ESD events increases (Akkachai, Kittipong, Darunee, & Duanghathai, 2014). Electrostatic dissipation reduces the charge buildup or allows the dissipation of the accumulated charges. To safely control and dissipate charges, it is recommended that the packaging have an electrical conductivity in the range of 10^{-9} and 10^{-2} S/m (Tolinski, 2015b; Trost, 1995a; Verma, Verma, Dhawan, & Choudhary, 2015). The change in electrical conductivity is dependent on time, temperature, and available moisture in the environment to work properly; nonetheless, it is also

susceptible to evaporation or leaching (Doyon et al., 2009; Paasi, Nurmi, Vuorinen, Strengell, & Maijala, 2001). It is worth mentioning that the concentration of antistatic additives needs to be about twice as high in crystalline polyolefins like HDPE for the same performance as in less crystalline ones like LDPE.

In addition to controlling electrostatic dissipation, it is also important to consider the potential for electromagnetic interference (EMI). EMI is a phenomenon in which an electromagnetic disturbance generated by an external source has the potential to disrupt or even damage electronic systems, depending on their susceptibility (Tong, 2016). To attenuate the propagation of electromagnetic fields, shielding structures typically rely on electrically conductive materials, resulting in the reflection of the incident field. In flexible packaging, EMI shielding can be achieved through the incorporation of an electrically conductive layer, such as aluminum. Although EMI shielding is not explicitly addressed as a requirement in commercial packaging standards for electronic devices, a military performance specification provides specific values for achieving a safe range of attenuation for their applications. This is particularly important for military devices used in naval and aviation applications, which are exposed to harsh environmental conditions. According to the military standard, depending on the application, an EMI attenuation of a minimum of 10 dB or 25 dB must be achieved in the 1 to 10 GHz frequency range (*MIL-PRF-81705 - Performance Specification: Barrier Materials, Flexible, Electrostatic Protective, Heat- Sealable*, 2009), translating to an attenuation of approximately 90% and 99.7% of the incident field, respectively.

The use of different materials to achieve multiple properties in current flexible packaging solutions has its drawbacks, including structural defects, dependence on environmental conditions, and susceptibility to corrosion as previously mentioned. Additionally, combining dissimilar materials in packaging presents a challenge for effective mechanical recycling, due to the difficulty and cost of separating adhered layers, leading to waste disposal problems (Cervantes-Reyes et al., 2015). One approach to overcome these drawbacks is to focus on designing multilayered packaging with sustainability and recyclability as priorities (C. T. de M. Soares et al., 2022). This can be achieved by using a structure that does not rely on the use

of adhesives and metallic layers but instead combines polymeric materials with fillers or coatings to control both barrier properties and electrical conductivity, allowing for EMI shielding. Considering these challenges, researchers have been exploring the use of polymeric composites based on nano sized fillers as a promising candidate for flexible packaging applications (Kausar, 2020). By combining polymeric composites with nano-sized particles, more specifically, carbonaceous fillers such as carbon nanotubes and graphene, the resulting packaging materials have improved electrical and barrier properties (Tan & Thomas, 2016). In the following sections, their properties will be discussed, and the most relevant research will be reviewed to identify gaps that might enable the development of a more sustainable packaging solution for protecting sensitive electronic devices on an industrial scale.

1.2 Carbonaceous-based composites and their use in packaging research

1.2.1 Potential carbon-based material candidates and their structure for flexible packaging applications

It is worth mentioning that many fillers have been investigated for use in polymer composites for packaging applications. These fillers can be divided into two broad groups: inorganic fillers based on mineral fillers such as clay, and organic fillers, such as carbonaceous fillers (Cui, Kundalwal, & Kumar, 2016; Tan & Thomas, 2016). Even though non-carbon fillers provide improvements in the barrier properties, they are beyond the scope of this literature review. Additionally, although most of the research is currently focused on biodegradable engineering polymers, as a route to reduce the negative environmental impact of slow degrading petroleum-based polymers, still, the biggest market share is dominated by commodity polyolefins, e.g. PE and PP (Jones, Saffar, Koutsos, & Ray, 2021; Tan & Thomas, 2016). These materials could benefit of reuse and recyclability, reducing the negative impacts of incineration and landfilling (Jones et al., 2021). Therefore, in this review, focus will be given to polymer-based composites with polyolefins and carbon-based fillers due to its inherently electrically conductive properties.

In the last decade, great attention has been dedicated to investigating polymer composites with nanomaterials (Balazs, Emrick, & Russell, 2006). Those materials can first be defined by their size, where one of their dimensions is between 1 and 100 nm. As the material gets smaller, the percentage of atoms exposed on its surface increases, creating a higher surface area and providing interesting properties at lower filler contents (Kreyling, Semmler-Behnke, & Chaudhry, 2010); however increases the material agglomeration. This allows for the research of different properties depending on the size and shape of the material. In this context, carbon-based materials stand out as versatile materials with many variations known as carbon allotropes (i.e., graphite, carbon black, and carbon nanotubes). Of those two specific materials, graphene-based materials and carbon nanotubes improve thermal, electrical, and mechanical properties (Geim & Novoselov, 2007; N et al., 2021; Watt & Gerhardt, 2020).

Graphene has distinctive thermal, electrical, and mechanical properties due to its structure (Balandin et al., 2008), increasing the interest and effort to harness such unique properties in different applications, including aerospace, electronics, inks, and textiles, to name a few (Dhinakaran, Lavanya, Vigneswari, Ravichandran, & Vijayakumar, 2020; Geim & Novoselov, 2007; Kauling et al., 2018). In general, the properties of the material rely on the material structure. And for graphene this means how closely the structure resembles its ideal form, i.e., a two-dimensional (2D) material with an atom thick hexagonal carbon arrangement and a sp^2 hybridization. Figure 1.4 illustrates the graphene structure, and how it can be understood as the building unit of other carbon allotropes, such as carbon nanotubes by rolling graphene to itself forming a hollow cylindrical structure and graphite, by stacking many graphene layers (>100 layers) on top of each other (J. Chen, Wei, & Xie, 2021; Geim & Novoselov, 2007; Kauling et al., 2018; Novoselov et al., 2004).

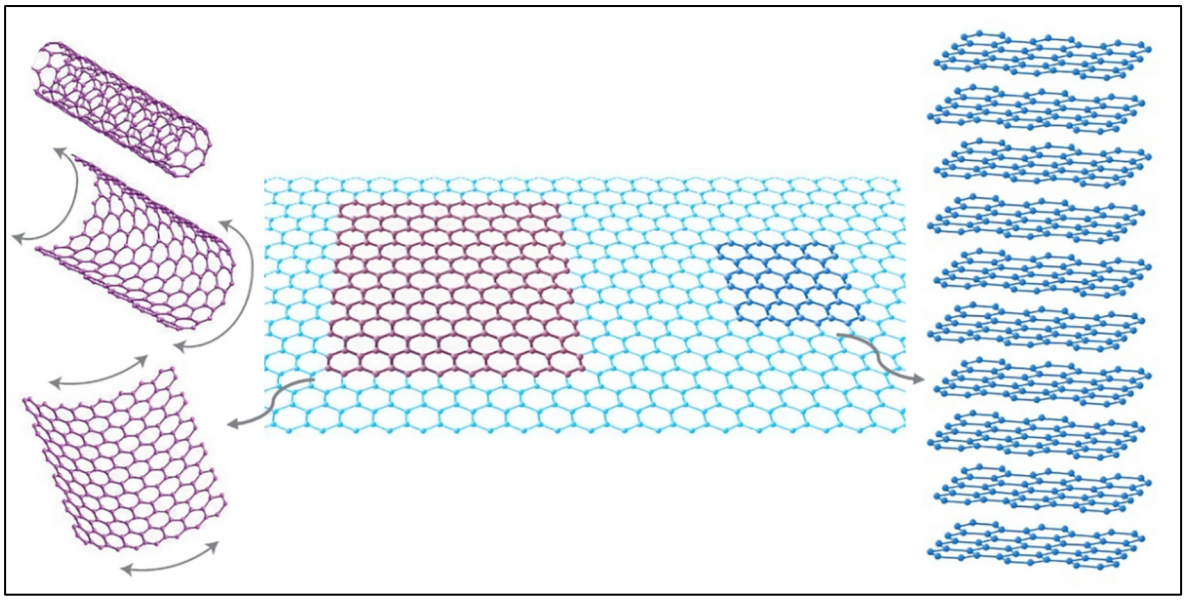

Figure 1.4 Graphene can be represented as the basic building material for carbon materials rolled into a nanotube highlighted in purple on the left or stacked into graphite represented in darker blue on the right. Adapted from Geim & Novoselov (2007, p. 184)

The most reliable method to obtain a graphene layer is the bottom-up approach, produced, for example, by the chemical vapor deposition (CVD) technique (Dhinakaran et al., 2020; Geim & Novoselov, 2007). Using this approach, Seethamraju (2016) demonstrated the potential of graphene for barrier applications in polymeric composite packaging with moisture barrier properties. (2016). With only one deposited graphene layer, they were able to achieve a great reduction in water permeation, between 10^4 and 10^6 times compared to neat polymers, depending on the polymeric matrix used, providing a higher barrier than aluminum foil. The findings were attributed to the low defect layer and to the high energy barrier of graphene due to its sp^2 periodic structure, that allow water molecules to penetrate only across defects (Seethamraju et al., 2016). However, the great barrier effect was only achievable when graphene was produced using the CVD method, which is currently costly and incompatible with inexpensive packaging products and large-scale production and is mainly used for research (Kauling et al., 2018).

A more feasible alternative to graphene are graphene-based materials (GBM), exemplified by reduced graphene oxide (Verma et al., 2015) and graphene nanoplatelets (GNP) (Boldt,

Leuteritz, Schob, Ziegenhorn, & Wagenknecht, 2020). Among the different varieties available on the market, for the necessary bulk-sized applications of flexible packaging, GNP has great potential due to its resemblance to graphene, cost-effectiveness, and bulk availability as well. Although the terminology of GBM lacked consensus both because it was more recently available and because of the high variability of products on the market (Wick et al., 2014), the International Organization for Standardization has proposed a standard for the common designation of GBM. In this standard, GNP was classified as having a few layers of graphene stacked with a lateral dimension of approximately 100 nm to 100 μm and thickness a between of 1 nm to 3 nm (*ISO Nanotechnologies — Vocabulary — Part 13: Graphene and Related Two-Dimensional (2D) Materials*, 2017). The cost-effectiveness of GNP is linked to its production method, accomplished by the top-down approach instead of the bottom-up, where graphite is used as the base material and processed by liquid-phase exfoliation by methods such as sonication and ball milling, resulting in a material with a statistical distribution of different number of layers (Kauling et al., 2018). The GNP layered structure still enables it to obtain composites with electrical and barrier properties, mainly due to a higher aspect ratio (Müller et al., 2017; Tan & Thomas, 2016), meaning the ratio between the materials longest dimension to its lowest dimension (Wolf, Angellier-Coussy, Gontard, Doghieri, & Guillard, 2018).

Another important material for the potential use in flexible packaging composites are carbon nanotubes (CNT). They have a well-established research history in the literature, with a longer development (Iijima & Ichihashi, 1993) compared to the more recently investigated graphene (Novoselov et al., 2004). CNTs have diameters in the nanometer range and lengths up to micrometers (Rathinavel, Priyadharshini, & Panda, 2021), presenting high aspect ratios. In terms of their structure, they can be classified as consisting of a single or multiple concentric hollow tubes, namely single-walled (SWCNT) and multi-walled carbon nanotubes (MWCNT), respectively (J. Chen et al., 2021). In composites research, MWCNTs have been more commonly used due to their lower cost compared to SWCNTs and have shown to achieve improved electrical, thermal, and mechanical properties (Singh, Patra, Obodo, & Rai, 2022; Watt & Gerhardt, 2020).

Both MWCNT and GNP based composites are promising candidates to be explored in flexible packaging to protect sensitive electronic devices due to their properties and bulk availability. To achieve the necessary properties for flexible packaging, specific morphologies are required to improve both barrier and shielding properties, which will be discussed in the next sections.

1.2.2 The permeability theory, tortuous path morphology to improve barrier properties in carbon based composites

1.2.2.1 Permeability theory in the context of polymer packaging

The objective of packaging barriers is to reduce the transmission rate of permeating species across the packaging material. Where the permeant moves through the material from the high to the low concentration side. How easily the permeation happens will depend on various factors such as the permeating species (e.g., water or oxygen), environmental conditions (e.g., temperature and humidity), and the barrier thickness. The barrier performance can be expressed by the permeability coefficient (P) as follows (Equation 1.1):

$$P = D \cdot S = \frac{QL}{At\Delta p} \tag{1.1}$$

Where P is the product of diffusion (D) and solubility (S) coefficients, or expressed by the mass of permeant (Q) across the material thickness (L), for the available surface area (A), for time (t) for a given permeant partial pressure difference across the film (Δp) (Mangaraj, Goswami, & Panda, 2015; Trinh, Chang, & Mekonnen, 2023). For a multilayered system the P can be calculated as the sum of the permeability constants of the individual layers (Mangaraj et al., 2015).

The permeation process involves three steps, adsorption of the permeant at the polymer surface, its solubilization and diffusion through the polymer. Hence, permeation will depend on the type of material as represented in Figure 1.2. This is notably true for polyethylene, a non-polar polymer, as it presents a higher barrier to water, due its lower solubility (Tan &

Thomas, 2016). One strategy to improve the polymer barrier properties is to restrict its diffusion, reducing the permeant ability to move within the polymer. This can accomplished by means of reducing the polymer chain mobility and the free volume, using polymers with less bulky side groups, narrower molecular weight distribution, fewer long-chain branching, higher chain stiffness, higher crystallinity or increased glass transition temperature (Haley & Borke, 2009; Morris, 2017c). Another strategy for enhancing polymer barrier properties is by using polymer composites with the addition of nanofillers (Jalali Dil, Ben Dhieb, & Ajji, 2019).

1.2.2.2 Enhancing barrier properties with tortuous path morphology

The use of tortuous path morphology is an effective way to the enhance barrier properties of polymer composites. The strategy used to reduce permeation is to delay the diffusion of the molecules by means of a physical barrier forming a tortuous path. In practical terms, an impenetrable phase is used to increase the molecules' diffusion path. This can be accomplished in two ways: by increasing the crystalline phase of the polymeric matrix or by using fillers to create a tortuous path within the composite. Figure 1.5 exemplifies this effect using a platelet-like filler, where the blue arrow indicates the free diffusion path of a molecule percolating an amorphous unfilled polymer (left side) and the longer path in orange with the addition of a filler with a platelet shape (right side).

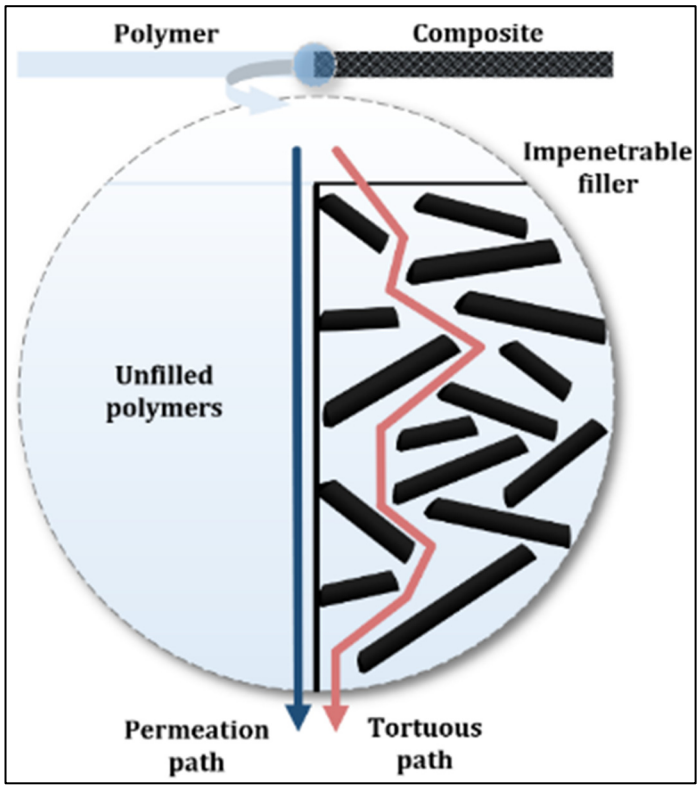

Figure 1.5 Tortuosity effect with the addition of layered particles in a polymeric matrix on the right side compared to an unfilled amorphous polymer on the left side

The shape of the filler is an important factor that influences the barrier property. The barrier efficiency increases depending on the particle's dimensions. Isodimensional particles (spherical shape) show the lowest barrier improvement, followed by elongated particles such as CNT. In turn, layered particles like GBM display the highest consistency in reducing permeability (Wolf et al., 2018) by creating a more tortuous path. However, to achieve a higher barrier effect based on a layered filler, it should be well dispersed throughout the matrix during processing and with appropriate orientation, as later discussed. A well-dispersed state includes the filler's layers exfoliation, increasing its availability within the composites. Figure 1.6 illustrates the distinct stages of distribution and dispersion of a layered filler in a polymeric matrix.

Figure 1.6 Different stages of separation of a filler with layered structure from a less desirable to a most desirable state

The last stage presented in Figure 1.6 is preferable for a barrier composite since it will result in the most efficient reduction of permeation since it is perpendicular to it. Some models have been proposed in the literature to describe and predict the permeability reduction as a function of filler content. Table 1.1 includes some of the proposed models that rely on the filler particles' shape, including aspect ratio, which specifies the length-to-thickness ratio. The first three models rely on the filler particles alignment at right angles to the diffusion direction. However, that's not always the case. The last presented model considers that by including an orientation function where the orientation of the particles relative to the permeation is considered, providing a better property prediction. Additional models can be found in the literature that consider additional parameters (Cui et al., 2016; Tan & Thomas, 2016).

Table 1.1 Relative permeability models available in the literature

Relative permeability models	Ref.
$$\frac{P}{P_0} = \frac{1-\varphi}{1+\left(\frac{L}{2D}\right)\cdot\varphi}$$ Where, P - permeability of the polymer composite P_0 - permeability of the unfilled polymer, L/D - the aspect ratio (length/ thickness) filler φ - is the volume fraction of the filler. Assuming: • Penetrants have an increased diffusion path because of the presence of impermeable filler particles. • Particles are aligned at right angles to the diffusion direction	1 (Nielsen, 1967)
$$\frac{P}{P_0} = \left(1+\frac{\alpha^2\varphi^2}{1-\varphi}\right)^{-1}$$ Where, α - Flake aspect ratio (d/a), d is half the flake width and 'a' is the flake thickness. (α is half the aspect ratio (L/D) of model 1) Assuming: • particles are aligned at right angles to the diffusion direction.	2 (Cussler, Hughes, Ward, & Aris, 1988)
$$\frac{P}{P_0} = \frac{1}{4}\left(\frac{1}{1+a_1 k\alpha\varphi}+\frac{1}{1+a_2 k\alpha\varphi}\right)^2$$ Where, α – aspect ratio defined as half the platelet width (which in this case is the platelet radius) divided by thickness. $a_1 = \frac{(2-\sqrt{2})}{4}$, $a_2 = \frac{(2+\sqrt{2})}{4}$, $k = \frac{\pi}{ln\alpha}$ Assuming – particles are aligned at right angles to the diffusion direction	3 (Fredrickson & Bicerano, 1999; Tan & Thomas, 2016)
$$\frac{P}{P_0} = \frac{1-\varphi}{1+\frac{L\varphi}{2W}\left(1-\sqrt{\frac{2}{3}(1-f)}\right)}$$ Where, f – Herman's orientation function, $f = \frac{1}{2}(3\cos^2\theta - 1)$ θ – angle between the diffusion direction and the normal vector of the filler particle. Then when the filler particles are orientated parallel (θ=0) to the direction of diffusion f=1, and particles are orientated perpendicular to the direction of diffusion (i.e. θ=π/2) then f=-0.5. When there is random orientation, then f=0.	4 (Jalali Dil et al., 2019)

Most of the models presented in the Table 1.1 assume that the filler particles are at right angles to the diffusion direction. In contrast, the last model introduces an orientation function to consider the angle between the diffusion direction and the normal vector of the filler particle, enabling a better representation of the average particle orientation, including random filler orientation. To better represent the influence of filler content, aspect ratio, and filler orientation on barrier properties, Figure 1.7 presents a comparison of predictions from the different models in terms of relative reduction of permeability. On the upper part, for a filler volume content of 1 vol.%, it illustrates the influence of the filler aspect ratio (AR). In the lower part, for a fixed AR of 50, it demonstrates the influence of the amount of filler in terms of volume in the composite. For both representations, the filler particles have either a random orientation or are parallel with the diffusion direction in the last model and oriented at right angles in the remaining models.

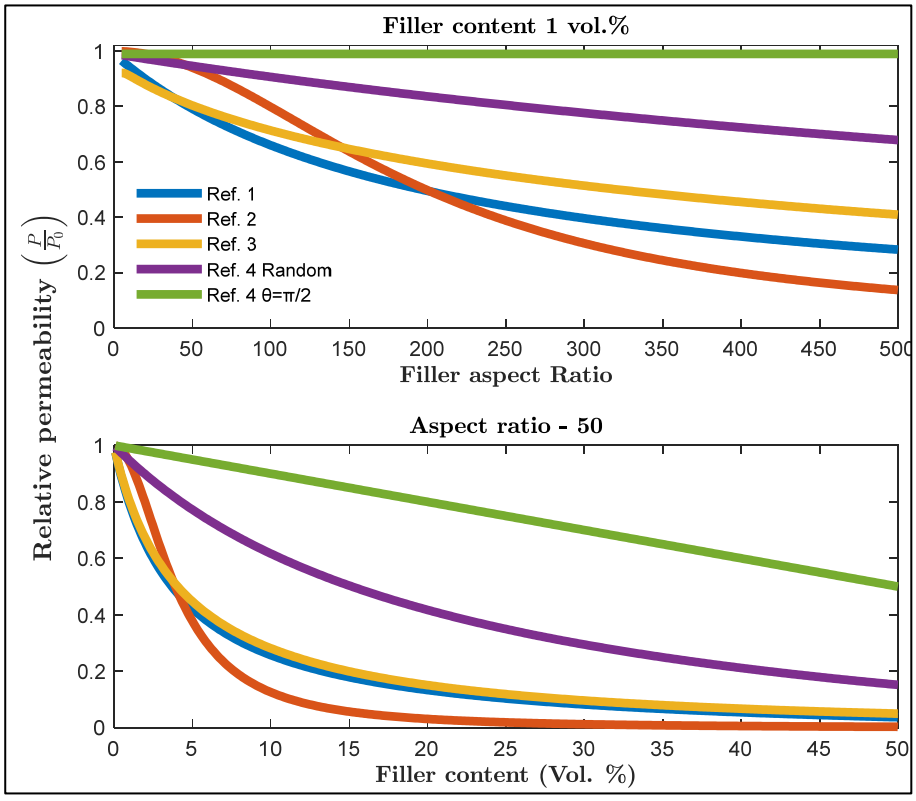

Figure 1.7 Relative permeability predictions for a filler content of 1 vol.% as a function of filler AR and for a fixed AR = 50 as a function of filler volume content

As illustrated in Figure 1.7, the orientation of the filler is fundamental to providing an effective barrier effect. If the filler is oriented parallel to the permeation direction, a high content of filler is necessary (green line). To reduce permeation by half, a content of 50 vol.% is required with an AR of 50, which can create challenges in processing the composite. However, even with a random orientation, an improvement in barrier properties can still be achieved (purple line). With a perpendicular orientation, increasing the AR results in a greater reduction of permeability compared to an unfilled polymer. For a fixed AR of 50, filler content provides the most significant improvements for values less than 5 vol.%.

1.2.2.3 Gas barrier performance of carbon-based nanocomposites

The barrier properties of a polymer composite can be significantly influenced by the morphology of the selected filler and the fabrication method employed. Table 1.2 presents the maximum reduction in permeability of various gases in polymer composites, given a specific filler content of carbon-based fillers, based on different matrices available in the literature. Additionally, the table presents the fabrication methods used as well as the morphologies and aspect ratios (AR) of the fillers.

Table 1.2 Permeability properties of polymer composites for different matrices and fabrication methods using different carbon-based fillers and their morphology

Matrix	Filler*	Filler morphology	Fabrication method	Filler content (wt. %)	Maximum Reduction** (%)	AR ***	Ref.
Polyimide	Graphene Oxide	Platelets	Solution casting	1	W – 90	N/A	(Tseng, Tsai, & Chung, 2014)
Poly(vinyl alcohol) PVA	Graphene oxide nanosheet		Solution casting	1	W – 68 O2 – 98	800	(Huang et al., 2012)
Polycarbonate (PC)	Graphene nanoplatelets		Extrusion and compression molding	7	W– 48 CO2 – 23 O2 – 40	9	(Oyarzabal et al., 2017)

Table 1.2 Permeability properties of polymer composites for different matrices and fabrication methods using different carbon-based fillers and their morphology (Continued)

Matrix	Filler*	Filler morphology	Fabrication method	Filler content (wt. %)	Maximum Reduction** (%)	AR ***	Ref.
Polyamide 11 (PA)	Chemical functionalized graphene from expandable graphite	Platelets	Melt compounding and compression molding	0.1	W – 49 O2 –38	16	(Jin, Rafiq, Gill, & Song, 2013)
Polyamide 12 (PA)				0.6	W – 38 O2 – 32		
Low density polyethylene (LDPE)	Natural graphite polymer-assisted liquid-exfoliation		Melt compounding and compression molding	0.3	W – 21	290	(Simon et al., 2017)
Polylactic acid (PLA)				0.3	W – 10		
Poly(ε-caprolactone)	Epoxy-functionalized graphene		Extrusion and injection mold	3	W – No barrier effect	N/A	(Bouakaz, Habi, Grohens, & Pillin, 2018)
Polyamide 6 (PA6)	Multiwalled carbon nanotubes	Elongated	Melt compounding	1	W – 10 O2 – 50	20	(Méndez et al., 2017)
	Thermally reduced graphene oxide	Platelets			W – 25 O2 – 70	6	
Thermoplastic polyurethane (TPU)	Solution assisted dispersion graphene oxide		Solution process and film blowing	0.2	W – 36	N/A	(Russo et al., 2015)
Polyamide 6/linear low-density polyethylene blends	Carbon black	Spheres	Melt compounding and compression molding	15	W – 4	N/A	(Silva et al., 2020)
Polyamide 6 (PA6)	Graphite	Platelets	Melt compounding and compression molding	12	He – 30 N2 – 45	20	(Kim & Macosko, 2009)
	Functionalized graphene sheets			3	He – 45 N2 – 36	90	

W – water, O – Oxygen gas, He – Helium gas, N – Nitrogen gas
* The designations were taken from their respective works.
** Relative to the pure unfilled material permeability.
*** Approximated from TEM micrographs when available.

Despite the limited number of studies on the use of fillers with different morphologies, the effect of particle shape on water barrier properties can be exemplified by comparing the performance of carbon nanotubes, carbon black, and platelet-like particles such as graphene and graphene oxide, as presented in Table 1.2. When compared to platelet-like particles, both carbon nanotubes and carbon black exhibited significantly lower barrier effects with permeability reductions ranging from 2.5 to 6.3 times less effective, even when used at filler contents up to 15 times higher, as observed with carbon black. A lower filler concentration usually helps to reduce the negative impact on the mechanical properties and material processing.

In addition to particle shape, the type of fabrication method of the polymer composites is another important factor that influences their barrier properties. Solution-based processing techniques are commonly used for producing polymer nanocomposites due to their flexibility in filler functionalization and higher filler orientation (G. Papageorgiou, Li, Liu, A. Kinloch, & J. Young, 2020; Wolf et al., 2018), providing improved barrier properties compared to melt processing techniques, as shown in Table 1.2 in terms of maximum reduction and higher AR. Compared to melt processing techniques that produce more random orientations and increase particle breakage and agglomeration (M. Liu et al., 2018; Wolf et al., 2018), affecting the final properties.

Overall, the barrier properties of polymer composites can be significantly influenced by the choice of particle type and fabrication method. When considering a more sustainable solution for multilayered packaging, it is important to note that the preferred approach should not rely on the use of solvents. While solution-based processing techniques have been shown to yield improved barrier effects at the laboratory scale, they are not as compatible with large-scale production as well-established industry techniques such as extrusion. Extrusion offers a more efficient production process with higher volume and a lower cost to produce polymer composites. Although research has been conducted on using extrusion for packaging applications, it is still limited by the use of compression molding, which is incompatible with

common industrial film forming techniques such as blown and cast film. These techniques produce more filler orientation during processing and provide design flexibility by allowing for the selection of different layer designs. Additionally, as supported by Table 1.2 the investigation of polyethylene is rather limited, despite being the most commonly used thermoplastic in the polymer packaging industry (G. M. McNally, Small, Murphy, & Garrett, 2005). Furthermore, further research is needed to investigate the multilayered polymer composite based on a layered filler such as GNP or GBMs, where morphology in terms of filler alignment and layer structure is designed using approaches that are compatible with common industrial film forming techniques to achieve improved barrier properties for packaging applications with a common packaging material such as HDPE. In addition to this, it is important to achieve appropriate electrical properties towards a complete packaging solution based on carbon-based particles.

1.2.3 Electrically Conductive Polymer Composites for Flexible Packaging

In polymer composites, the incorporation of platelet-like carbon material to create a tortuous path morphology has been shown to effectively create a barrier effect against the permeation of undesired molecules through the film. While this has been investigated in the context of flexible packaging research, studies on electrically conductive polymer composites (ECPC) for flexible packaging remain limited, as this type of technological application is not commonly an objective of such studies (Table 1.2). ECPCs are systems composed of an electrically insulating polymeric matrix and a conductive filler, characterized by an abrupt transition in electrical conductivity related to a critical value of the filler, known as the percolation threshold (Nan, Shen et Ma, 2010). In this context, achieving the percolation threshold, where a continuous network of conductive fillers is formed within the composite, is an important morphology for controlling electrical conductivity and obtaining electrostatic dissipation and electromagnetic shielding properties. Combining this morphology with the tortuous path morphology are important steps for producing a composite suitable for protecting electronic devices using flexible packaging.

1.2.3.1 Percolation Threshold and Electrical Conductivity in Carbon-Based ECPCs

ECPC's electric conductivity behavior is dependent on the amount (mass or volumetric) of its filler. A typical expected behavior of ECPC is depicted in Figure 1.8, representing three distinct regions in the curve that compose the transition from an insulating to a more conductive phase. This behavior can be described as a function of the filler content. At low concentrations, the filler particles do not show enough proximity, so the composite's conductivity is the same as the insulating polymer. As the concentration increases, the particles get closer, allowing for quantum phenomena such as tunneling and the formation of a continuous path through the matrix. This raises the composite's conductivity up to the percolation threshold. Adding more filler results in a less pronounced increase in the composite electrical conductivity, as it only improves an already formed conducting network (Lux, 1993; Nan, Shen, & Ma, 2010).

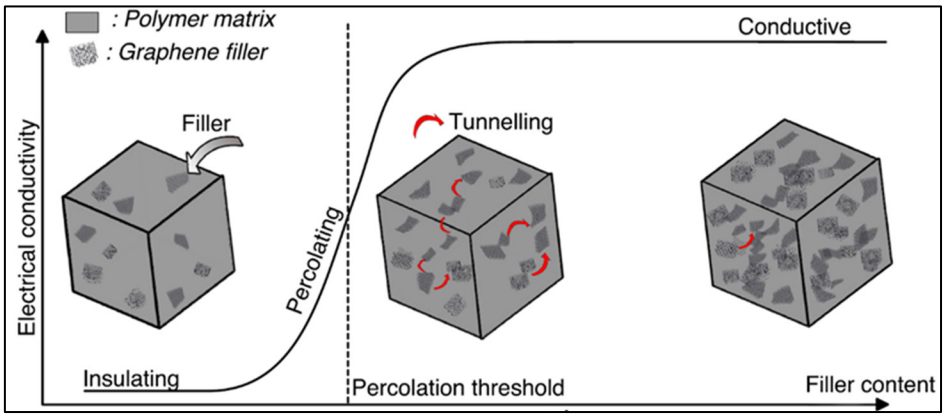

Figure 1.8 Effect of the conductive filler content in an insulating polymer matrix. For small concentrations, the composite is insulating; above a critical amount of filler, there is a marked increase in the electrical conductivity. Taken from Marsden et al. (2018, p. 6)

A common model used to estimate the percolation threshold concentration is based on the classical percolation theory (Kirkpatrick, 1973), also known as the power law or scaling law (Rahaman et al., 2017). Which can be determined using Equation 1.2:

$$\sigma_c = \sigma_0 (V_f - V_{fc})^t, \text{ with } V_f > V_{fc} \quad (1.2)$$

Where the composite's electrical conductivity (σ_c) is given by a constant (σ_0) times the difference between the volume fraction of the filler (V_f) and the volume fraction of the filler at the percolation threshold (V_{fc}) to the power of a critical exponent (t). The percolation threshold can be estimated by a linear regression of Equation 1.3:

$$\log \sigma_c = \log \sigma_0 + t(V_f - V_{fc}) \tag{1.3}$$

With the experimental conductivity values for different filler concentrations of the composite, the percolation threshold is obtained by continuously varying V_{fc} values until the best linear fit is obtained based on the coefficient of correlation. Several factors influence the percolation threshold and the electrical conductivity of the ECPCs. Among them are the filler type, processing technique, its shape and distribution, and the interactions between matrix and filler (Lux, 1993). This complexity of factors and possible interactions prevents the existence of a universal model to predict the percolation threshold behavior and design optimized properties. But nonetheless, other models have been proposed in the literature and can be found elsewhere (Lux, 1993; Rahaman et al., 2017; Taherian, 2016).

1.2.3.2 Effects of Processing Methods, Matrix Choice, and Polymer Properties on the Electrical Conductivity of Carbon-based polymer composites

The type of conductive particle used in an ECPC can significantly impact its electrical conductivity (EC). For instance, in a study by Rousseaux and colleagues (2013), ESD packaging was developed using polystyrene with either carbon nanotubes (CNT) or carbon black (CB) as the conductive filler. The resulting composite packaging using CNT was more conductive than that using CB and did not shed, while requiring a much lower filler content of around 1 wt.% compared to the 15-30 wt.% typically used with CB (Rousseaux, Lhost, & Lodefier, 2013). Factors such as size, shape, dispersion, and intrinsic conductivity of the particles within the polymer matrix can influence the formation of a conductive network and the overall EC of the composite. The most apparent property of the conductive filler is its intrinsic EC. Conductive filler powders have been investigated and their ECs compared for carbon black, graphene, graphite, and MWCNTs (Marinho, Ghislandi, Tkalya, Koning, & de

With, 2012). Although single-particle conductivity can vary by three to five times higher depending on the conductive filler, the EC of the powders is much closer than expected for nanostructured materials such as MWCNT and graphene. This is due to the orientation and particle contact having a greater effect on the EC of these nanostructured fillers. As a result, the conductivities of these materials varying between 10^1 to 10^3 S/m, in order from highest to lowest, were MWCNTs > Graphene > Carbon black > graphite (Marinho et al., 2012). The dependence on filler type is illustrated in Table 1.3, which shows different fillers in polyethylene matrices obtained by melt processing along with their percolation threshold, maximum concentration, and conductivity.

Table 1.3 Melt-Processed Carbon-Based Polyethylene Composite: Processing method, Percolation Threshold, Maximum Filler Concentration, and Electrical Conductivity

Matrix	Filler	Processing method	Percolation threshold (wt.%)	Maximum Concentration (wt.%)	Maximum Conductivity (S/m)	Ref.
Low density Polyethylene	Carbon black	Extrusion and compression molding	>20	20	10^{-9}	(Paszkiewicz et al., 2020)
	Graphene nanoplatelets		2.5-5		10^{-5}	(Paszkiewicz et al., 2018)
	MWCNT		1.5		10^{2}	
		Melt compounding and compression molding	1-4	10	10^{-1}	(Sabet & Soleimani, 2014)
Medium density Polyethylene	MWCNT	Extrusion and compression molding	7.5	10	10^{-2}	(T. McNally et al., 2005)
High density Polyethylene			1.9	10	10^{-2}	(Xiang, Harkin-Jones, & Linton, 2014)
			1-2	4	10^{-1}	(Xiang, Harkin-Jones FREng, & Linton, 2014)
		Melt compounding and compression molding	2.5	16	10^{-2}	(Al-Saleh, 2016a)
			4.5	10	10^{-1}	(Linares et al., 2008)
		Melt compounding and injection molding	10-19.7	28	10^{1}	(Jiang & Drzal, 2011)
	Graphene nanoplatelets		>28		10^{-4}	

As exemplified in Table 1.3, the lowest percolation values were achieved with MWCNT, usually ranging from 1 wt.% to nearly 8 wt.%, followed by graphene nanoplatelets and carbon black. A higher percolation with MWCNT was primarily attributed to the processing technique; injection molding was unable to adequately disperse the filler, thus reducing both the interconnection between particles and the EC (Jiang & Drzal, 2011). Furthermore, even at high filler concentrations (10 wt.%), the electrical conductivity remained relatively constant around 10^{-2} to 10^{-1} in most of the cases for HDPE, indicating that are diminishing returns in

increasing the filler content. Among conductive fillers, carbon nanotubes have been extensively studied in ECPCs due to their high aspect ratio and higher electrical properties, providing further support to the findings on how varied factors affect the EC of ECPCs.

In this context, the processing method has also been a focus of research in the development of ECPCs. Similarly to the barrier properties, the electrical performance of composites produced via solution processing is superior to that obtained via melt processing. This is exemplified in Figure 1.9, which illustrates the percolation threshold for polymethyl methacrylate (PMMA), PE, and PP matrices with carbon nanotubes as a conductive filler. While solution processing yields percolations closer to 1 wt.%, for melting processing, the values are widely distributed (Watt & Gerhardt, 2020). In another example, a tenfold reduction in percolation threshold was more readily achieved with solution processing rather than with melt processing (Jouni et al., 2014). But, as previously mentioned, solution processing is not as compatible with large-scale production of flexible packaging films. Additionally, considering the importance of HDPE for flexible packaging applications and its use as a polymeric matrix in ECPCs, it is important to consider that its crystallinity and viscosity will affect the final EC, as exemplified in Figure 1.9 in terms of percolation threshold.

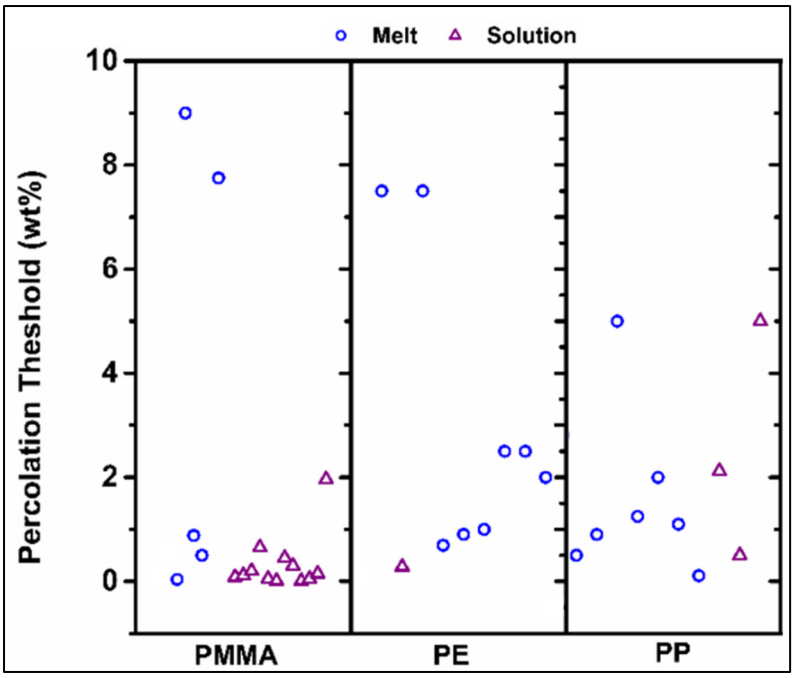

Figure 1.9 Percolation threshold for different carbon nanotube/polymer composites for two processing methods for PMMA, PE, and PP matrices. Adapted from Watt & Gerhardt (2020, p. 11)

As shown in Figure 1.9, the choice of matrix will also impact the ECPCs properties. It has been demonstrated that polymer melt viscosity influences the EC and percolation threshold. Lower viscosity results in higher EC compared to higher viscosity, increasing the percolation threshold threefold for a PP/MWCNT composite obtained by melt-mixing (Pötschke, Mothes, Krause, & Voit, 2019). The effect of viscosity on EC has also been confirmed for other polymeric matrices, including polyamide 12, polybutylene terephthalate, polycarbonate, polyetheretherketone, and low-density polyethylene (Socher, Krause, Müller, Boldt, & Pötschke, 2012). With lower viscosities, the infiltration process of filler agglomerates by the polymer chains is enhanced, reducing filler shortening, improving dispersion, and increasing the EC (Pötschke et al., 2019; Socher et al., 2012). It should be noted that carbon nanotubes are rather polar, which can cause issues during processing of non-polar polyolefin melts (Alig et al., 2012), such as polyethylene. Both filler polarity and viscosity partially account for the differences in percolation threshold shown in Table 1.3.

In addition to the effects of viscosity on electrical conductivity, the crystallinity of the polymeric matrix also plays a role. Compared to amorphous polymers, semi-crystalline polymers usually require larger amounts of conductive filler to achieve a similar EC due to their phase structure (Lim, Min, & Kim, 2010; Watt & Gerhardt, 2020), formed by amorphous and crystalline phases, that may limit the filler's participation in the conductive network (Kazemi et al., 2017; Tarani et al., 2016; J. Wang et al., 2020). This is particularly significant for ECPC based on HDPE as polymeric matrix due to its higher degree of crystallinity. More recently, two potential alternatives that are still not fully explored for HDPE composites to enhance its electrical conductivity and could facilitate its use for ESD control and shielding: hybrid systems and thermal treatment.

Hybrid composites combine conductive fillers to enhance the EC of an ECPC through a synergistic effect. Although the definition of synergism may vary depending on the study, it can be described as occurring when the hybrid's EC is greater than the sum of the highest EC attained by each filler separately (Qu, Nilsson, & Schubert, 2019). The basis for the synergistic effect is still being researched, but it is suggested that the combination of different particle shapes and aspect ratio variations could enhance tunneling and EC in the hybrid composite (Qu et al., 2019). Experimentally, synergism is investigated by varying the ratio between the different fillers and monitoring its effect on conductivity. Using this approach, different matrices have been investigated with CNT as the primary filler combined with GNP, for example, epoxy (Kranauskaitė et al., 2018) and a styrene-ethylene/butylene-styrene thermoplastic elastomer (Kuester, Demarquette, Ferreira, Soares, & Barra, 2017). However, there has been little investigation of HDPE based hybrid composites. One of the few studies was conducted by Wang et al (2018) that obtained a hybrid composite based on HDPE with 1 wt.% of MWCNT and 0.5 wt.% of GNP, compatibilized with ethylene-vinyl acetate, by melt blending. This hybrid composite showed improved electrical conductivity sufficient to reach the ESD range (Q. Wang et al., 2018). However, the authors did not compare the same filler content for each individual material as part of their investigation nor did they investigate hybrid composites above the percolation threshold, essential for effective shielding properties.

Another approach to improve the EC of HDPE based composites is through thermal treatment, specifically targeting its crystalline phase. This allows for two types of time-dependent heat treatments of a semi-crystalline composite: annealing above the melting point or controlling the cooling rate (J. Wang et al., 2020; Strugova, Ferreira Junior, David, & Demarquette, 2021). Both can improve EC through different mechanisms: annealing enhances EC by allowing filler diffusion (Alig, Lellinger, Engel, Skipa, & Pötschke, 2008; Helal et al., 2019) in the polymer melt, while slower cooling rates during crystallization promote an increase in the volume exclusion effect of the crystalline phase (J. Wang et al., 2020). This increases the probability of filler-filler contact and leads to higher EC. Despite its importance, the effect of time-dependent heat treatments on the stability of synergism in hybrid systems of HPDE/CNT/G remains unclear.

In addition to improving the electrical conductivity of HDPE-based composites, achieving higher levels of electrical conductivity is also important for effective shielding properties. Shielding is a critical aspect in flexible packaging applications where electromagnetic interference can compromise the performance of electronic devices.

1.2.3.3 EMI shielding concepts and the requirements for flexible packaging

As EMI shielding is related to a composite's electrical conductivity, it can be controlled by properly adjusting the shielding effect through the electrical properties. For shielding applications, an electrical conductivity greater than 10^{-2} S/m is recommended (Sankaran, Deshmukh, Ahamed, & Khadheer Pasha, 2018; Sudha, Sivakala, Patel, & Radhakrishnan Nair, 2010). This makes ECPCs interesting candidates for shielding due to their lower density and greater corrosion resistance when compared to usual shielding materials, which are typically metals with its high electrical conductivity (Saini & Aror, 2012; Tong, 2016).

The effectiveness of a shielding material in reducing an incident electromagnetic wave or radiation is expressed as shielding effectiveness (SE) in decibels (dB), denoting an energy reduction in a logarithmic scale by the ratio between the transmitted and incident energy (Saini

& Aror, 2012). The SE for any EMI depends on the contribution of three mechanisms of a shielding material: reflection, absorption, and multiple internal reflections (B. G. Soares, Barra, & Indrusiak, 2021) and is represented by the Equation 1.4 (Ravindren, Mondal, Nath, & Das, 2019):

$$SE = SE_R + SE_A + SE_{MR} \tag{1.4}$$

SE_R represents the shielding by reflection, SE_A the shielding by absorption, and SE_{MR} shielding by multiple internal reflections. The last one is usually disregarded for SE_A higher than 10 dB (Ravindren, Mondal, Nath, & Das, 2019). Shielding effectiveness can be experimentally evaluated with a two-port vector network analyzer (VNA) by measuring the scattering parameters (S-parameters) (Peng & Qin, 2021; Schmitz, Soares, Barra, & Santana, 2023) after interacting with the analyzed material over a given range of frequency, usually in GHz, inside a waveguide. Where the coefficients reflection (R), transmission (T) and absorption (A) of the material are given by:

$$A + R + T = 1 \tag{1.5}$$

$$R = |S_{11}|^2 = |S_{22}|^2 \tag{1.6}$$

$$T = |S_{12}|^2 = |S_{21}|^2 \tag{1.7}$$

The indices 1 and 2 of the scattering parameters (S) represent the VNA ports. Where 1 indicates the port that receives the EMI radiation, and 2 represents the port that transmits the incident energy. Shielding effectiveness is related to R and T by the following (Cao et al., 2019):

$$SE(dB) = 10 \cdot log_{10}\left(\frac{1}{T}\right) \tag{1.8}$$

$$SE_R(dB) = 10 \cdot log_{10}\left(\frac{1}{1-R}\right) \tag{1.9}$$

$$SE_A(dB) = 10 \cdot log_{10}\left(\frac{1-R}{T}\right) \tag{1.10}$$

The total SE and the contribution of each mechanism can be obtained by replacing R and T for the scattering parameters:

$$SE(dB) = 10 \cdot log_{10}\left(\frac{1}{T}\right) = 10 \cdot log_{10}\left|\frac{1}{|S_{21}|^2}\right| \tag{1.11}$$

$$SE_R(dB) = 10 \cdot log_{10}\left(\frac{1}{1-R}\right) = 10 \cdot log_{10}\left|\frac{1}{1-|S_{21}|^2}\right| \tag{1.12}$$

$$SE_A(dB) = 10 \cdot log_{10}\left(\frac{1-R}{T}\right) = 10 \cdot log_{10}\left|\frac{|S_{11}|^2}{1-|S_{21}|^2}\right| \tag{1.13}$$

Reflection is the primary shielding mechanism in metals, while carbon-based materials have an increased ability to shield by absorption due to their dielectric properties, which reduce the amount of electromagnetic radiation (David et al., 2023). The SE can also be expressed in terms of shielding efficiency (%) (Li et al., 2017) and represents the percentage of the incident wave that is reduced by the shielding material for a certain amount of SE, as given by:

$$Shielding\ efficiency\ (\%) = 100 - \left(\frac{1}{10^{\frac{SE}{10}}}\right) \cdot 100 \tag{1.14}$$

Figure 1.10 shows the shielding efficiency as function of SE and highlights the recommended SE for packing material with shielding values according to the military standard (*MIL-PRF-81705 - Performance Specification: Barrier Materials, Flexible, Electrostatic Protective, Heat- Sealable*, 2009).

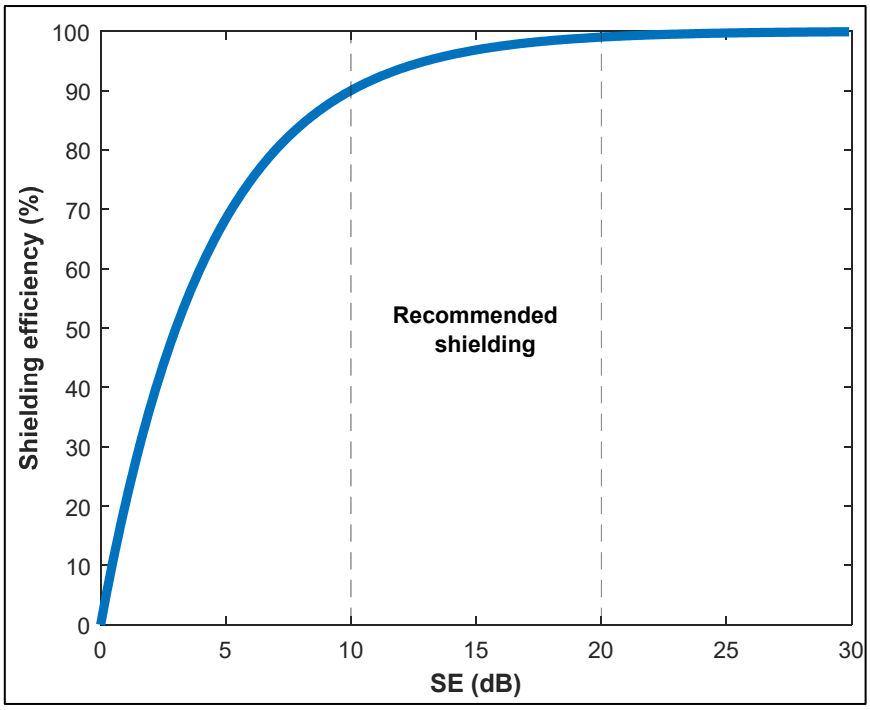

Figure 1.10 Shielding efficiency as function of SE including the recommended values for a packaging material

The required shielding in the standard in the 1 to 10 GHz frequency range of 10 dB or 25 dB as shown in Figure 1.10 results in an attenuation of approximately 90 % and 99.7 % of the incident field, respectively. However, shielding is rather limited to being evaluated for sheet samples with thicknesses in the millimetric range, rather than for flexible films which have thicknesses less than 250 µm. This difference may be one of the reasons for the limited literature with carbon-based materials and the necessary combined properties, barrier, ESD, shielding, for such a packaging material. One example of a composite for ESD and shielding application was investigated by Verma et al. (2015), which combined thermoplastic polyurethane (TPU) and thermally reduced graphene oxide (RGO). Solution blending and compression molding techniques were employed as fabrication method for the composite. With 0.6 wt.% of RGO, the composite's electrical conductivity was within the static dissipative range (10^{-9} to 10^{-4} S/m) and had an SE of -3 dB. Increased filler content improved both static dissipative and shielding properties, with SE increasing to -21 dB at 10 wt.% RGO and a thickness of 3 mm, with absorption dissipation as main shielding mechanism (Verma et al.,

2015). Despite the potential limitations of the fabrication route for industrial scale-up, the work effectively demonstrates the feasibility of combining both properties for packaging applications. Additionally, to the combination of properties by tailoring multilayered structures optimal properties can be explored. This was demonstrated by Danlée and colleagues (2012), who achieved improved shielding in the 8 to 40 GHz region by adjusting the alternation of pure layers of polycarbonate (PC) and conductive layers of PC coated with MWCNT, while simultaneously decreasing the total thickness of the composite (Danlée, Huynen, & Bailly, 2012). As highlighted by the authors, the arrangement of the layers is essential for absorption. An alternating sequence of insulating and conductive layers enables the wave to travel deeper into the material, increasing absorption and reducing the reflection of incident waves.

1.2.4 Multilayered structures obtained by coextrusion technique for flexible packaging nanocomposites

To achieve a multilayered flexible packaging nanocomposite for the protection of sensitive electronics, the coextrusion technique is key to exploring new layer designs based on barrier and electrical properties towards increased reuse and recycling solutions. Coextrusion is a process that allows the obtention of a thin flexible multilayered film, having less than 250 μm, by simultaneously extruding two or more polymers and joining them together to form a single structure with multiple layers by combining multiple molten polymers (Sanchez V. et al., 1996). Conventionally, in an industrial setting, there are two ways to obtain those films: either by cast film or blown film coextrusion.

Simply put, in the cast film extrusion process, a polymer is extruded through a flat die with a wide slit and narrow spacing (Langhe & Ponting, 2016). The molten material is then stretched in the machine direction by attaching it to a rotating roll and drawing it down to a specific thickness (Morris, 2017b). Multilayered structures can be obtained by combining the polymer melt streams from multiple extruders into a feedblock, where the layers are arranged in a specific order and the final width is achieved in the die (Kanai & Campbell, 1999b; Morris, 2017b), as exemplified in Figure 1.11 a). Alternatively, as represented in Figure 1.11 b) tubular films can be obtained with the blown film coextrusion. In this process, concentric layers are

formed in an annular die. Air pressure is used to fill the melt extrudate and blow a bubble as it exits the die (Kanai & Campbell, 1999a; Langhe & Ponting, 2016). It is important to notice that this technique results in biaxial orientation of the film in both the machine and transverse directions (Morris, 2017b). And in orientation studies of HDPE/MWCNT composites, it was found that while biaxial orientation resulted in improved mechanical properties, the composite experienced a great reduction in electrical conductivity by a factor of approximately 10^{10}. As a result, the composite's conductivity became much more similar to the insulative matrix of HDPE (Xiang, Harkin-Jones, & Linton, 2015). Based on that, we selected cast film coextrusion as one of the processing techniques to design specific multilayered composite structures.

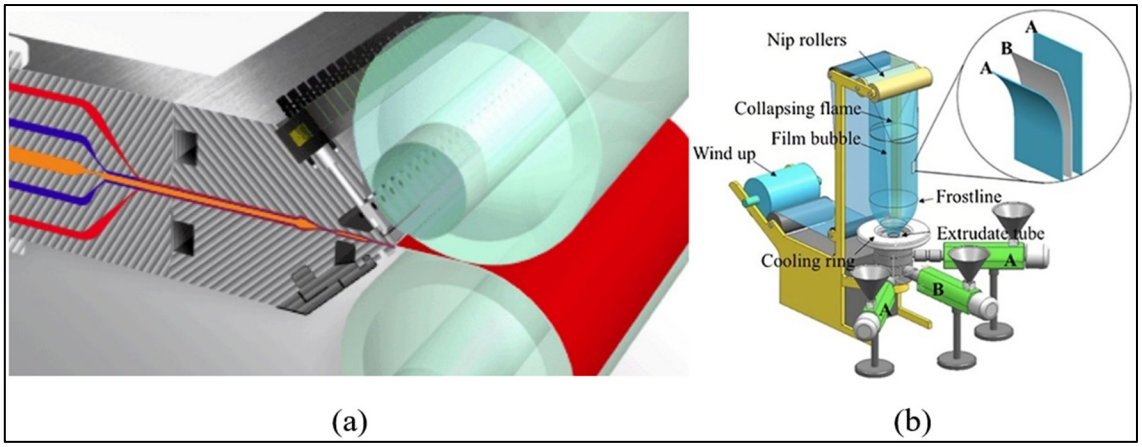

Figure 1.11 Coextrusion techniques a) cast film extrusion with a cross section showing the joining of different flows highlighted in different colors forming a final multilayered film. Taken from Smart Ecofilms (2023) and a b) blown film extrusion line with an ABA structure. Taken from Winotapun et al. (2019, p. 3)

Another possible technique that allows for the obtention of a composite with more than a few layers compared to cast film coextrusion is by the use of a multiplying element, also referred as forced assembly, microlayer technology, or nanolayer technology (Langhe & Ponting, 2016; Morris, 2017c). This approach uses a multiplication element within the feedblock to sequentially split in half the combined melt and stake it, doubling the number of layers. Therefore, starting with two melt flows A and B will produce a structure with 2n+1 layers, depending on the number of multiplying elements, denoted by n. The resulting structure will

be a multilayered material with an ABA alternating structure (Langhe & Ponting, 2016; Messin et al., 2017), as illustrated in Figure 1.12.

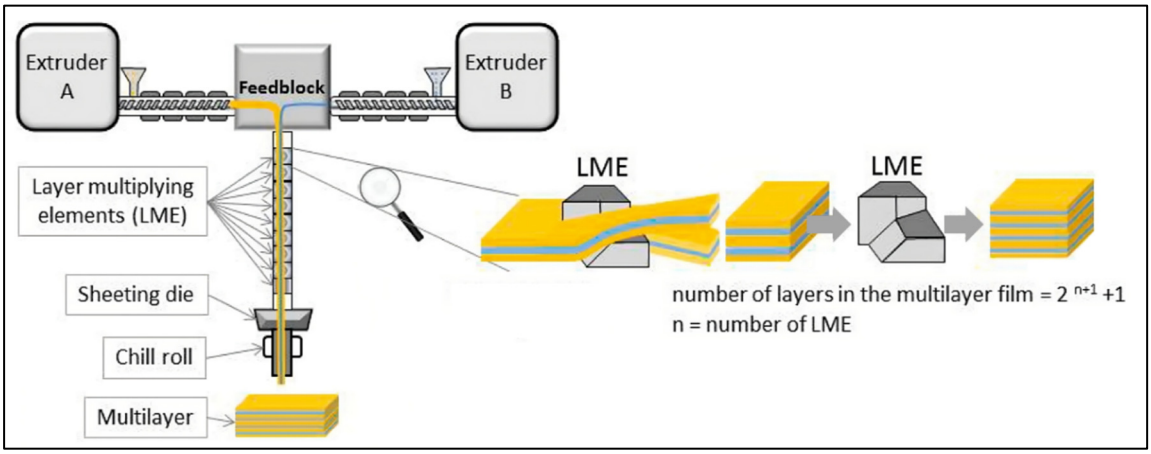

Figure 1.12 Coextrusion process with a layer multiplying element. Adapted from Messin et al. (2017, p. 3)

The obtention of microlayers have been reported to improve resistance to pin-hole formation, a detrimental defect to barrier films shown improved barrier properties (P. C. Lee, Dooley, Robacki, Jenkins, & Wrisley, 2014), barrier (Zhang, Lee, Jenkins, Dooley, & Baer, 2014), electrical conductivity (W. Gao, Shen, & Guo, 2014), among others. Using a layer-multiplying element combined properties were obtained by He et al. (2020). The study successfully achieved a composite with both shielding and flame-retarding properties. Although polyolefin matrices were not investigated, an alternating layer of poly (butylene succinate) and MWCNT with layers of thermoplastic polyurethane (TPU), MWCNT and intumescent flame retardants were used. The study identified an optimal number of layers, with 16 layers a shielding effectiveness of 33 dB was observed with a 4 wt.% of MWCNT and 1.7 mm thick sample (L. He et al., 2020).

1.2.4.1 Microwave absorption

In recent years, significant research attention has been dedicated to investigating composites capable of reducing electromagnetic pollution accomplished by increased absorption effects.

The loss process is an important and practical way to reduce electromagnetic pollution by absorption instead of simply reflecting it (Danlée, Huynen et Bailly, 2012), as opposed to metal, where it's shielding due to its high conductivity, promoting the reflection of the incident EM wave. The ability to absorb the incident EM wave is given by a high reflection loss (RL), by converting the incident EM waves into thermal energy (Zeng, Cheng, Yu, & Stucky, 2020). Experimentally, the absorption measurement is performed with the same equipment as shielding measurements, using only one port, and the investigated material is backed by a metallic plate to reflect the incident wave towards port 1. RL is given by Equation 1.15 (Schmitz et al., 2023):

$$RL(dB) = 20 \cdot log|S_{11}| \tag{1.15}$$

RL can also be expressed by Equation 1.16 (Z. Liu et al., 2007):

$$RL = 20 \log \left| \frac{Z_{in} - Z_0}{Z_{in} + Z_0} \right| \tag{1.16}$$

Where, Z_0 is the characteristic impedance of free space, and Z_{in} is the input impedance at the interface of free space and material. The absorption is improved with matching impedances, otherwise there will be no dissipation (Zeng et al., 2020). The material's ability to absorb and dissipate the radiation will depend on its thickness, dielectric, and magnetic losses (P. He, Cao, Cao, & Yuan, 2021; Zeng et al., 2020). Although magnetic materials are investigated for increased microwave absorption, carbon-based materials have dielectric losses as the main contributor to microwave absorption (Z. Liu et al., 2007). The absorption can be further improved with multilayer structures, allowing the wave to travel further within the composite (X. Gao et al., 2016). Gao and colleagues (2015) obtained enhanced microwave absorbing composites of PP/carbon black (CB) with multilayered structures. By investigating the effect of the number of alternating layers of conductive (PP/CB) and insulating (PP), both electrical conductivity and reflection loss increased with an increasing number of layers. The maximum reflection loss increased from -12 dB for a 2-layer structure to -32 dB with 128 layers for a

composite with a filler loading of 7 wt.% and a 1.5 mm thick sample. The improved absorption was attributed to the higher interfacial polarization, resulting from an increased electrical charge accumulation on the interfaces with the increasing number of layers (W. Gao, Zheng, Shen, & Guo, 2015). Considering those results, a flexible packaging composite that could simultaneously fulfill a variety of functional requirements, e.g., barrier, shielding, and microwave absorption, remains to be investigated. It is important to note that none of the previous studies assessed the performance of flexible films but rather focused on the evaluation of sheet composites.

CHAPTER 2

RESEARCH OBJECTIVES

To address the issue of using dissimilar materials in flexible packaging, the primary objective of this research project is to develop a flexible, multilayered polymeric composite as a more recycling-friendly packaging solution. To achieve this, materials and processing techniques most compatible for industrial use were employed. We combined a high-density polyethylene (HDPE) matrix, a common, chemically simple, and hydrophobic packaging material, with carbon-based fillers possessing specific properties: industrial-grade graphene (G) with a platelet-like morphology and multilayered carbon nanotubes with high electrical conductivity to achieve gas barrier and electromagnetic shielding. To this end, three steps were taken successively by focusing on the following specific objectives.

2.1 Specific objectives

The specific objectives are each explored in depth within their own individual chapters, as shown in the parentheses.

- Investigate the effect of G on the barrier and electrical properties at low filler content in a HDPE multilayered cast film (Chapter 3).

- Examine the influence of G as a secondary filler on the barrier and electrical properties of hybrid composites of HDPE and CNT in a single-layer film (Chapter 4).

- Investigate the feasibility of a multilayer structure with combined barrier and shielding properties and compare its performance to that of single-layer composites (Chapter 5).

CHAPTER 3

INVESTIGATING THE EFFECTS OF INDUSTRIAL GRADE GRAPHENE CONTENT AND SURFACE FINISHING ON HDPE MULTILAYERED FILMS

3.1 Chapter overview

Graphene-based composites are promising candidates to improve properties in flexible packaging applications. However, the literature hardly addresses industrial-scale requirements. In this work, high-density polyethylene (HDPE), a common packaging material, and industrial-grade graphene (G) were used to prepare multilayered composites by coextrusion cast film, a flexible-packaging-industry-compatible technique. The effects of G content and surface finishing on HDPE films' performance were investigated. Results showed that although surface finishing improved visible light transmittance by reducing surface roughness, it also induced defects and increased permeability. These detrimental effects can be successfully prevented by layer design during coextrusion. A maximum permeability reduction of 43% at 0.5 wt.% of G was achieved. Such a result was associated with good dispersion efficiency and a the filler aspect ratio. However, it has been found that as the G content increased, the dispersion efficiency was reduced, decreasing both the barrier efficiency and the mechanical reinforcement effect. Moreover, for the maximum investigated G content of 1 wt.%, the composite's electrical conductivity remained the same. In summary, the present study showed the feasibility of industrial-scale production of G-based flexible packaging film applications, emphasizing the importance of G dispersion and layer design to achieve improved properties. This work was published in Materials Today Communications, in Volume 31, June 2022, 103470.

3.2 Literature review

Flexible packaging ensures the protection of electronic devices against damaging effects such as those caused by moisture or electrostatic discharge. In this context, polymer-based composites are versatile candidates for the flexible package industry, allowing for tuning key

properties such as permeability. One of the main strategies used to control and reduce permeability in polymer-based composites is to increase the tortuous path (Tan & Thomas, 2016) of the permeating species by dispersing a layered filler in a polymer matrix, improving its barrier effect. Dispersion is typically achieved by intercalation and exfoliation of the layered filler (e.g., clays, graphite, and graphene) by means of solvents, polymer melt blending, and/or filler modification (Jalali Dil et al., 2019; Tan & Thomas, 2016). At the research laboratory scale, polymer-based composites for barrier applications are usually obtained via solution processing. However, this technique is not suitable for cost-effective industrial applications due to the large amounts of material required and scale-up limitations. Thus, to promote the transfer of research findings on barrier properties to technological applications for flexible packaging, one should direct efforts towards processing techniques and materials suitable for an industrial scale, i.e., melt compounding of thermoplastics and large scale produced fillers. Still, there is little published research on the topic.

Simultaneously with other advancements in the field, there has been a growing interest in research on carbonaceous-based polymeric composites over the past decade. Typically, fillers like carbon nanotubes, graphene, and their derivatives. These functional fillers enhance specific properties of polymeric composites, in particular thermal conductivity, gas barrier, and electrical conductivity (antistatic and electromagnetic shielding effects), to name a few. In particular, graphene and its derivatives, can offer an interesting way to improve the performance of polymeric films used in the flexible packaging industry. For example, mechanical and electrical conductivity (Yadav et al., 2013), barrier properties (J.-T. Chen et al., 2014), among others (Sundramoorthy & Gunasekaran, 2014).

To take advantage of the promising properties of graphene, great efforts have been made recently to develop and optimize its cost-effective powder production on an industrial scale (Kauling et al., 2018; Kovtun et al., 2019), suitable for melt compounding. The literature concerning industrial graphene, however, mainly deals with materials of high structural variability (Kauling et al., 2018), leading to large differences in terms of reported nomenclature and results (Kauling et al., 2018; Mohan, Lau, Hui, & Bhattacharyya, 2018). Thus, for the sake

of simplicity, the performance evaluation of materials designated as graphene, graphene nanoplatelets, graphene microplates, or graphite microplates will, hereafter, be referred to as graphene-based materials (GBM).

Some studies have therefore been conducted on graphene-based materials in polymeric composites and demonstrated that it is an effective way to reduce permeability. Permeability reductions of 18% to 45% with a filler weight content up to 7 wt.% in different thermoplastic matrices, such as polypropylene (Kalaitzidou, Fukushima, & Drzal, 2007), polyamide (Boldt et al., 2020), and polycarbonate (Oyarzabal et al., 2017), compounded by means of extrusion, have been reported. However, in order to ensure lower cost and processability, as low as possible filler concentrations are usually recommended. Additionally, high filler concentrations adversely affect film transparency and coloring control, as well as, diminish barrier efficiency due to increased filler agglomeration (Jin et al., 2013). Although some studies demonstrate the feasibility and potential use of graphene-based composites to improve barrier properties, two main drawbacks can be pointed out from a literature analysis. First, the composites are usually produced by the compression molding technique, and it is known that the barrier properties depend significantly on the manufacturing technique (Morris, 2017a). Thus, those results are not directly transferable (Boldt et al., 2020) to commonly used fabrication techniques in the flexible packaging industry, like blown and cast film processes. Second, the most commonly used thermoplastic in the polymer packaging industry is polyethylene (G. M. McNally et al., 2005). Polyethylene, however, is seldom used as a polymeric matrix in studies of permeability involving graphene-based composites (Tan & Thomas, 2016). Therefore, in order to address some of the shortcomings found in the literature regarding the processing technique and matrix on the composites performance, this study aims to extend the results to flexible packaging applications for electronics protection at the industrial scale based on cast film composites of high-density polyethylene (HDPE) and industrial-grade graphene.

Herein, multilayered composite films of HDPE, the most common flexible packaging material, with an industrial (commercial) grade graphene (G) are produced in a coextrusion cast film

line, allowing flexibility to design the layers The commercial graphene employed is produced through liquid-phase exfoliation of graphite. This production route's main advantages are low cost and environmental sustainability by using water as a processing medium (Madinehei, Kuester, Kaydanova, Moghimian, & David, 2021). Additionally, it has been shown that this G has a lower health risk than other fillers (Moghimian & Nazarpour, 2020).

The two main investigated parameters in this study are the surface finish, to produce more homogenous film surfaces, and filler loading up to a maximum of 1 wt.% to reduce agglomeration and the negative impact on film transparency. The influence of those parameters on, the oxygen and water vapour permeability, electrical conductivity, and mechanical properties were investigated. Furthermore, a discussion of the effect of filler agglomeration on these properties is presented. Finally, permeability and mechanical response are evaluated in light of theoretical models in order to validate and interpret the obtained results.

3.3 Experimental

3.3.1 Materials

The polymeric composite films were prepared using high density polyethylene-hexene copolymer pellets under the commercial name Formolene HB5502B (Formosa plastics, USA). The reported physical properties are a density of 0.955 g/cm^3 and a melt flow index of 0.35 g/10 min (190 °C/2.16 kg). A commercial graphene grade was used in the form of masterbatch (MB) pellets composed of HDPE Formolene HB5502B and 40 wt.% of GrapheneBlack 3X (Nanoxplore Inc., Canada) (NanoXplore, 2021). An electrical conductivity of 1.2×10^0 S/m was measured for the hot-pressed MB sample using the four-point probe method. All materials were used as received and kindly supplied by Nanoxplore Inc. (Canada).

3.3.2 Methods

3.3.2.1 Film fabrication

Films of 8 layers were fabricated using a coextrusion cast line (LabTech engineering, Thailand) with four single screw extruders with a ratio length/diameter of 30 and equipped with Maddock mixing screws. The MB was diluted with HDPE into three different compositions: 0.1 wt.%, 0.5 wt.%, and 1 wt.% of G directly in the single screw extruders (SSE). Those concentrations were kept the same for each one of the eight layers. Neat films were prepared for comparison with the composites. Temperatures from the feeding zone to the metering zone were 200 °C, 220 °C, and 240 °C with a screw speed of 20 rpm for all extruders. The connection pipes from the extruders to the die were set at 220°C and the flat die at 240 °C. A 300 mm flat die with a lip opening of 150 µm was used to achieve films with an average thickness of 100 µm, resulting in a draw ratio between 1.3 and 1.5 considering the final film thickness. The casting roll and die exit distance were set to less than 20 mm with parallel alignment to avoid melt sagging. Rolls were used in a vertical alignment position with chill rolls set to 90 °C to reduce surface defects and promote a more symmetrical microstructure (Duffo, Monasse, & Haudin, 1990).

To compare the effect of the surface finish on the film's properties, a polishing roll was used to nip the samples with 0.2 MPa at 90 °C, resulting in a film with a smooth surface. Those samples were identified as nipped (N) and compared against the reference group without surface finishing, which was identified as non-nipped (NN).

3.3.2.2 Characterization

The transparency, morphology, barrier, mechanical, and electrical properties of the obtained samples were characterized using different analytical techniques at room temperature. The measurements were performed in duplicate on samples arbitrarily taken from the center of the fabricated films for each composition and surface finishing, unless otherwise stated. When

relevant, the orientation in which the samples were tested is indicated by machine direction (MD) and transverse direction (TD) throughout the chapter.

The transparency of the produced films was estimated by evaluating the light transmittance in the visible range (340 – or to 1000 nm) of square-shaped films with a side length of 50 mm using a UV-Vis Thermo Scientific SPECTRONIC 200.

The morphology of the samples was characterized by optical microscopy (OM), scanning electron microscopy (SEM), transmission electron microscopy (TEM), and atomic force microscopy (AFM).

The surface (top view) and cross section (MD) of the films (SI) were observed with an optical microscope in transmission mode (model Olympus BX51). The images were captured using an OptixCam Summit SK2-5.2X digital camera. Pictures of the surface and cross section were taken at 100- and 1000-times magnification, respectively, both from at least 3 random areas. An automated approach was employed using the Image Processing Toolbox of MATLAB 2020a software to investigate the filler dispersion, alignment, and size. The main operations of the automated approach were: noise reduction, polymeric matrix background removal, particle identification, and summation of the projected particle area within different focused regions of the same area under analysis. A conversion factor was applied to the identified particles based on the picture's pixel information and sample size through a micrometer calibration procedure in the microscope. The obtained data based on top view pictures were: average particle length size, D50, D90, and maximum particle size. The average G particle thickness was obtained from the image processing of cross-section pictures. To clarify, particle size in this context refers to the size (length or thickness) of the G agglomerate instead of the smallest constituent unit of a material. Samples were also observed with a SEM Hitachi MEB-3600-N at an accelerating voltage of 5 kV and by TEM using a JEOL model JEM-2100F at 200 kV. In this case, films embedded in a mounting resin were prepared by ultracryomicrotomy at -160 ºC. These samples were analyzed in the machine-transverse (M-T) plane to investigate the G aspect ratio. The surface roughness of 10-mm samples (25 μm^2 of analyzed area) was

determined using a Bruker EnviroScope AFM in tapping mode. It was calculated by averaging the absolute values of the obtained profiles.

The water permeability was evaluated in a MOCON AQUATRAN model 1 using an exposed area of 50 cm². The amount of water vapor transmitted across the films was determined at 37.8 °C in a saturated atmosphere (100% relative humidity). The duplicates were tested at the same time, with 24 hours of conditioning before each measurement. The oxygen transmission rates were assessed using MOCON OX-TRAN 2/21 ST equipment at 23 °C and 0% relative humidity with an exposed area of 100 cm² and 4 hours of conditioning. At least 4 measurements were done for each sample, and the reported permeability is given by averaging those measurements. Both water and oxygen permeability results were normalized by the film thickness obtained from four measurements with a micrometer screw gauge.

The crystallinity of the films was determined by differential scanning calorimetry (DSC) (PerkinElmer model Pyris 1) to evaluate its possible influence on oxygen and water permeability results. For that, a sample was taken from the center of the same films tested for permeability. The sample was encapsulated in an aluminum pan and analyzed in the range of 50 °C to 200 °C at a heating rate of 10 °C/min. The percentage of crystallinity was determined according to Equation 3.1:

$$X_c = \left(\frac{\Delta H_f}{\Delta H_f^0 \cdot \phi}\right) \cdot 100 \tag{3.1}$$

Where ΔH_f is the experimental heat of fusion and ΔH^0_f is the enthalpy of fusion of a theoretical 100% crystalline HDPE, which was assumed to be 293 J/g based on literature (Ehrenstein, Riedel, & Trawiel, 2004), and ϕ is the weight fraction of HDPE in the composite.

The mechanical properties of the obtained films were obtained in tensile mode using Instron ElectroPuls E3000 equipment with a load cell of 250 N at a 2 mm/sec rate. Samples in the machine direction (MD) and transversal direction (TD) were cut from the produced films into

rectangular shapes of 20 mm × 80 mm. They were fixed between pneumatic grips with the help of rubber pieces to avoid sample slippage.

Volume resistivity (ρ) measurements were conducted using the two-probe standard method with a Keithley 6517B electrometer and a Keithley 8009 test fixture. Volumetric conductivity (σ) values in S/m were obtained according to Equation 3.2:

$$\sigma = \frac{1}{\rho} = \frac{1}{\left(\frac{A \cdot V}{i \cdot t}\right)} \tag{3.2}$$

A voltage V of 200 V was applied for 180 seconds, followed by 180 seconds of discharge. The current i was taken as the average value after 60 seconds of the initial applied electrical potential. The effective area of the measuring electrode is represented by A. Thickness t was determined by averaging five values taken from random regions using a micrometer screw gauge.

3.4 Results and discussions

3.4.1 Surface roughness and light transmittance

Surface finishing and optical properties are important requirements in the flexible packaging industry since they can give the manufacturer the ability to display the product inside the packaging (Morris, 2017a). The average surface roughness (SR) of the samples, as well as the average peak and valley height, are presented in Table 3.1. As expected, the non-nipped (NN) sample presents rougher surfaces when compared to the nipped (N) one. The restricted cooling and pressure imposed by the chilled rolls on the nipped samples result in a more homogeneous and smoother surface, with smaller peaks and valleys and lower variability among them. It can also be seen from Table 3.1 that the increase in G content also resulted in an increase in the SR of the surface-finished films.

Table 3.1 Average values of surface roughness (SR), peaks and valleys height

Group	Filler weight Content (%)	Average SR (nm)	Average peak height (nm)	Average valley height (nm)
Nipped (N)	0	4.8±2.5	13.7±12.3	4.7±8.3
	0.1	7.1±7.8	23.1±13.2	16.3±15.6
	0.5	7.5±4.2	27.7±20.3	15.0±15.6
	1.0	8.5±2.3	19.0±13.7	8.7±9.7
Non-nipped (NN)	0	30.0±19.8	70.4±35.6	25.1±32.3
	0.1	29.3±27.0	61.9±29.0	17.4±31.4
	0.5	19.9±22.1	52.6±46.7	16.0±35.0
	1.0	23.1±34.6	80.8±58.7	108.7±91.3

Figure 3.1 presents the percentage of transmitted light as a function of SR for N and NN films. The surface finish resulted in an increase ranging from 1.9% to 49.6% in light transmission for the neat HDPE. This transparency enhancement can be explained by the reduction of SR, which results in a more homogenous surface and decreases light scattering effects at the surface. The introduction of graphene led to light transmission attenuation due to increased light scattering and absorption effects (Marini & Bretas, 2017; Palomba et al., 2018). A further increase in G content led to a 99.8% reduction in transmittance at 1 wt.% compared to the neat N material. In contrast, a similar trend of decrease in transmittance and increase in SR was not observed for the NN composite films. This could be attributed to a high variation in the SR of NN samples, as shown in Table 3.1. Interestingly, N 0.1 wt.% films exhibited higher light transmittance than the NN neat HDPE films. These results are in good agreement with the visual appearance of the composite films, with the N films being more transparent to the naked eye than the NN films.

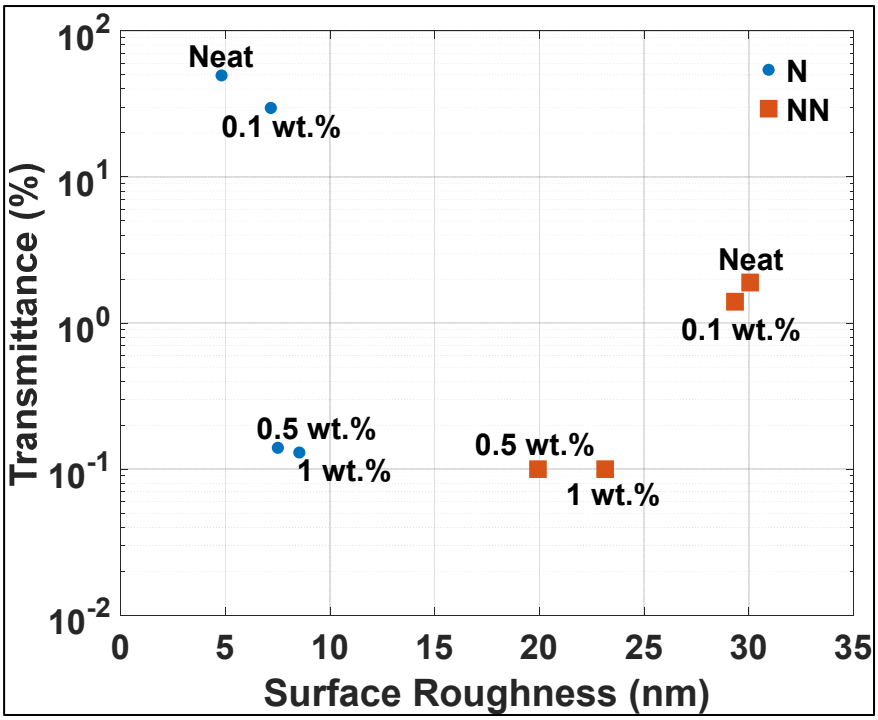

Figure 3.1 Percentage of transmitted light in 500 nm as function of surface roughness for nipped and non-nipped samples

3.4.2 Filler average size, dispersion, alignment, and aspect ratio

The gas permeability performance of a composite material depends on the state of the dispersed phase inside the film. Taking that into account, optical microscopy (OM) was used as a fast tool to identify the dispersion state of the fabricated films from top view and cross section. Both matrix and the G phase were easily distinguished in transmission mode due to the small amounts of G and the small film thickness (100 µm). Figure 3.2 depicts the top and cross-section view images of a NN sample after image processing for the three evaluated graphene contents used for the quantification of the particles' parameters. The N samples presented similar results.

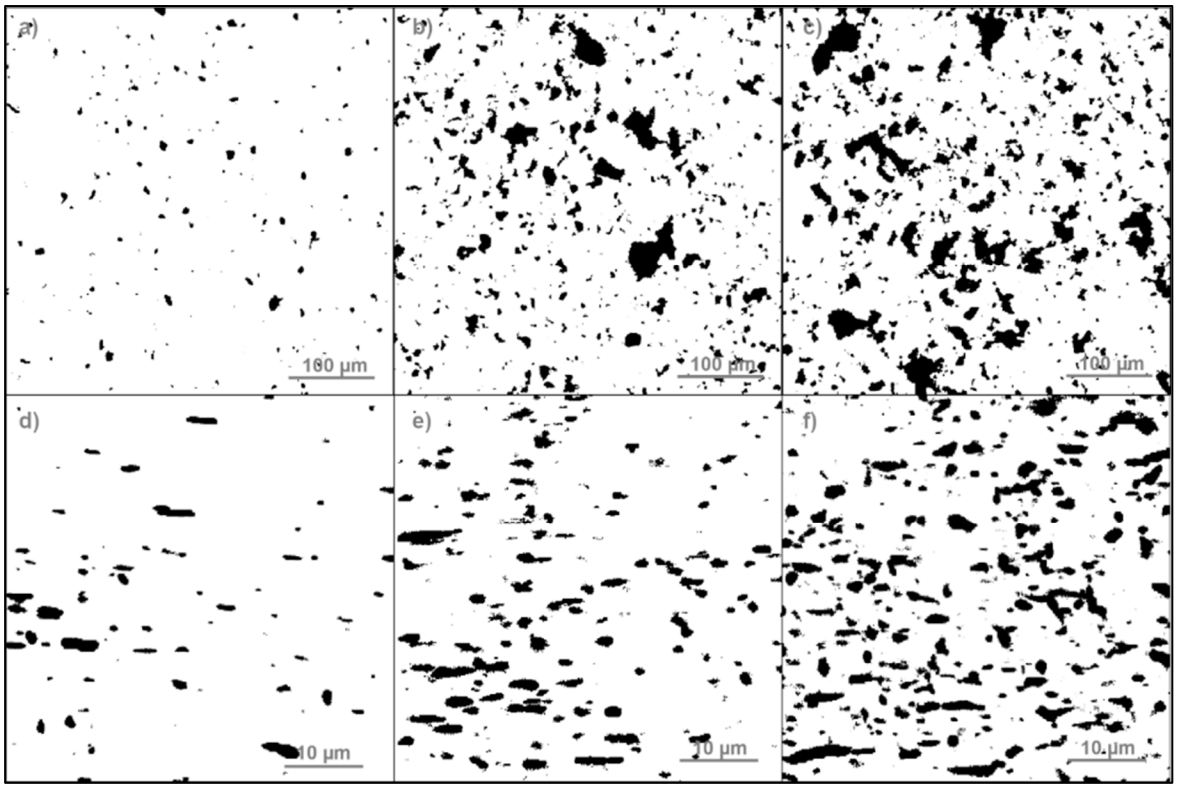

Figure 3.2 The top row presents top view pictures of NN samples a) 0.1 wt.% G, b) 0.5 wt.% G and c) 1 wt.% G. The bottom row presents cross section pictures of d) 0.1 wt.% G, e) 0.5 wt.% G and f) 1 wt.% G

A good dispersion and distribution of graphene can be qualitatively observed in Figure 3.2. The graphene displays a platelet shape and preferential alignment parallel to the film's surface, induced by the processing technique as presented in Fig.2 d)-f). Such alignment is desired and beneficial to reduce composites permeability (Jalali Dil et al., 2019).

Table 3.2 summarizes the average graphene particle size, D50, D90 and maximum size in terms of length size of graphene agglomerates and average graphene agglomerate thickness measured for both studied groups (N and NN). Length and thickness are assumed based on the preferential alignment observed. For the same graphene content, both N and NN samples show a similar average size, with half of the fillers being less than 3 µm in length and a similar distribution throughout the matrix. The increase in G content resulted in a higher number of larger agglomerates. This agglomeration effect is observed with an increase in the average G

length, D90, and maximum particle size found in the matrix. The increase in G content is accompanied by an increase of graphene agglomerate thickness (Table 3.2), indicating that filler is indeed dispersed in the form of agglomerates. This observation suggests a reduction in extruder efficiency to deagglomerate the G at higher contents. Considering the limitations of OM in observing smaller particles, a TEM analysis was carried out for the 0.5 wt.% G films in the machine-transverse (M-T) plane for both N and NN groups. The TEM images are depicted in Figure 3.3.

Table 3.2 Summary of size measurements, average values, D50, D90, maximum size (Max.), average thickness of G agglomerates for nipped and non-nipped samples

Group	Graphene weight content (%)	Average G length size (μm)	D50 (μm)	D90 (μm)	Max. (μm)	Average G agglomerate thickness (μm)
Nipped (N)	0.1	3.1±0.1	2.3	6.1	45.8	0.6±0.4
	0.5	4.0±0.1	2.5	8.5	87.1	0.7±0.2
	1.0	4.7±0.0	2.5	10.3	143.7	1.0±0.8
Non-nipped (NN)	0.1	3.2±0.0	2.4	6.3	47.5	0.5±0.4
	0.5	4.3±0.1	2.6	9.4	125.5	0.9±0.5
	1.0	4.8±0.1	2.5	10.7	123.8	1.1±0.8

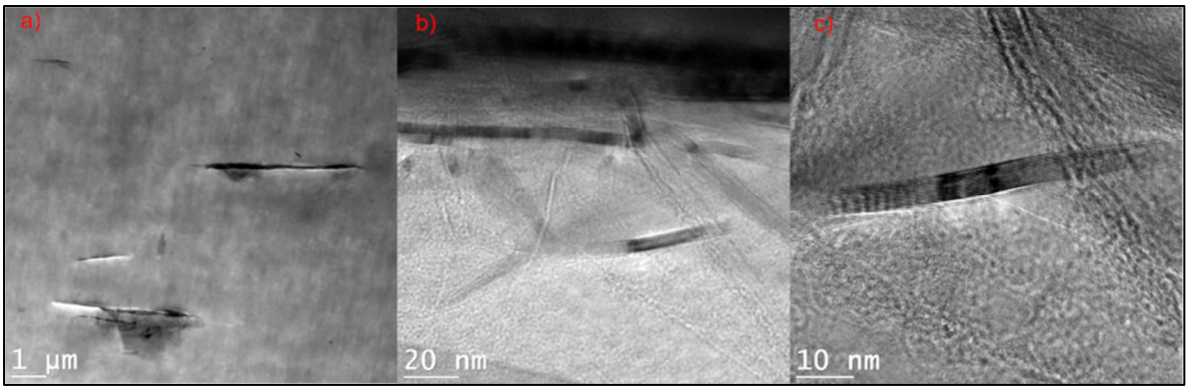

Figure 3.3 TEM in the M-T plane showing a) primary agglomerates, b) non-exfoliated graphene and c) Few layers of graphene in the 0.5 wt.% NN composite

TEM confirms the existence of primary agglomerates, as shown in Figure 3.3 a) and suggested by OM cross-section analysis, comprised of smaller particle agglomerates with few graphene layers (Figure 3.3c)). Thus, TEM and OM results indicate that the extrusion by SSE is inefficient to properly deagglomerate the primary agglomerates (Fig. 3.3 b)), which therefore limits the G barrier effect as the filler content increases to 1 wt.% in the nipped samples (Jin et al., 2013), as discussed in section 3.3. No great differences were found between the techniques. Furthermore, the TEM analysis indicated that the graphene agglomerates presented an average aspect ratio (AR) of 16±13.

3.4.3 Water and oxygen permeability performance

The use of an impenetrable phase is an important strategy to improve barrier performance in flexible packaging. In the present work, both the crystalline phase of HDPE and the dispersed graphene filler act as impenetrable phases for permeating species. Table 3.3 shows the performance of both nipped and non-nipped HDPE/G films in terms of water and oxygen permeability and their average crystallinity.

Table 3.3 Summary of water and oxygen permeability and average crystallinity percentage for nipped and non-nipped samples

Group	Filler content (wt.%)	Water Permeability ($mg \cdot mm/m^2 \cdot day$)	Oxygen Permeability ($cm^3 \cdot mm/m^2 \cdot day$)	Average Crystallinity (%)
Nipped (N)	0	260±2	125±3	58±1
	0.1	162±6	79±1	58±2
	0.5	152±1	71±2	58±1
	1	231±2	107±2	57±1
Non-nipped (NN)	0	169±3	79±1	60±1
	0.1	156±1	73±1	59±2
	0.5	155±1	65±1	58±1
	1	151±1	67±1	59±1

Nipping the samples resulted in an increase in permeability for all films. In the case of the films without graphene, this increase was more than 35%, which cannot be explained by a decrease in the crystallinity of the samples as the crystallinity of all samples was the same within experimental error. In any case, according to the Nielsen Model (Nielsen, 1967) (Equation 3.3) and considering the crystalline phase as a filler of AR equal to one (Duan & Thomas, 2014), the decrease in permeability originating from a change in crystallinity would not be more than 13%.

$$\frac{P}{P_0} = \frac{1 - \varphi_s}{1 + \frac{L}{W} \cdot \frac{\varphi_s}{2}} \tag{3.3}$$

Where the P_c/P_m ratio is the permeability ratio of the composite compared to the polymeric matrix, L/W is the aspect ratio (AR) of the barrier particle given by the length L and thickness W, and φ_s is the particle volume fraction in the composite. Therefore, the observed increase in permeability was attributed to the presence of defects at the surface of the films induced during the surface finishing, as will be discussed in the next paragraphs.

Meanwhile, G filler presented the expected effect of decreasing permeability for all samples, however, to varying extents depending on whether the films had been nipped or not. In general, for NN samples, a decrease in permeability with increasing G content was observed to a

maximum of 18% with 0.5 wt.% G in oxygen permeability. As for the N samples, a maximum reduction of 43% was obtained for the same G content and permeability test. But an unexpected behavior is observed at 1 wt.% G with an increase of more than 50% in permeability compared to samples with 0.5 wt.% G content.

To better understand the inconsistent results of G content and surface finishing on the permeability properties, a different layer design was used, and new films were prepared with no filler at the surface layers at both nipping and no nipping conditions. By adopting this configuration, the top and bottom layers were made only of HDPE, and the inside layers were set to 1 wt.% G content. The measured oxygen permeability of the nipped and non-nipped samples were 73±1 and 72±3 $cm^3 \cdot mm/m^2 \cdot day$, respectively, corresponding to a permeability reduction of 42% and 9% compared to the neat HDPE films. Those results lead to two possible conclusions: first, the surface treatment has a dependency on the amount of filler at the surface, and second, the permeability response is dominated by the structure developed at the surface. SEM and AFM analysis of N samples indicated the presence of surface defects such as holes and poor interface filler/polymer which possibly created preferential pathways to increase permeation. The density of defects is further increased at higher G contents, which correlates with larger agglomeration sizes (Table 3.2) that are expected to lead to more defects in the films (Appendix I). Second, considering the NN samples, the presence of G at the surface is beneficial to the overall barrier ability of the films acting as physical barrier.

The permeability experimental results were compared to the Nielsen prediction model (Equation 3.3) to assess the performance of the surface finishing and the G. Figure 3.4 depicts experimental data and the permeability ratio as a function of graphene content, assuming filler alignment perpendicular to the surface as verified by OM and TEM. Composites with particles perpendicularly aligned to the surface and with increasing AR, from 5 to 1000, were used as input in Eq.3.3 to plot theoretical result profiles (grey lines). The WP and OP abbreviations stand for water and oxygen permeability, respectively.

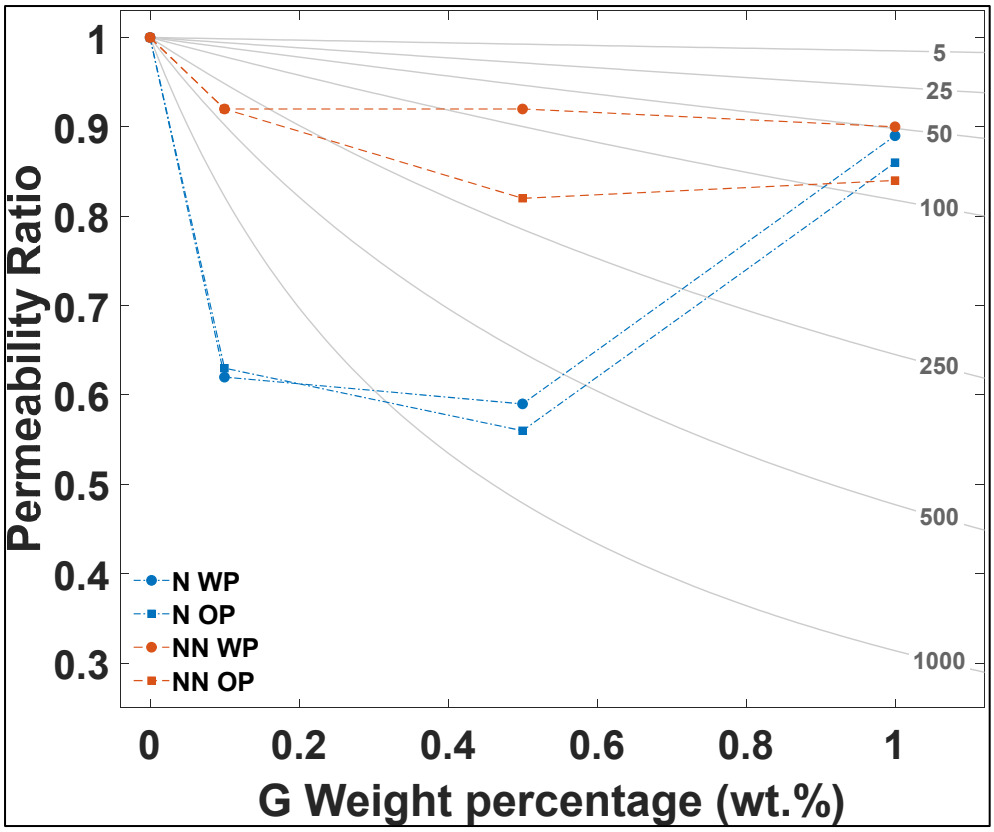

Figure 3.4 Permeability ratio as function of filler weight concentration for experimental and predicted data. The lines between the experimental data points are just a guide to the eyes. The indicated numbers in the grey lines are the used AR

The model predicts a continuous permeability ratio decrease as a function of filler content for a composite with both alignment and AR fixed. Comparing the predicted results to the experimental data, G shows two behaviors depending on the sample group considered. For the NN group, a permeability reduction is obtained with G acting as a physical barrier, with AR of 250-500 at 0.1 wt.% G to AR of 50-100 at 1 wt.% G, which indicates that with increasing G content, the deagglomeration efficiency is reduced. For the N samples, a pronounced reduction is obtained, indicating that G would act as a filler with an AR higher than 1000, which is not compatible with OM and TEM analysis. Instead of having higher AR, it is possible that G hinders the influence of defects developed during surface finishing compared to the neat N sample and effectively reduces the permeability until 0.5 wt.% G. At 1 wt.% G, the magnitude of reduction in permeability is hindered by increased agglomeration and reduced

deagglomeration efficiency of single screw extruders at low speeds. Furthermore, the most effective barrier reduction was found for oxygen as a permeant rather than water. A smaller reduction in water permeability with the addition of G could be related to the chemical nature of HDPE itself. As HDPE is a hydrophobic material, it already acts as a good barrier against water, and hence, the relative difference between the neat polymer and the composites is less pronounced.

3.4.4 Mechanical response under tensile stress

The mechanical response of the neat and composite films was evaluated since it provides valuable data regarding the packaging material to guarantee product integrity (Morris, 2017d). The main mechanical responses of the composites under tensile stress are summarized in Table 3.4 in the MD and TD.

Table 3.4 Summary of mechanical properties of neat and composites films in the machine and transversal directions for both groups

Group	Filler content (wt.%)	E (MPa)		Elongation at break (%) *		E ratio
		MD	TD	MD	TD (range)	
Nipped (N)	0	370±40	360±30	500	230-500	1.0
	0.1	400±30	390±30		280-500	1.0
	0.5	400±30	390±20		280-500	1.0
	1	390±30	410±50		280-490	0.9
Non-nipped (NN)	0	390±40	380±20	500	200-500	1.0
	0.1	400±30	400±20		250-500	1.0
	0.5	400±30	410±30		230-500	1.0
	1	420±20	430±20		190-360	1.0

* Elongation at break values of 500% means samples failed to break due the equipment's maximum displacement

As the E ratio shows (MD to TD modulus ratio), no significant anisotropic response was observed. Nonetheless, the elongation at break behavior was different and is only presented for TD. Since in MD, the breakage of the samples would exceed the displacement limit of the tensile equipment. This elongation behavior could be ascribed to the processing alignment of the crystalline phase experienced during processing, as supported by FTIR results (Appendix I)

and the literature (Fatahi, Ajji, & Lafleur, 2005; Yadegari, Morshedian, Khonakdar, & Wagenknecht, 2016a).

Since it was not possible to identify a clear trend in composite's Young modulus (E) with surface finish or increasing G content, the Halpin-Tsai model (Dul et al., 2019; King, Klimek, Miskioglu, & Odegard, 2015) (Equation 3.4) was employed to evaluate and compare experimental results with the model predictions. The Halpin-Tsai model is commonly used to predict the Young's module of a polymer composite (Shokrieh & Moshrefzadeh-Sani, 2016):

$$E_L = E_m \left(\frac{1 + \eta_L \xi V_f}{1 - \eta_L V_f} \right) \tag{3.4}$$

The parameters η_L and ξ are defined as:

$$\eta_L = \frac{\left(\frac{E_f}{E_m}\right) - 1}{\left(\frac{E_f}{E_m}\right) + \xi} \tag{3.5}$$

$$\xi = \frac{2}{3} \times \frac{L}{W} \tag{3.6}$$

$$E_C = E_L \tag{3.7}$$

Where the E_c, E_L, E_m, and E_f are the composite, longitudinal, matrix, and filler Young's moduli, respectively. V_f is the G volume fraction in the composite, and L/W is the filler length L and thickness W ratio. Experimental results in MD were compared to composites containing up to 1 wt.% of G with AR ranging from 5 to 50 (TEM measurements), filler density of 2.2 g/cm^3, aligned with the processing direction, and a Young's module of 36.5 GPa that corresponds to the exfoliation between G layers (King et al., 2015). The results are presented in Figure 3.5.

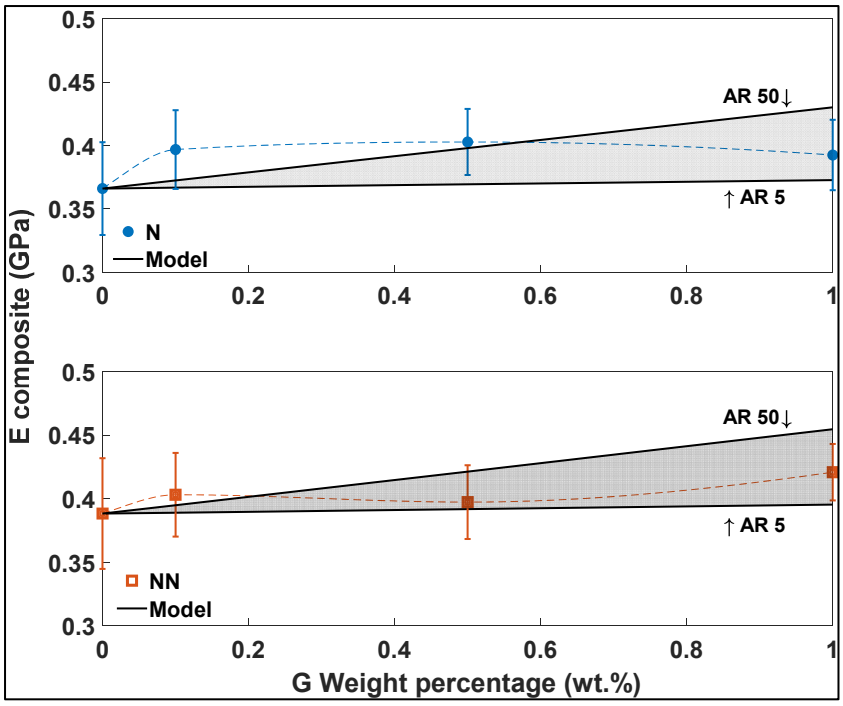

Figure 3.5 Young's modulus of composites and model with AR between 5 and 50 for nipped and non-nipped samples

As shown in Figure 3.5, although the use of G increases the average Young's modulus of the composites compared to the neat samples, they all fall within the experimental error, which reduces the confidence of the observed effect of reinforcement. However, in general, the experimental data agrees with the proposed model for both groups since the AR is reduced due to the higher number of agglomerates, as evidenced in the previous analyses. It is noteworthy that increased AR leads to more pronounced effects, as observed by the predicted line of AR 50.

3.4.5 Electrical conductivity

In flexible packaging, a certain level of electrical conductivity is desired to promote safe charge dissipation to protect electronics from undesired electrical discharges. For a 100 µm thick film, an electrical conductivity between 10^{-04} to 10^{-09} S/m is advised (Tolinski, 2015a). Commercial-grade graphene is a conductive material. Taking this into account, the electrical conductivity was measured to evaluate if the graphene addition at contents up to 1 wt.% would be able to

cause any changes in the electrical conductivity. For the investigated filler content range, the electrical conductivity for both groups varied between 6 and 8 × 10^{-16} S/m. So, a maximum filler concentration of 1 wt.% has no significant impact on electrical conductivity and is less than the desired range to promote safe charge dissipation. The low electrical conductivity is a result of the reduced amount of filler, which is below the percolation threshold required to increase the composite conductivity. To achieve higher electrical conductivity by melt compounding, higher concentrations of filler are usually needed (Batista et al., 2019).

3.5 Conclusions

The effect of industrial-grade graphene and surface finishing on multilayered cast HDPE films was investigated. At low filler concentrations, G improved permeability properties independently of surface finishing. Additionally, it was also found that, although the surface finishing favors light transmittance by reducing the surface roughness of the films, the nipping process induces some defects affecting permeability. The detrimental effect of surface finishing is counteracted by layer design or the filler at concentrations lower than 1 wt.%. At this same weight concentration, the addition of graphene was not enough to cause a significant difference in terms of electrical conductivity, and the barrier properties were compromised. As the theoretical model indicates, this was attributed to the dispersion state of the filler, where a smaller AR resulted in decreased barrier efficiency and a low mechanical reinforcement effect. To conclude, the use of industrial-grade graphene at low concentrations is attainable for industrial-scale production of flexible multilayer films with improved properties. At 0.1 wt.% G, a good combination of barrier properties and light transmittance was achieved through surface finishing. Nevertheless, the incorporation of 1 wt.% of graphene seems to be a limiting content at which detrimental effects on the mechanical and barrier properties were observed due to reduced dispersion efficiency. A drawback that can be partially overcome in nipped films by removing graphene from the outer layer.

CHAPTER 4

THE INFLUENCE OF PROCESSING PARAMETERS TOWARDS A SYNERGISTIC EFFECT IN POLYETHYLENE-CARBON-BASED HYBRID COMPOSITES

4.1 Chapter overview

Carbon-based hybrid thermoplastic composites are promising candidates for flexible packaging to protect electronics, as they can present synergistic properties by combining more than one filler. In this work, composites consisting of a high-density polyethylene (HDPE) matrix, a common packaging material, carbon nanotubes (CNT) as the main electrically conductive filler, and industrial-grade graphene (G) as the second filler were combined by extrusion and shaped by compression molding. The effect of adding G as a second filler on the electrical and barrier properties of the hybrid composites was evaluated above the percolation threshold. A synergistic effect on the electrical conductivity was observed at a CNT:G ratio of 99:1 at 9 wt.% content. The use of 0.1 wt.% of G reinforced the electrical network formed by CNT, achieving synergism that further improved the electrical conductivity when combined with a solid-state treatment. Experimental data suggested that the effect on the electrical conductivity was mostly influenced by the thermal history linked to morphological changes. The research results represent a further step towards developing hybrid or structured carbon-based thermoplastic flexible packaging solutions.

4.2 Literature review

As electronic devices have grown in both number and variety, it has become more challenging to ensure their performance, correct operation, and safe shipment. Currently, at the commercial level, this is assured by a multilayer flexible packaging. The combination of polymeric layers and a metallic aluminum layer results in a structure with properties such as gas and moisture barriers, as well as electromagnetic shielding. However, there are important drawbacks to this current approach, including layer delamination, corrosion of the aluminum layer, and low recyclability (Kaiser et al., 2017; Twede et al., 2009; Yam, Yam, & Davis, 2009).

Alternatively, carbon-based thermoplastic composites are promising candidates to overcome these drawbacks, providing a corrosion-free, lightweight, recyclable, and industry-compatible approach. In our previous work, we showed that a high-density polyethylene multilayered flexible composite with industrial-grade graphene (G), an electrically conductive carbon-based material, acted as a good barrier against water and oxygen by decreasing permeation by around 38% at 0.1 wt.% G (Ferreira Junior et al., 2022). However, low G filler fraction yielded an insulating composite below the electrical percolation threshold (EPT). The EPT is the minimum amount of filler required to create a conductive network, resulting in an electrically conductive material (Nan et al., 2010), which is essential for electromagnetic shielding. Thus, enhancing the EC of carbon-based thermoplastic composites is expected to provide improved shielding properties that, combined with barrier properties, could offer a more complete solution for the protection of electronic devices. In this regard, to keep the G barrier properties at low filler content and achieve electrically conductive composites, its combination with carbon nanotubes (CNT) represents a feasible approach.

In the literature, hybrid composites combine two or more conductive fillers, e.g., carbon black (CB), CNT, or graphene nanoplatelets (GNP) (Al-Saleh, 2016b), aiming to enhance the EC through a synergistic effect. A synergistic effect occurs when the hybrid's EC is greater than the sum of the highest EC attained by each filler separately at a fixed filler fraction (Qu et al., 2019). The mechanism behind synergism is still under investigation, but models suggest that different particle shapes (1D, 2D, 3D) and/or aspect ratio, could lead to higher tunneling chances, increasing EC (Gbaguidi, Namilae, & Kim, 2020). Therefore, experimentally, synergism is investigated by varying the ratio between fillers at a certain concentration and monitoring its effect on the conductivity (Al-Saleh, 2016b; Kranauskaitė et al., 2018; Kuester et al., 2017; Rostami & Moosavi, 2020; Q. Wang et al., 2018). However, no specific filler ratio has been found to consistently lead to synergism in carbon-based composites, as different materials and methods may influence the synergetic relationship. Synergistic effects have been observed in hybrid composites containing CNT as the primary filler combined with GNP, for example, at the weight ratios of CNT:GNP 5:1 (Kranauskaitė et al., 2018) and 1.5:1 (Kuester

et al., 2017). Meanwhile, in composites in which the CNT content was equal to or lower than CB (Socher, Krause, Hermasch, Wursche, & Pötschke, 2011; Q. Wang et al., 2018) or GNP (Al-Saleh, 2016b; Rostami & Moosavi, 2020) only improvements in the EC were observed without synergism. This difference has been attributed to the CNT geometry, that favors the formation of conductive networks (Al-Saleh, 2016b). Previous studies with CNT hybrids have been limited to evaluating the effect of the main filler on properties such as EPT (Kranauskaitė et al., 2018; Socher et al., 2011), and crystallinity (Socher et al., 2011), but the influence of the second filler on a hybrid composite remains unclear, especially above the EPT. This is particularly relevant considering that particle size affects the EC, as exemplified in PLA/GNP composites (Y. Gao et al., 2017). Furthermore, gas permeability and other properties may also be influenced by not only characteristics of the second filler but also the thermal history of the composite, requiring additional investigation.

The influence of processing parameters and the resulting thermal history on the EC of carbon-based thermoplastic composites through morphological changes is well established (Alig et al., 2008; Y. Gao et al., 2017; Socher et al., 2011; Strugova et al., 2021). However, few studies have investigated the influence of thermal history on the stability and extent of synergism in these composites (Y. Gao et al., 2017; Garzón & Palza, 2014). The effects of thermal history are evidenced by the post-processing heat treatment that induce additional morphological changes not only in blends (Strugova et al., 2021) but also in single-polymer composites containing CNT (J. Wang et al., 2020). These treatments are especially relevant for semi-crystalline polymers (J. Wang et al., 2020), which are widely used in flexible packaging and account for most of the global plastic production (Geyer et al., 2017). Compared to amorphous polymers, semi-crystalline polymers usually require larger amounts of conductive filler to achieve a similar EC due to their phase structure (Lim et al., 2010; Watt & Gerhardt, 2020), formed by amorphous and crystalline phases, that may limit the filler's participation in the conductive network (Kazemi et al., 2017; Tarani et al., 2016; J. Wang et al., 2020). The crystalline phase allows for two types of time-dependent heat treatments: more commonly done either above the melting point, designated as annealing or by controlling the cooling rate

(Strugova et al., 2021; J. Wang et al., 2020). Both treatments can improve EC, but by different mechanisms: annealing enhances EC by allowing the filler diffusion (Alig et al., 2008; Helal et al., 2019) in the polymer melt, creating richer filler regions referred to as secondary agglomeration (J. Wang et al., 2020). While, slower cooling rates during both non-isothermal and isothermal crystallization conditions (Wurm et al., 2014) promote an increase in the volume exclusion effect of the crystalline phase due to crystal growth. Consequently, the probability of filler-filler contact increases leading to higher EC. Despite its importance, the effect of time-dependent heat treatments on the synergism stability of hybrid systems containing CNT/G is still unclear.

In this context, the aim of this work was to evaluate the electrical and barrier properties of a hybrid composite based on CNT and industrial grade graphene (G) in a semi-crystalline matrix of high-density polyethylene. The reasoning behind these material choices was to combine the high EC provided by CNT with the proved barrier effect of G (Ferreira Junior et al., 2022) in addition to the possibility of promoting a synergistic effect on EC above the EPT. The influence of thermal history on EC by comparing pre- and post-heat treatment was also addressed. The synergism was investigated in the light of the evolution of the EC as function of time and temperature.

4.3 Experimental

4.3.1 Materials

High-density polyethylene-hexene copolymer pellets (HDPE, Formolene HB5502B, Formosa plastics, USA) was employed as the polymer matrix. HDPE presents a density of 0.955 g/cm^3 and a melt flow index of 0.35 g/10 min (190 °C/2.16 kg) according to the manufacturer's datasheet. Multi-walled carbon nanotubes (CNT, NC7000, Nanocyl, Belgium) with an average diameter of 9.5 nm and length of 1.5 μm (Nanocyl, 2016) were used as supplied. An industrial-

grade graphene (G, heXo-G V20 graphene nanoplatelets, a former commercial grade produced by Nanoxplore Inc., Canada). Both HDPE and G were kindly supplied by NanoXplore.

4.3.2 Methods

4.3.2.1 Filler preparation

To obtain hybrid composites a fractioning step was conducted by manually sieving the G powder (100 g) through a sieve with an opening of 25 μm. The collected material was then identified as G, showing an average length size of 24 μm, as opposed to the as received, with 58 μm. The sieved powder was characterized in terms of agglomerate size using a scanning electron microscopy, as detailed below.

4.3.2.2 Masterbatch preparation

Two masterbatches (MB) with a filler content of 13 wt.% were produced using a Haake Rheomix OS PTW16 twin-screw extruder with a length/diameter ratio of 40, screw speed of 100 RPM, and a temperature profile of 180 °C in the feeding zone, 200-240 °C in the metering and compression zones, and the die at 220 °C. The MBs were cooled with an air knife, pelletized, and reprocessed under the same conditions to improve the filler's homogenization. The produced MB were identified based on the fillers used: HDPE/CNT and HDPE/G. All the investigated concentrations were obtained by MB dilution and/or mixture.

4.3.2.3 Composites preparation and synergism investigation

A preliminary investigation was carried out to determine the electrical conductivity of HDPE/CNT composites as a function of CNT concentration ranging from 0 to 13 wt.% and the percolation threshold (p_c) of the composite, which was evaluated using Equation 4.1 (Strugova et al., 2021):

$$\sigma = k \cdot (p - p_C)^t, \text{ with } p > p_c \quad (4.1)$$

Where p is the filler mass fraction, t is the critical exponent, and k is the proportionality constant. The p_c can be estimated by a linear regression of a log(σ) vs. log(p – p_c) plot. A fixed value of 9 wt.% was chosen for further studies since it was above the p_c, allowing for a higher electrical conductivity and a more stable system, where further increases in conductivity would benefit shielding properties. Using this value as a starting point, composites with various CNT:G weight percentage ratios were examined to see if synergism could be achieved in HDPE/CNT/G hybrids. The ratios investigated were (0:100), (30:70), (50:50), (80:20), (90:10), and (99:1). Synergism was found for the 99:1 ratio composition and was used to investigate the effect of the second filler on the hybrid's synergism. All the previous composites were obtained with a co-rotating twin-screw extruder, MiniLab II Haake Rheomex CTW5, with a screw speed of 200 RPM, 240 °C and 6 min of mixing. The samples characterizations were performed in as extruded material, and hot-pressed films (100 µm thick, 240 ºC, 10 MPa for 10 min), cooled down to room temperature without controlling the cooling rate. Additionally, due to shape constraints imposed by permeability measurements, these samples were fabricated using the same extruder and under similar conditions as for MB production, except that the composites were extruded only once at a screw speed of 200 RPM, followed by hot pressing under the same conditions mentioned above.

4.3.2.4 Composite post-treatments and their effect on synergism

Two heat treatment protocols were proposed to evaluate the influence of the thermal history on the synergism stability of a semicrystalline-based composite. The post-treatments consisted of either annealing the hot-pressed samples in the molten state or heating them up in the solid state, where both treatments promote morphological changes by different mechanisms, namely diffusion and an increased volume exclusion effect, as we previously observed in polymeric blends based on a semicrystalline polymer and CNT (Strugova et al., 2021). In the molten state, samples were hot pressed at 240 ºC and 10 MPa for 120 min and cooled to room temperature.

For the solid-state treatment, samples were kept inside an oven in the crystallization region at 120 ºC (Figure AII.1) for 120 min without additional pressure.

4.3.2.5 Characterization techniques

The free powder G and composites were characterized by scanning electron microscopy (SEM) Hitachi S-3600-N with an accelerating voltage of 5kV. The filler size before and after MB production were characterized by optical microscopy (OM). An optical microscope (OM) model Olympus BX51 was used to characterize filler size before and after MB production. The images were obtained with an OptixCam Summit SK2-5.2X digital camera at a 100-times magnification, from at least three random areas. An automated approach was employed using the Image Processing Toolbox of MATLAB 2021b software to investigate the average agglomerate length size, D50, D90, and maximum particle size as detailed in the section 3.3.2.2.

The permeability performance against water and oxygen was evaluated in a MOCON AQUATRAN model 1 and a MOCON OX-TRAN 2/21 ST with exposed areas of 50 and 100 cm^2, respectively. Specific conditions can be found in the section 3.3.2.2. The reported permeability is the average of at least four measurements for each sample. The results were normalized by the sample thickness obtained from at least five measurements with a micrometer screw gauge.

The melting behaviour and samples' crystallinity were determined by DSC (PerkinElmer model Pyris 1) to evaluate the influence of the processing conditions and-post treatments. Amounts varying between 10 and 20 mg of material were taken from the samples as extruded, pressed, annealed, and solid-state. The samples were encapsulated in an aluminum pan and tested in the range of 50°C to 180 °C at a heating rate of 10 °C/min. The percentage of crystallinity was calculated according to Equation 4.2:

$$X_c = \left(\frac{\Delta H_f}{\Delta H_f^0 \cdot \phi}\right) \cdot 100 \quad (4.2)$$

Where ΔH_f is the experimental heat of fusion and ΔH^0_f is the enthalpy of fusion of a theoretical 100% crystalline HDPE, which was assumed to be 293 J/g (Ehrenstein et al., 2004), and ϕ is the weight fraction of HDPE in the composite.

Volume resistivity measurements (ρ) were conducted using two techniques depending on the sample's electrical conductivity. For less-conductive samples, the two-probe standard method was used, with a Keithley 6517B electrometer and a Keithley 8009 test fixture. Volumetric conductivity (σ) values in S/m were obtained according to Equation 4.3:

$$\sigma = \frac{1}{\rho} = \frac{1}{\left(\frac{A \cdot V}{i \cdot t}\right)} \quad (4.3)$$

A constant voltage V of 200 V was applied for 180 seconds, followed by 180 seconds of discharge. The current i was taken as the average value after 60 seconds. The effective area of the measuring electrode is represented by A. Thickness t was determined by averaging five values taken from random regions using a micrometer screw gauge.

More conductive samples were characterized with the four-probe method, using a Keithley 237 as a current source, and the voltage was monitored with an Agilent 3458A multimeter. The σ was obtained according to Equation 4.4 (Yilmaz, 2015):

$$\sigma = \frac{1}{\rho} = \frac{1}{\left(\frac{V \cdot F}{i}\right)} \quad (4.4)$$

F is the geometric factor (Yilmaz, 2015), and it is related to the sample's shape and dimensions. Circular samples and as extruded rectangular strands had their dimensions determined by averaging five values using a micrometer screw gauge.

The AC electrical conductivity evolution of pressed samples of HDPE/CNT, and hybrid composites was evaluated at room temperature and 120 ºC. The measurements were carried out in a broadband dielectric spectrometer (BDS) (Novocontrol Technologies) at 1 Hz and 3V for at least 2 hours with gold-covered samples. A rheo-electrical device using a rotational rheometer MCR 501 (Anton Paar) with a LCR meter ST2826/A (SOURCETRONIC) was employed to verify the EC ratio evolution under annealing conditions (240 ºC, 120 min). The rheo-electrical measurements were conducted under the following conditions: cone-plate geometry, an angular frequency of 0.05 rad/s, 20 Hz, 1V, and 240 ºC. The electrical conductivity was obtained based on the complex impedance of the samples (Strugova, David, & Demarquette, 2022). Both tests were performed on 1-mm thick samples with a diameter close to 25 mm. All measurements were performed at least in duplicate.

4.4 Results and discussions

4.4.1 Investigation of synergism in HDPE/CNT/G hybrid composites

Figure 4.1 shows the EC as a function of the CNT weight percentage in HDPE/CNT and HDPE/CNT/G hybrid composites. Hybrid composites contain 9 wt.% of filler at varied ratios of CNT:G. The calculated electrical percolation threshold (p_c) of HDPE/CNT composite is indicated by a vertical line. The DC electrical conductivity (EC) is frequently used to infer the effectiveness of dispersion of the CNT in the polymeric matrix since the filler connectivity will increase the composite EC.

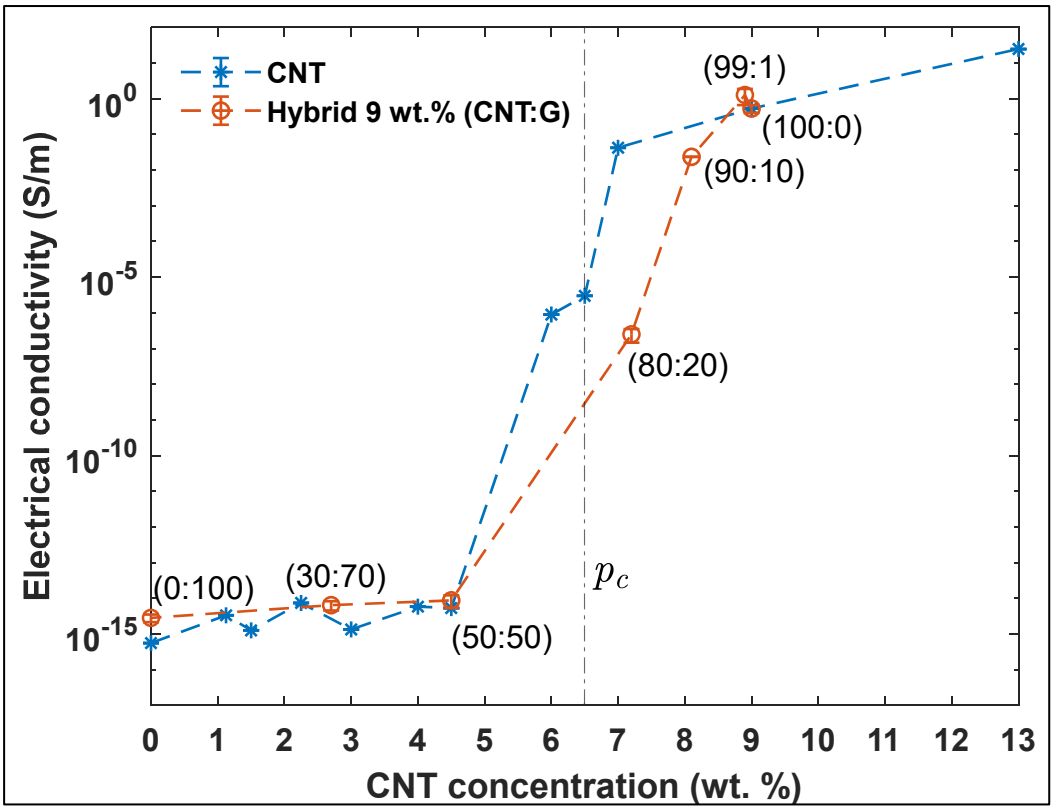

Figure 4.1 Electrical conductivity as function of CNT concentration for CNT and hybrid composites. The respective weight percentage ratio of CNT:G are given in parentheses

The calculated p_c value (R^2 = 0.99) of 6.49 wt.% (grey dash-dotted line) is within the reported range in the literature for polyethylene/CNT composites (T. McNally et al., 2005) and also in the ESD range (Verma et al., 2015). A higher p_c is expected by using a non-polar polymeric matrix and a high viscosity HDPE, since p_c can be up to three times higher compared to a lower viscosity HDPE (Ha, Kim, & Ha, 2010). Furthermore, for a semicrystalline polymer such as HDPE, it has been hypothesized that the polymer covers the conductive filler during heterogeneous nucleation, reducing both the filler availability and the composite EC (Kazemi et al., 2017; Tarani et al., 2016; J. Wang et al., 2020).

Synergism with G was investigated above the p_c at a fixed concentration of 9 wt.%, since at this concentration a more stable system was achieved, and as well, a further increase in EC

could benefit shielding. As shown in Fig. 1, a significant EC reduction happens with increasing G content and decreasing CNT content (0:100 CNT:G). Interestingly, a synergistic effect was observed for the 99:1 CNT%:G% ratio that is equivalent to 0.1 wt.% of G, which is lower than the ratio values reported in the literature (Kranauskaitė et al., 2018; Kuester et al., 2017). Owing to further interpretation, this ratio could be taken as the ideal ratio between CNT and G in this study under the processing conditions used, in which there is just enough G to promote better particle-particle contact. The 99:1 ratio was fixed and the effect of the secondary filler on the composite's synergism and permeability was investigated.

4.4.2 Effect of secondary filler on composites' permeability and electrical conductivity

The particle size has been shown to affect the EC of a composite (Y. Gao et al., 2017). Thus, the G morphology was analyzed. Figure 4.2 shows the morphology of the free graphene powder at different magnifications.

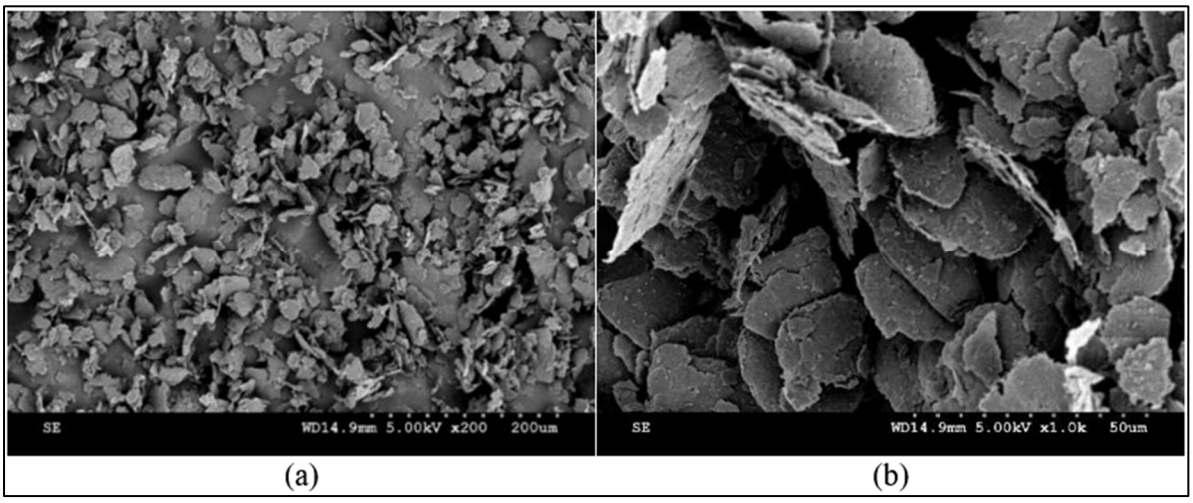

Figure 4.2 Powder morphology of graphene at (a) 200x and (b) 1000x times magnification by SEM

A characteristic platelet like shape can be observed in Figure 4.2. Table 4.1 gives the average filler length size, D50, D90, and maximum particle size (agglomerate) measured by image

processing of the free powder and the composite after MB dilution of HDPE/G to 0.1 wt.%, equivalent to the hybrid's composition in the 99:1 ratio.

Table 4.1 Summary of average filler length size, D50, D90 and maximum agglomerate size for the free powder and composite

Description	Average filler length size (μm)	D50 (μm)	D90 (μm)	Max. (μm)
Free powder	24.2±2.5	31.0	97.9	122.0
Composite	3.0±0.1	2.0	6.7	32.5

As shown in Table 4.1, after processing, a reduction ratio of 8 times was obtained for the average filler length, showing an effective reduction of the agglomerate size. Figure 4.3 shows the HDPE/CNT and hybrids' morphology with a 99:1 at 9 wt.%.

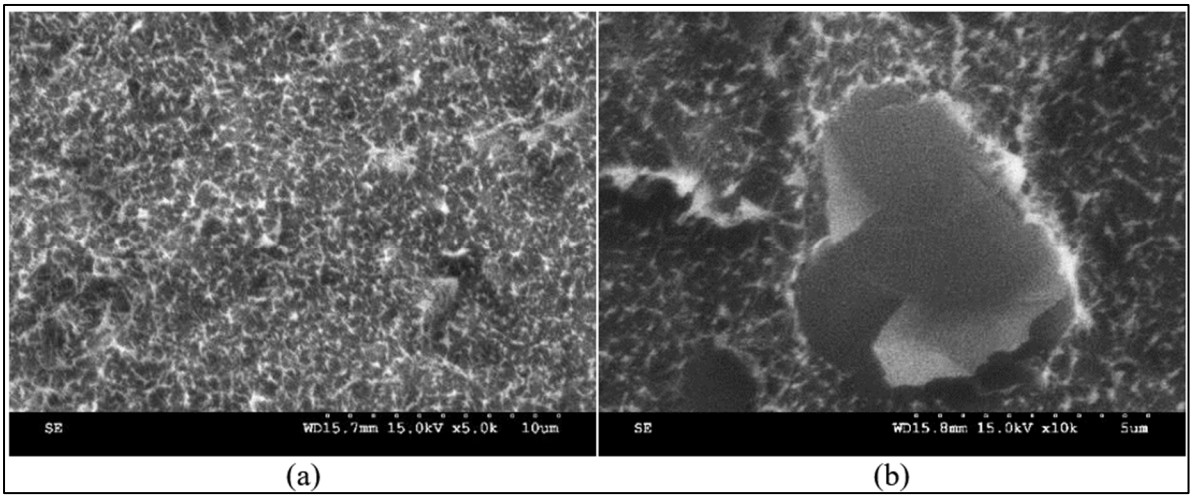

Figure 4.3 SEM imaging of composites morphology containing (a) only CNT and (b) hybrids, emphasizing the secondary filler

As shown in Figure 4.3 the hybrid composite shows a good interface between the matrix and G, with a particle size of around 7 μm. This value falls within the D90 distribution of the composite, as determined by OM. Despite the reduction in size, the particles' platelet shape is well-preserved.

As shown in the previous chapter, the addition of 0.1% G decreased permeation by around 38% demonstrating an increase in the barrier effect against water and oxygen, which is beneficial to flexible packaging. In order to verify the effect of using hybrid composites on the same barrier properties, Table 4.2 shows the water and oxygen permeability performance of hybrid composites containing 9 wt.% of CNT:G at a 99:1 ratio. Their results are compared to those of neat HDPE and CNT-only composites. Crystallinity percentage is included to complement the discussion, considering that the crystalline phase also contributes to the barrier properties.

Table 4.2 Summary of water and oxygen permeability and average crystallinity percentage for neat material and composites

Sample	Filler content (wt.%)	Filler ratio CNT:G	Water Permeability ($mg \cdot mm/m^2 \cdot day$)	Oxygen Permeability ($cm^3 \cdot mm/m^2 \cdot day$)	Average Crystallinity (%)
Neat HDPE	0	0	91±2	40±2	57±2
HPDE/CNT	9	100:0	135±3	60±4	62±1
Hybrid		99:1	135±1	56±1	63±1

Although the composites exhibited higher crystallinity compared to pure HDPE, an increased permeation was observed. This increase in permeation was expected for composites containing CNT at the investigated filler content (Méndez et al., 2017). The addition of G at the chosen ratio was insufficient to form an impenetrable phase and enhance barrier performance. Oxygen permeability and its standard deviation were marginally lowered compared to HDPE/CNT, suggesting that in higher concentration G could potentially improve the permeability properties. The EC of the CNT and hybrids composites are shown in Table 4.3 of the compressed molded samples and identified as pressed samples.

Table 4.3 EC of the CNT, hybrids as received and sieved composites

Group	Filler content (wt. %)	CNT:G ratio	As pressed EC (S/m)
CNT	9	100:0	$(5.3 \pm 1.3) \times 10^{-1}$
Hybrid		99:1	$(3.3 \pm 1.0) \times 10^{-1}$

As Table 4.3 shows, CNT composites had higher electrical conductivity than hybrid composites, despite the initial expectation of synergism with 0.1 wt.% G in a 99:1 ratio. A possible explanation is that the composite thermal history during shaping, particularly cooling, affects the EC change. However, this factor was not controlled for both the preliminary and the new pressed samples in Table 4.3. Based on those results and to better understand the relationship between the EC increase in CNT composites and synergism stability, two annealing protocols were conducted. Since the most important steps during sample shaping are the melt and solidification, two different strategies were chosen to thermally treat the samples: one in the solid-state at crystallization (120 ºC) and one at the processing temperature at the molten state (240 ºC), both for a fixed time of 120 min, and comparing the resulting EC to the materials as obtained after extrusion and pressing. Previous studies have shown that both approaches could affect the final EC of the composites (Strugova et al., 2021; J. Wang et al., 2020). The crystallization step was chosen to be done in the solid state at a fixed temperature within the crystallization region since the control of cooling rate was not possible to be accurately reproduced.

4.4.3 The effect of annealing in the molten state on composites' electrical conductivity

To account for the influence of thermal history on EC results, Figure 4.4 compares the EC of composites with different thermal histories, namely: as obtained by extrusion; as hot pressed; and after annealing hot pressed samples in the molten state and their melting behavior.

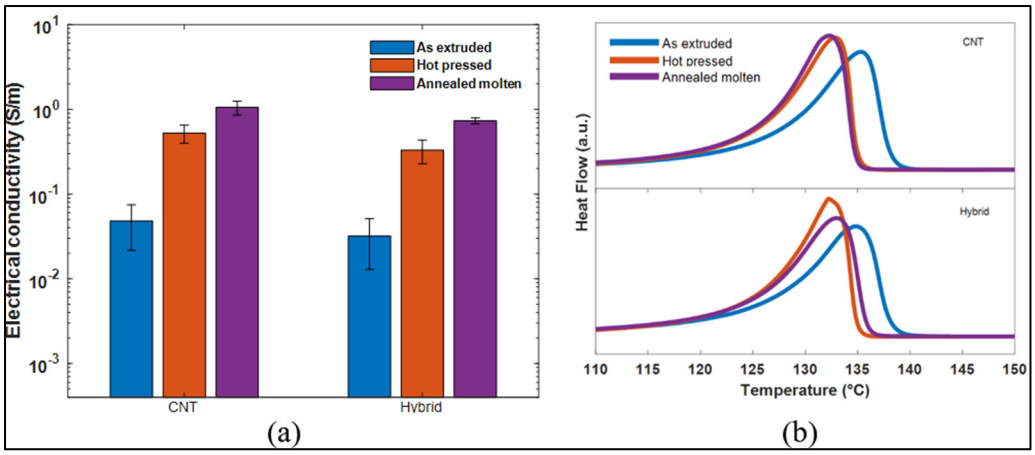

Figure 4.4 (a) EC comparison between as obtained by extrusion, hot pressed and heat-treated samples, and their (b) melting behavior

Both hot pressing and annealing increased the EC when compared to the extruded sample, as shown in Figure 4.4 a). Hot pressing increased the EC by one order of magnitude, while annealing in the molten state for longer times increased the EC of all samples but to a lesser extent, with the highest values found for CNT-based samples. This indicates that at high temperatures, diffusion is facilitated, improving the electrical conductivity of filler networks (Alig et al., 2008). Additionally, the heat treatment was unable to induce the synergistic effect in hybrid composites. Figure 4.4 b) depicts the DSC melting curves for the investigated conditions, namely extrusion, hot pressing, and annealing in the molten state. Both the hot pressing and annealing steps slightly decreased the melting point peak to lower temperatures, around 2 ºC less, with almost no change to the amount of crystallinity, varying between 61% and 63%. The small shift to increased values in the melting curves of the extruded samples is a result of the processing conditions. After exiting the die, these samples experienced a slower cooling rate in air than those subjected to faster cooling during cooling steps of pressed and molten state treatment samples.

To better understand the differences in the increase of EC due to annealing in the molten state as a function of time, the EC was monitored under the same time and temperature conditions as used during the treatment, i.e., 240 ºC and 2 hours, and were carried out by rheo-electrical

measurements. Samples had their resistance monitored during constant deformation in the linear viscoelastic region to track their changes in EC and viscoelastic properties. Figure 4.5 a) shows the evolution of EC as a function of time compared to its initial value of 240 ºC, and Figure 4.5 b) shows the complex storage modulus ratio. Figure 4.5 also illustrates the addition of G influenced the CNT network reorganization with annealing in the molten state and prevented the formation of a longer electric path within the conductive network.

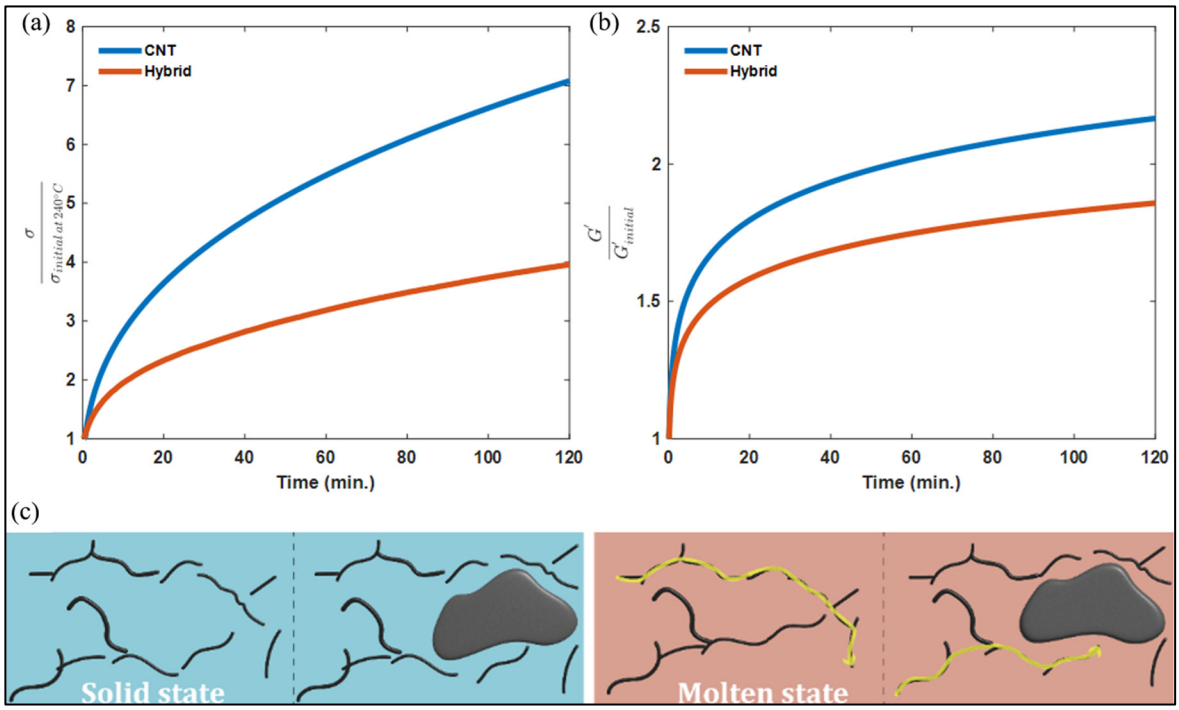

Figure 4.5 (a) EC evolution ratio relative to treatment temperature (240 ºC) and (b) complex storage modulus ratio as a function of time for each group of sample, (c) a comparison of the effect of the G (larger particle) addition on the CNT (tubes) network reorganization with annealing in the molten state, an electrical path, is highlighted in yellow

Under the set conditions, all samples showed an increase in EC as a function of time, with the CNT/HDPE composite displaying the greatest change and highest EC after treatment (Figure 4.3), where the highest change rate occurred in the first 20 minutes. The driving force behind the EC changes in the molten state is the reorganization of the filler due to increased HDPE

chain mobility (Y. Gao et al., 2017), leading to secondary agglomeration (Alig et al., 2012) of CNT. With the addition of 0.1 wt. % G the EC change rate is reduced by around 50%, likely due to the hampering of the secondary agglomeration process as indicated by the decrease of the storage modulus ratio in Figure 4.5 b) reducing the final EC. Moreover, the differences in EC after the heat treatment (Figure 4.3) could be explained by the influence of G. G particles reduced EC more significantly and caused a reduction in storage modulus, Fig. 4.5 b), affecting HPDE chain mobility (Y. Gao et al., 2017). Figure 4.5 c) illustrates how G hindered CNT network formation from the solid state (in blue) to the molten state (in red), with a new and shorter electrical path forming from network reorganization (highlighted in yellow).

4.4.4 The effect of annealing in the solid state on composites' electrical conductivity

Figure 4.6 shows the EC comparison of composites as obtained by extrusion, hot pressing, and after either annealing in the molten or solid state, as well as their melting behaviour.

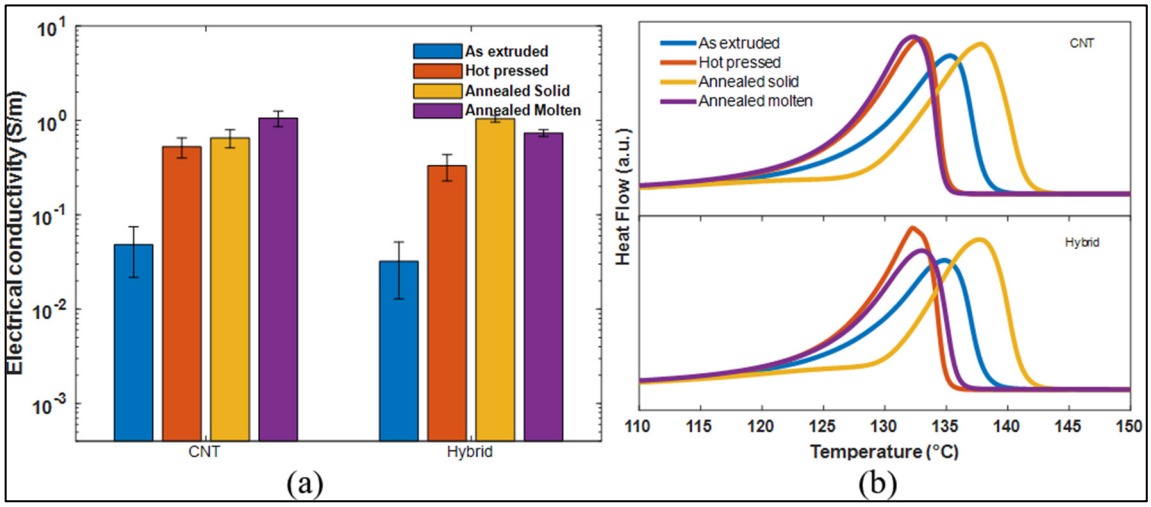

Figure 4.6 (a) EC comparison between as obtained by extrusion, hot pressed and heat-treated samples, and their (b) melting behavior

As shown in Figure 4.6 a), the heat treatment in the solid state resulted in a higher EC at a lower temperature (120 ºC) compared to annealing in the molten state (240 ºC). Furthermore,

the solid-state treatment resulted in a synergistic effect in hybrid samples compared to the CNT/HDPE composite. The heat treatment in the solid state induced more significant morphological changes to the polymeric matrix and shifted the melting peaks to higher temperatures compared to the other conditions for all groups (Fig. 4.6 b), which were followed by as extruded > hot pressed > annealed in the molten state. The observed differences in behaviour could be attributed primarily to the samples' thermal history, which was dominated by two effects: annealing in the solid state and cooling conditions. Solid-state annealing led the samples to reduce the amorphous phase and increase their crystalline regions towards a more thermodynamically stable condition (Hedesiu et al., 2007), with an increase in crystallinity to 67%, representing an increase between 6 and 10% compared to the other conditions. In turn, the cooling conditions were the main factor affecting the EC results for the extruded, pressed, and molten state treatments, as previously explained. To better understand the effects obtained, the changes in EC as function of time during solid-state were performed inside a temperature-controlled oven and monitored using a BDS. Figure 4.7 presents the relative change in EC over time relative to their initial EC at two different temperatures: 4.7 a) at the heat treatment temperature (120ºC) and 4.7 b) at the room temperature (RT), including the cooling step. The annealing effect in the solid state is illustrated in Figure 4.7 c).

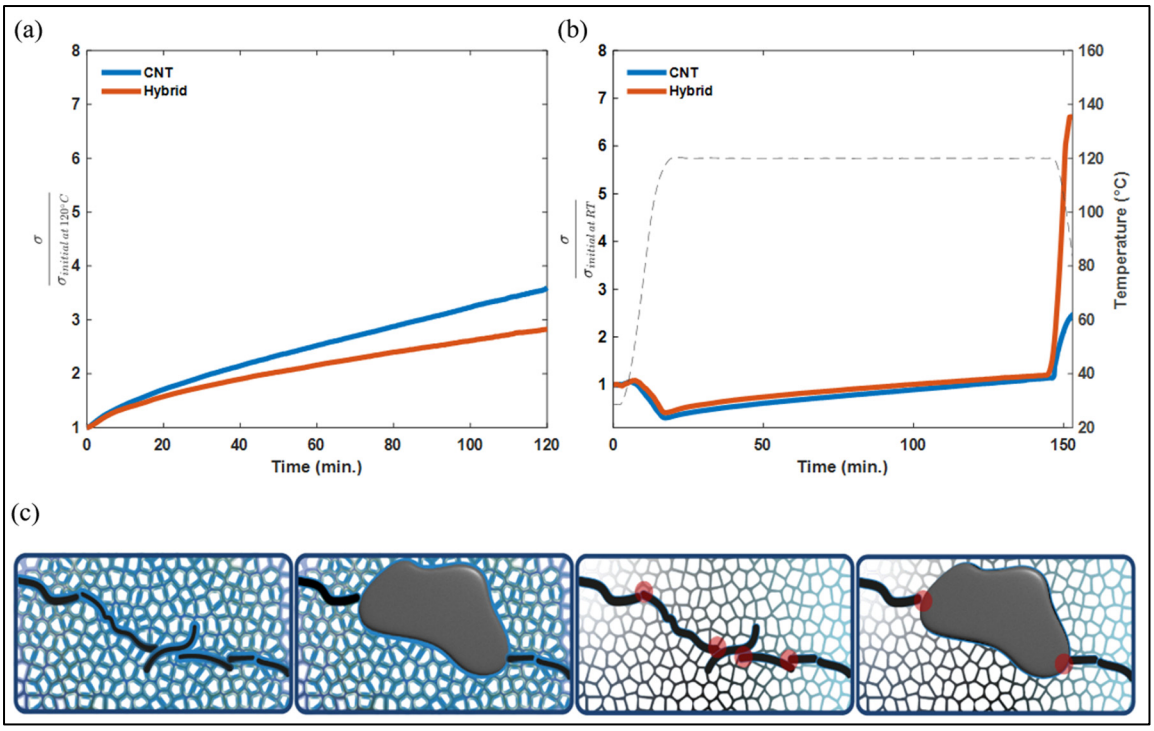

Figure 4.7 (a) Evolution of EC ratio as function of time relative to the EC at the initial temperature of 120 ºC (b) and the full test with the EC ratio evolution relative at room temperature. The grey dashed line shows the temperature change during the test, (c) a comparison of before and after annealing in the solid state shows the changes in crystallinity with the decrease of the amorphous phase (in blue) and the increase in filler availability, resistance points between filler are highlighted in red

Although the EC ratio in the solid-state treatment (Figure 4.7a) shows a similar profile to the molten state (Figure 4.5a), the underlying mechanism is different considering both treatment temperatures. In the solid state, the observed changes can be attributed to changes in the crystalline regions by reducing the amorphous areas, as corroborated by the increase in the degree of crystallinity. Meanwhile, in the molten state, chain mobility is higher and favours secondary agglomeration. As depicted in Figure 4.7 b), the EC remained constant (≈1) until approximately 80 ºC, followed by a drop with a maximum around the treatment temperature. This reduction could be explained by a thermal expansion of the matrix, increasing the interparticle distance, and reducing the EC. For the duration of the treatment, a low and constant increase in EC is observed, which is assigned to crystalline changes. A sharp increase in EC is observed for all samples after the onset of cooling step starts, with the most significant

increase for the sample containing G. Such behavior is different from that of the molten state treatment, in which EC changed more for CNT than for G. As Figure 4.6 shows, a synergistic effect was induced in hybrids by the solid-state treatment, with a clear increase in the EC ratio occurring at the cooling step (Figure 4.7b) and reduced tunnelling distance (Wurm et al., 2014). Those changes indicate a combination of two effects: volume exclusion and increased availability of G and CNT for participation on electrical conduction. During the heat treatment in the solid-state, with increased crystallinity, the available space for filler particles is reduced, increasing the volume exclusion effect and the likelihood of particle-to-particle interaction. Additionally, it has been suggested that both G and CNT could be covered by the insulating polymer phase (Kazemi et al., 2017; Tarani et al., 2016), but with temperatures within the melting regions, those particles could be more available to participate in the electrical conduction. Figure 4.7 illustrates those morphological changes after the annealing in the solid state, with the reduction of the insulating polymeric phase around the fillers and with G increasing the conductivity path by reducing the number of resistance points (in red) between particles.

4.5 Conclusions

Heat treatment in the solid state of hybrid composites based on a semicrystalline matrix induced a synergistic effect. The result suggests that the thermal history and, more importantly, the cooling conditions are fundamental in influencing the final electrical conductivity of the composite and possibly inducing synergistic effects on hybrid composites. We hope that a similar solid-state treatment of semicrystalline matrix composites could be implemented to improve the electrical conductivity of finished films or parts without losing their shape. The contribution of the second filler of the hybrid composite to the EC could be more significant if conducted in a sub-percolated system. Future work would possibly benefit from investigating hybrid composites based on an amorphous matrix and greater amounts of G to further improve the barrier properties.

CHAPTER 5

EXPLORING THE POTENTIAL OF CARBON-BASED HYBRID HDPE COMPOSITES FOR MULTILAYERED FLEXIBLE PACKAGING SOLUTIONS

5.1 Chapter overview

There is a growing need for more recyclable-friendly multilayered flexible packaging solutions. Previous research has proposed chemical recycling as a route for such complex, multilayered structures. However, the contribution of carbon-based hybrid thermoplastic composites towards simpler multilayered structures has received little attention. This study investigated the barrier, shielding, and microwave absorption performance of single polymer film composites of high-density polyethylene (HDPE), industrial-grade graphene (G), and multiwalled carbon nanotubes (CNT) with compositions up to 4.5 wt.%. Multilayered structures with 129 layers were obtained by the coextrusion technique with a multiplying element. Morphological investigation confirmed the successful creation of different alternating layer designs. Compared to single-layered films, the multilayered structures exhibited improved barrier and shielding properties due to selective filler placement and increased dielectric properties. The results of this study support the view that simpler multilayered structures could be developed towards more recyclable-friendly flexible packaging solutions.

5.2 Literature review

Multilayered flexible packaging is an essential part of the protection of electronic devices, offering safekeeping against handling abuse and environmental conditions such as high humidity or electromagnetic interference. However, the ever-growing number of electronic devices challenges the handling of such packaging material with low recyclability, creating an environmental problem due to its complex structure. To achieve the desired protective properties, mismatched materials must be combined, such as aluminum, different polymers, and adhesives, negatively impacting the reuse, and separation of materials and their recycling. Although recycling of multilayer structures is available using layer delamination or selective

layer dissolution to separate their core materials, these steps are time- and energy-intensive (Cervantes-Reyes et al., 2015; Horodytska et al., 2018; Kaiser et al., 2017). A more sustainable alternative is to design multilayered packaging for recyclability (C. T. de M. Soares et al., 2022). One approach to improve recyclability is the use of biodegradable engineering polymers, such as poly(lactic acid) and polycaprolactone, to oppose the negative environmental impact of slow-degrading petroleum-based polymers. Research has focused on enhancing their barrier properties and processability for use in flexible packaging (Abdallah, Mirzadeh, Tan, & Kamal, 2018; Mirzadeh, Ghasemi, Mahrous, & Kamal, 2015). But the biggest market share is still dominated by commodity polyolefins like polyethylene and polypropylene. To increase their recyclability, one strategy is to reduce the complexity of their multilayered structures. One approach to achieving simpler structures while maintaining functional properties for the protection of electronic devices involves two steps: materials selection and processing method.

Carbon-based thermoplastic composites are promising candidates as materials for flexible packaging to protect sensitive electronic devices. These materials offer a corrosion-free, lightweight, more recyclable, and industry-compatible approach. The main properties of interest for this type of packaging, barrier and shielding, can be controlled by using different carbon materials and particle shapes. Dispersing a layered filler such as graphene-based materials (GBM) in a polymer matrix has shown to increase the tortuous path of permeating species, allowing for control of their barrier effect (Tan & Thomas, 2016), thus reducing the permeability to different permeating species, nitrogen (Kim & Macosko, 2009), oxygen (Jin et al., 2013; Méndez et al., 2017), and water (Simon et al., 2017; Tseng et al., 2014) at low filler content, to cite a few. Shielding can be achieved by using conductive particles, with carbon nanotubes (CNT) being the preferred one (Sankaran et al., 2018). CNT-based composites with a wide range of electrical properties can be obtained in a variety of common polymeric matrices, including low- (Paszkiewicz et al., 2018) and high-density polyethylene (Al-Saleh, 2016a), polypropylene (J. Wang et al., 2020), polycarbonate (Socher et al., 2012), and polyamide (Logakis et al., 2009). When the composite reaches a critical concentration of filler,

known as the percolation threshold, a conductive network is formed, resulting in an exponential increase in its electrical conductivity compared to the insulating polymeric matrix. This control allows for the adjustment of conductivity for different applications, including ESD (Rousseaux et al., 2013) or shielding (Kuester et al., 2017). To achieve the necessary multilayered structures, different strategies have been used, such as stacking of coated films (Danlée et al., 2012) or melt-mixed films followed by compression molding (X. Gao et al., 2016). However, these techniques lack the necessary production efficiency to obtain multilayered structures compared with coextrusion.

By using the coextrusion technique with a multiplying element, a greater number of alternating layer arrangements from micro to nanolayers have been accomplished, improving mechanical (W. Gao et al., 2015), barrier (Boufarguine, Guinault, Miquelard-Garnier, & Sollogoub, 2013; Messin et al., 2017; Zhang et al., 2014), electrical conductivity (W. Gao et al., 2014), shielding (L. He et al., 2020), and microwave absorption (X. Gao et al., 2016) properties. The effect of the number of layers on barrier and shielding properties should be considered when trying to achieve improved properties for a potential flexible composite, as the composite properties may vary with the number of layers. Barrier properties did not show improvement with more than 129 layers (Boufarguine et al., 2013; Lei, Du, Li, Li, & Guo, 2013), and even with increased crystallinity (Boufarguine et al., 2013), which are a result of competing morphological and orientation effects (Zhang et al., 2014). In contrast, electrical conductivity has shown improvements with increasing number of layers up to 128 layers in one study (W. Gao et al., 2015) while in another study found that electrical conductivity decreased with an increasing number of layers (L. He et al., 2020). This decrease in electrical conductivity also reduced shielding effectiveness, with an optimum observed at 16 layers (L. He et al., 2020). It is important to consider those differences towards the obtention of single-polymer structures, which represent a significant step towards the development of more recyclable flexible packaging solutions. As to ensure the quality of the recycled polyethylene (PE) flexible film in mechanical recycling, a minimum of 90% PE by weight is needed (APR, 2022). However, it should be pointed out that only two of the few studies available in the literature conducted

investigations exclusively with one polymer and carbon-based material: either polyvinyl chloride/multi-walled CNT (X. Gao et al., 2016) or polypropylene/carbon black (W. Gao et al., 2015). Furthermore, these two studies did not examine the permeability performance of their composites, which may potentially be improved through the incorporation of a layered filler.

To date, no experimental work has been conducted with the most common flexible packaging material, HDPE, neither with hybrid structures designed to achieve both barrier and electromagnetic shielding properties in flexible packaging. The objectives of this study are two-fold: firstly, to compare the barrier and shielding properties of single-layer and multilayered films at equivalent filler content; and secondly, to examine the effect of layer design on these properties. To this end, single-layer and multilayered composites with 129 alternating layers based on HDPE and carbon-based fillers - multiwalled carbon nanotubes (CNT) and/or industrial-grade graphene (G) - were fabricated by compression molding with a maximum filler content of 4.5 wt.%. The primary properties evaluated were barrier and shielding properties, comparing the effect of different layer designs on the performance of the films. Additionally, the microwave absorption performance was also evaluated as a function of the structure type and thickness.

5.3 Experimental

5.3.1 Materials

Single and multilayered composite films were prepared using a hexene-copolymer high-density polyethylene (HDPE) (Formolene HB5502B, Formosa Plastics, USA) as the polymeric matrix. This HDPE has a density of 0.955 g/cm^3 and a melt flow index of 0.35 g/10 min (190 °C/2.16 kg). Two fillers were investigated within this study: multi-walled carbon nanotubes (CNTs) (NC7000, Nanocyl, Belgium) provided in the powder form with an average diameter of 9.5 nm and length of 1.5 μm (Nanocyl, 2016). And an industrial-grade graphene (G,

GrapheneBlack 3X, Nanoxplore Inc., Canada) provided as a masterbatch (MB) in the pellets form using the same HDPE matrix with a 40 wt.% of GrapheneBlack 3X (Nanoxplore Inc., Canada).

5.3.2 Methods

5.3.2.1 Masterbatch preparation

Masterbatch dilution was chosen to obtain the composites as it results in improved dispersion compared to direct incorporation (Pötschke et al., 2019). Accordingly, HDPE/CNT MB with a filler content of 13 wt.% was produced using a Haake Rheomix OS PTW16 twin-screw extruder. The extruder had a length/diameter ratio of 40, a screw speed of 100 RPM, and a temperature profile of 180 °C in the feeding zone, 200-240 °C in the metering and compression zones, and 220 °C at the die. The MB were cooled using an air knife, pelletized, and reprocessed under the same conditions to enhance filler homogenization.

5.3.2.2 Multilayered composites preparation

Given that single-screw extruders are employed in the stage of obtaining the multilayered structures, a previous dilution step was carried out. Dilutions were performed under the same conditions as the MB production, including the reprocessing stage for improved homogenization. The following concentrations were obtained: HDPE/CNT with 4.5 wt.%, and HDPE/G with 0.5, and 4.5 %. A preliminary step was conducted to assess the processing compatibility between the viscosities of the different concentrations by measuring the complex viscosity of various filler concentrations at a strain of 0.3%. The measurements indicated the ratio between viscosities did not exceed 2 at higher frequencies (Figure AIII.1). The multilayered composites were fabricated using an in-house coextrusion line with a multiplying element (University of Toronto), producing 129-layer composites with an ABA structure. Two single screw extruders with a screw speed of 20 RPM were used, with processing temperatures

ranging from 180°C to 220°C from the hopper to the die, increasing in 20°C intervals. A sheet die with an opening of 3 mm was used, and samples were calendered to achieve a tape shape and a thickness reduction of 3 to 5 times. Multilayered tapes and pellets were compression molded into flexible films of 100 μm thick under 140°C, at 10 MPa for 5 min. The compositions were chosen based on previously obtained results for electrical conductivity and permeability (Chapters 3 and 4). Table 5.1 shows the composition of each layer for the investigated multilayered compositions.

Table 5.1 Composition of each layer for the investigated multilayered compositions

Structure type	Same layer composition		Alternating layer composition				
Layer A (Filler wt.% and type)	HDPE	0.5 G	HDPE	HDPE	HDPE	1 G	HDPE
Layer B (Filler wt.% and type)	HDPE	0.5 G	1 G	9 G	9 C	8 G	9 C + 1 G
Composites total filler content (wt. %)	0	0.5	4.5				

In total, four distinct sample types were made, differentiated by their thickness and structure. The multilayered structure was composed of sheets, tapes, and flexible films, with average thicknesses of 3.4 mm, 0.7 mm, and 0.1 mm, respectively. The films were fabricated using a compression molding technique with mono- and multilayered structures.

5.3.2.3 Characterization

The morphology of the tape and flexible films was examined using an Olympus BX51 optical microscope (OM). Images were captured using an OptixCam Summit SK2-5.2X digital camera at a 100-times magnification. Samples were microtomed in the transversal direction of the processing direction to a thickness of approximately 10 μm. The morphology of the sheet samples was analysed in the same direction and were examined using a Nikon SMZ800N microscope with a Clemex Lt545RC-CLX camera. ImageJ software was used for size analysis.

The barrier properties against water and oxygen were evaluated using a MOCON AQUATRAN model 1 and a MOCON OX-TRAN 2/21 ST, with multilayered and monolayered films having exposed areas of 3.1 cm². Specific conditions can be found in the section 3.3.2.2. The reported permeability is the average of at least four measurements for each sample, with the results being normalized by the sample thickness obtained from at least four measurements using a micrometer screw gauge.

The crystallinity of the multilayered and monolayered films used in the permeability measurements was quantified using DSC (PerkinElmer model Pyris 1), to validate their performance. Samples, ranging from 6 to 16 mg, were extracted from the center of the films, and measured in duplicate. The samples were encapsulated in an aluminum pan and tested in the range from 50°C to 180 °C, with a heating rate of 10 °C/min. The percentage of crystallinity was calculated according to Equation 5.1:

$$X_c = \left(\frac{\Delta H_f}{\Delta H_f^0 \cdot \phi}\right) \cdot 100 \tag{5.1}$$

Where ΔH_f is the experimental heat of fusion and ΔH^0_f is the enthalpy of fusion of a theoretical 100% crystalline HDPE, which was assumed to be 293 J/g (Ehrenstein et al., 2004), and ϕ is the weight fraction of HDPE in the composite.

Volume resistivity measurements (ρ) were performed using two techniques, depending on the electrical conductivity of the sample. For less conductive samples, the two-probe standard method was employed, using a Keithley 6517B electrometer and a Keithley 8009 test fixture. Volumetric conductivity (σ) values in S/m were calculated according to Equation 5.2:

$$\sigma = \frac{1}{\rho} = \frac{1}{\left(\frac{A \cdot V}{i \cdot t}\right)} \tag{5.2}$$

A constant voltage V of 200 V was applied for 180 seconds, followed by 180 seconds of discharge. The current i was taken as the average value after 60 seconds. The effective area of the measuring electrode is represented by A. The thickness t was determined by averaging four values taken from random regions using a micrometer screw gauge.

More conductive samples were characterized with the four-probe method, with a Keithley 237 as the current source and the voltage being monitored with an Agilent 3458A multimeter. The σ was obtained according to Equation 5.3 (Yilmaz, 2015):

$$\sigma = \frac{1}{\rho} = \frac{1}{\left(\frac{V \cdot F}{i}\right)} \tag{5.3}$$

F is the geometric factor (Yilmaz, 2015) and it is related to the sample shape and dimensions. Circular samples had their dimensions determined by averaging four values using a micrometer screw gauge.

The electromagnetic properties of the samples, SE, and RL were measured using a vector network analyzer, Keysight model E5080B. The microwave frequency ranges of 8.2 – 12.4 GHz and 12.4 GHz–18 GHz, designed as X and Ku bands, respectively, were investigated using a rectangular waveguide at the Federal University of Rio de Janeiro. Those bands are used in radar and satellite communications (Sankaran et al., 2018) and are often evaluated within carbon-based materials for shielding purposes. The obtained electromagnetic parameters included scattering factors, complex relative permittivity, and permeability. Equation 5.4 was used to obtain the SE:

$$SE(dB) = 10 \cdot log_{10} \left| \frac{1}{|S_{21}|^2} \right| \tag{5.4}$$

The reflection loss (RL) measurements were conducted using a metal backing configuration, consisting of a metal plate fixed to the sample holder, which acted as a perfect reflector.

5.4 Results and discussions

5.4.1 Morphology of multilayered structures as function of thickness

The morphology of the different multilayered structures is depicted in Figure 5.1. Figures 5.1 a)-c) all have the same composition, consisting of HDPE/G with 4.5 wt.%. As illustrated in Figure 5.1 a) a continuous and parallel layered structure was achieved, characterized by continuous and relatively evenly distributed layers. This type of structure is important for achieving improved barrier properties. In the figure, the brighter layers are composed of HDPE, while the darker ones are made of HDPE/G with 4.5 wt.%. The HDPE layer had an average thickness of 37±16 µm, while the other layer had an average thickness of 25±12 µm, with an expected layer thickness of 30 µm based on the sample's total thickness. This difference could be attributed to variations in the flow of materials during extrusion. Similar structures were observed for other compositions. Figure 5.1 b) shows the structure of alternating layers is still maintained after the calendaring process. Nevertheless, the distinction between individual layers becomes more challenging as the thickness decreases by approximately 4.5 times from the sheet material to the tape form. Figure 5.1 c) shows the structure of the flexible film obtained by compression molding of the tape material shown in Figure 5.1 b). At this stage, the distinction between layers is even harder to make, but it is still possible to identify continuous darker layers in some regions, mainly in the bottom region. This indicates that the pressing conditions did not disrupt the layered structure.

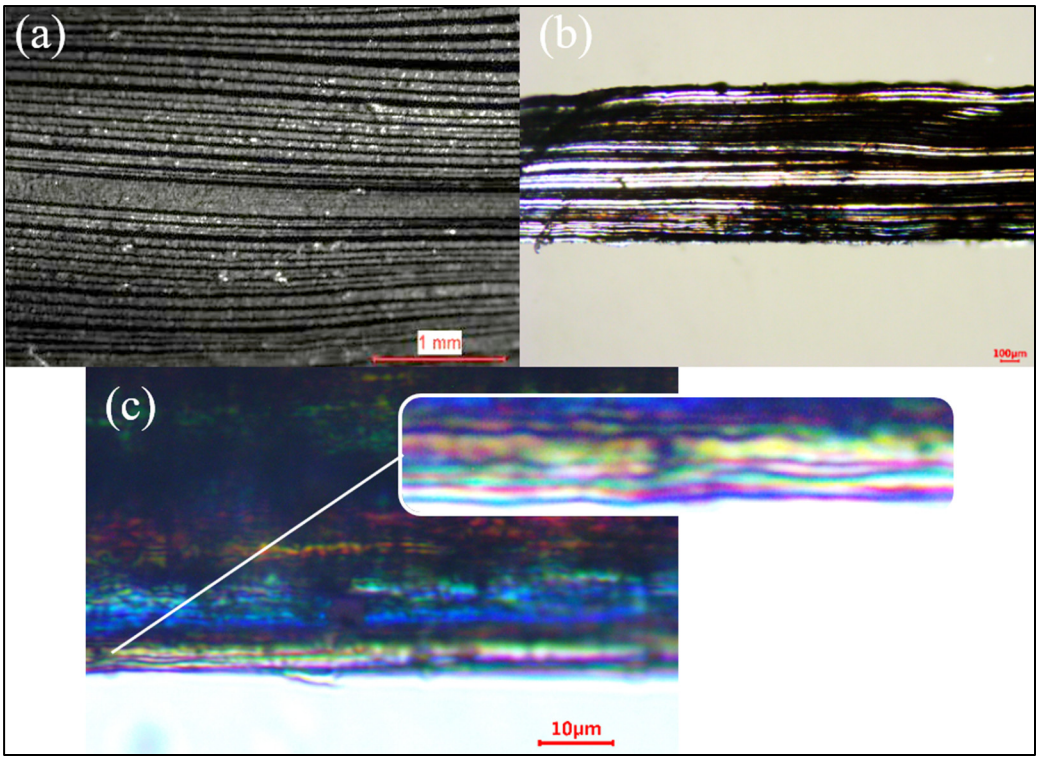

Figure 5.1 Multilayered composites of HDPE/G with 4.5 wt.% filler content with different thicknesses (a) sheet, (b) tape and (c) flexible film

5.4.2 Permeability and morphology – the importance of layer design

The processing technique can play a significant role in enhancing barrier performance by directing the distribution and arrangement of the impenetrable phase. Thus, an initial analysis examined the influence of the processing technique on the permeability properties by comparing multilayered samples to monolayered films, both obtained by compression molding. This was followed by an evaluation of the influence of layer design. The investigated morphology is represented in Figure 5.2 by multilayered tapes. In Figure 5.2 a) the tapes only contain layers with 0.5 wt.% G and shows a good distribution of the filler. In Figure 5.2 b) the tapes have an equivalent total content of filler, but with alternating layers of HDPE and 1 wt.% G, where a well-defined structure can be observed. In both composites, the filler exhibited a preferred parallel alignment with the surface, which is an important attribute to improve the barrier effect of the composite.

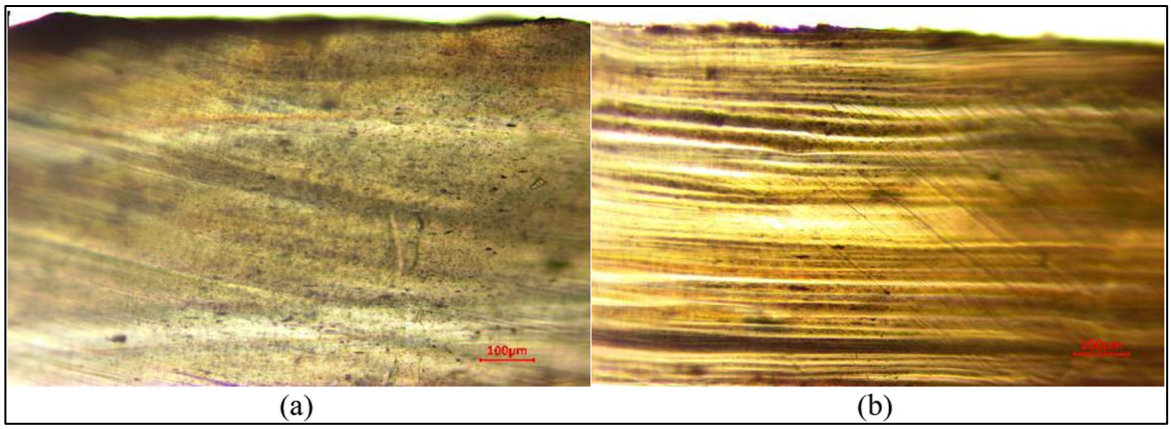

Figure 5.2 Multilayered tapes (a) with only layers composed of 0.5 wt.% G (b) alternating layers of HDPE and 1 wt.% G

The permeability and crystallinity results are presented in Table 5.2. The table shows the values obtained for each type of sample and its structures, allowing for a comparison of the influence of processing technique and layer design on these properties.

Table 5.2 Water and oxygen permeability and respective crystallinities for pure and composites containing 0.5 wt.% G

Group	Structure	Water Permeability ($mg \cdot mm/m^2 \cdot day$)	Oxygen Permeability ($cm^3 \cdot mm/m^2 \cdot day$)	Average Crystallinity (%)
Monolayer	HDPE	162±7	72±3	63±1
	Single layer with 0.5 G wt.%	174±24	71±12	63±0
Multilayered	Only HDPE layers	133±14	53±2	64±0
	Only 0.5 wt.% G layers	177±11	70±7	63±1
	Alternating layers of HDPE and 1 wt.% G	114±16	42±6	63±0

The influence of the coextrusion processing method can be observed with films only containing HDPE. By using the coextrusion technique to achieve a multilayered structure, a reduction of 18% in water permeability and 26% in oxygen permeability was achieved, with no significant change in crystallinity. This can be attributed to a change in the morphology of the HDPE spherulites to a longer disk shape, which increases the material tortuosity within the confined

HDPE layer (Zhang et al., 2014). These results suggest that the coextrusion method with a multiplying element may also improve the permeability properties of other semicrystalline polymers used in flexible packaging. When filler was added at 0.5 wt.%, either in the monolayer or in all the layers, an increase in permeability was observed. As was also the case in our previous study (chapter 3) in cast film extrusion and assigned to the formation of preferential pathways at the surface of the films. However, with proper layer design and the selection of specific layers to distribute the filler, a further reduction of 14% in water permeability and 20% in oxygen permeability was achieved with only 0.5 wt.%. These results are consistent with our previous study (section 3.3.3.3), which showed reductions of 10% and 18%, respectively, but with a lower crystallinity content of around 60%.

5.4.3 Multilayered samples morphology and permeability performance of flexible films

The influence on permeability properties depending on the filler type and with higher concentrations, similarly to chapter 4, particularly in the conductive range, were also examined. To achieve composites that can simultaneously fulfill barrier and shielding properties. For this purpose, the same total concentration of 4.5 wt.% of G and CNT were analyzed. To reduce electromagnetic reflection during shielding characterization, CNT was not present at the surfaces. For hybrid composites, G was either arranged in the layer A configuration, making it the surface layer, or combined with CNT in layer B to produce a hybrid layer, with layer A remaining pure HDPE. Figure 5.3 depicts both the structures described, respectively. The specific amounts of filler and configurations are detailed in Table 5.1. As demonstrated in Figure 5.3 a), Layer A contains G displaying a good distribution of the filler, an ellipsoid shape, and a parallel alignment with the surface, in contrast to the pure HDPE Layer A shown in Figure 5.3 b). Layers containing CNT (Layer B) are completely dark.

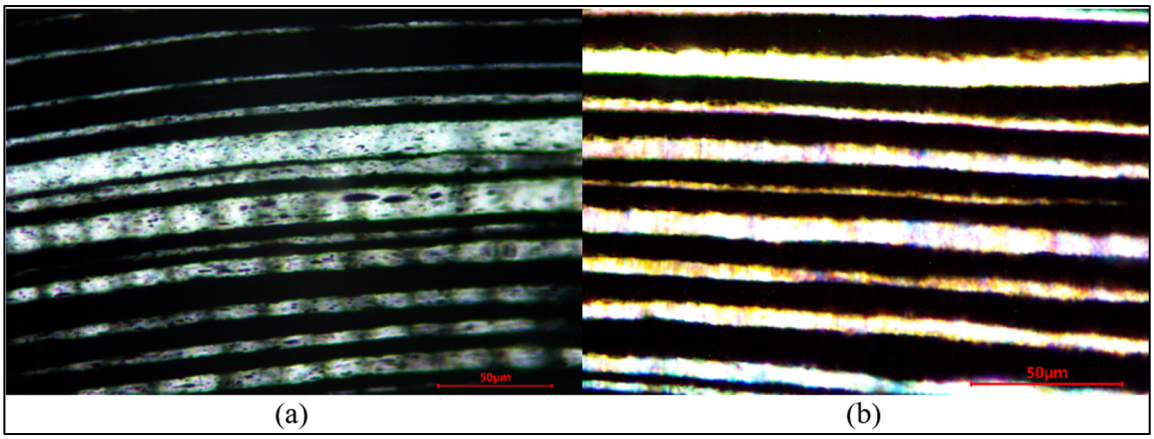

Figure 5.3 Multilayered tapes with (a) alternating layers of HDPE/0.5 wt.% G and HDPE/4 wt.% CNT, and (b) alternating layers of HDPE/CNT/G with a 4.5% wt.% loading

The effect of filler type and its location on the permeability properties of HDPE composites was also investigated. G and CNT fillers were added to the HDPE samples, either in the monolayers or multilayers structures, and their impact on water and oxygen permeability was measured. The results are summarized in Figure 5.4, which shows the permeability of all samples and for each filler type and different designs tested.

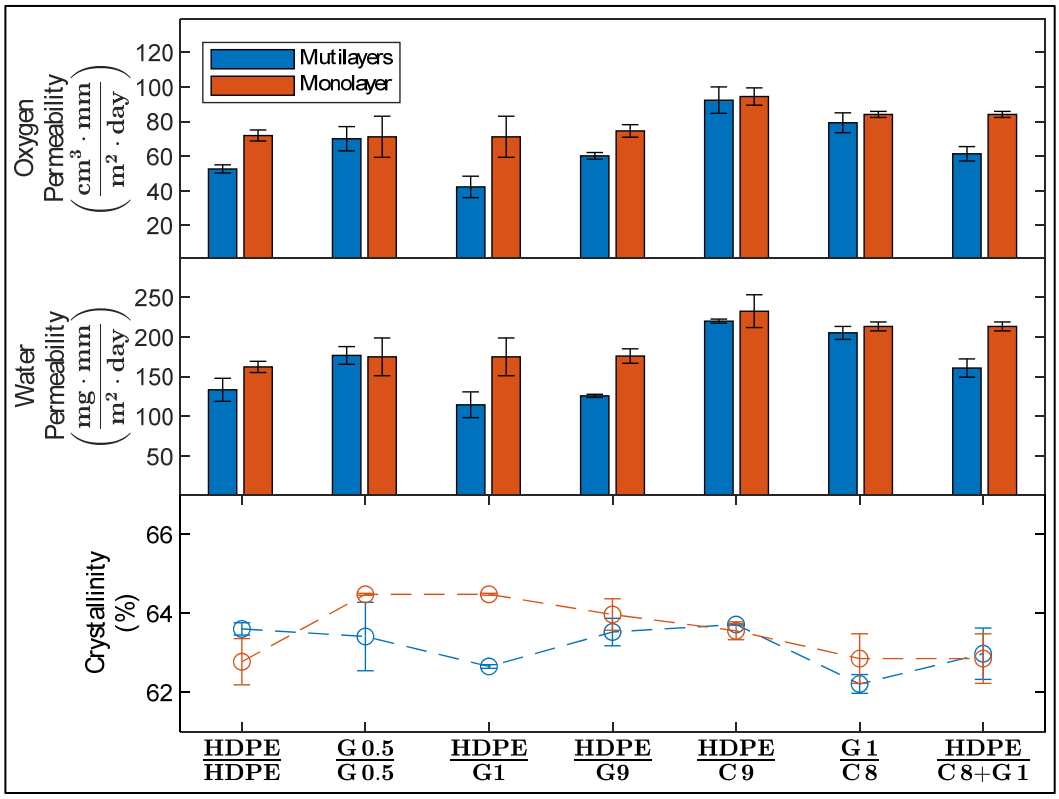

Figure 5.4 Water and oxygen permeability and respective crystallinities for the investigated structures. Each structure type is shown in the bottom of the figure, where Layer A is represented on top and Layer B on the bottom. The same compositions were used for the monolayered films. The average crystallinities are provided for each composition, the dashed lines are just a guide to the eye

Considering only the processing technique, an overall improvement was obtained by using coextrusion processing, even though monolayered samples exhibited an increased amount of crystallinity for certain compositions. When evaluating the effect of filler type, while CNT increased permeation between 30 to 75%, similarly to chapter 4, G at the same concentration of (4.5 wt.%) showed an 6% improvement in the barrier effect for water, but a 14% decrease in the barrier effect for oxygen compared to the pure material. Effective dispersion becomes more challenging at higher concentration. The differences in permeability can be attributed to the morphology of the filler, as the platelet-like morphology of graphene results in a more tortuous path than CNT. Considering hybrid composites, by partially replacing CNT with an equivalent amount of 0.5 wt.% G in layer A, did not result in any barrier improvement

compared to the pure HDPE. But a reduction in the negative impact of CNT was observed, with reductions as high as 30% for multilayered. The use of hybrid layers led to a further decrease in the negative impacts of CNT, yielding better performance than the multilayer structure containing 0.5 wt.% G in all layers, even with a nine times higher concentration of filler. This achievement is noteworthy, as it is generally necessary to use larger quantities of conductive filler to achieve desirable shielding properties.

5.4.4 Electrical conductivity of flexible films

For shielding applications, an electrical conductivity greater than 10^{-2} S/m is recommended (Sankaran et al., 2018; Sudha et al., 2010). Based on this, the electrical conductivity of the flexible films was investigated. But, due to constraints in layer arrangement and the small thickness of multilayered flexible films, the DC conductivity of the monolayered films was assessed as a suitable approximation of the layer electrical conductivity (EC) properties of the composite. The EC of the CNT and hybrids composites are shown in Table 5.3.

Table 5.3 EC of flexible films containing CNT, G, and hybrid composites

Material	Total filler content (wt. %)	CNT:G ratio	As pressed EC (S/m)
HDPE	0	-	$(7.0 \pm 0.8) \times 10^{-16}$
G	1	0:100	$(7.8 \pm 2.6) \times 10^{-16}$
CNT	9	100:0	$(1.2 \pm 0.3) \times 10^{-1}$
G		0:100	$(5.1 \pm 1.0) \times 10^{-15}$
CNT/G		90:10	$(1.1 \pm 0.6) \times 10^{-1}$

As Table 5.3 shows for composites containing CNT the recommended electrical conductivity for shielding was achieved, and no synergistic effect was observed for the hybrid composite containing CNT/G. So, it is expected that individual layers are conductive enough for shielding. At the investigated loading of G, no significant improvement on the electrical conductivity was observed.

5.4.5 Electromagnetic shielding

For the protection of sensitive electronic devices, the packaging material may need to possess shielding properties, with a minimum shielding effectiveness of 10 dB in the GHz frequency range, resulting in an attenuation of approximately 90% of the incident field. To evaluate the performance of flexible films as a shielding packaging material an initial comparison of the shielding performance of monolayered and multilayered films was conducted. Figure 5.5 a) presents the shielding efficiency (SE) normalized by the sample thickness for both groups, a vertical break line was used to separate the different bands (X and Ku) and in Figure 5.5 b) an average of the SE for the investigated frequency range is presented for multilayered and monolayered samples.

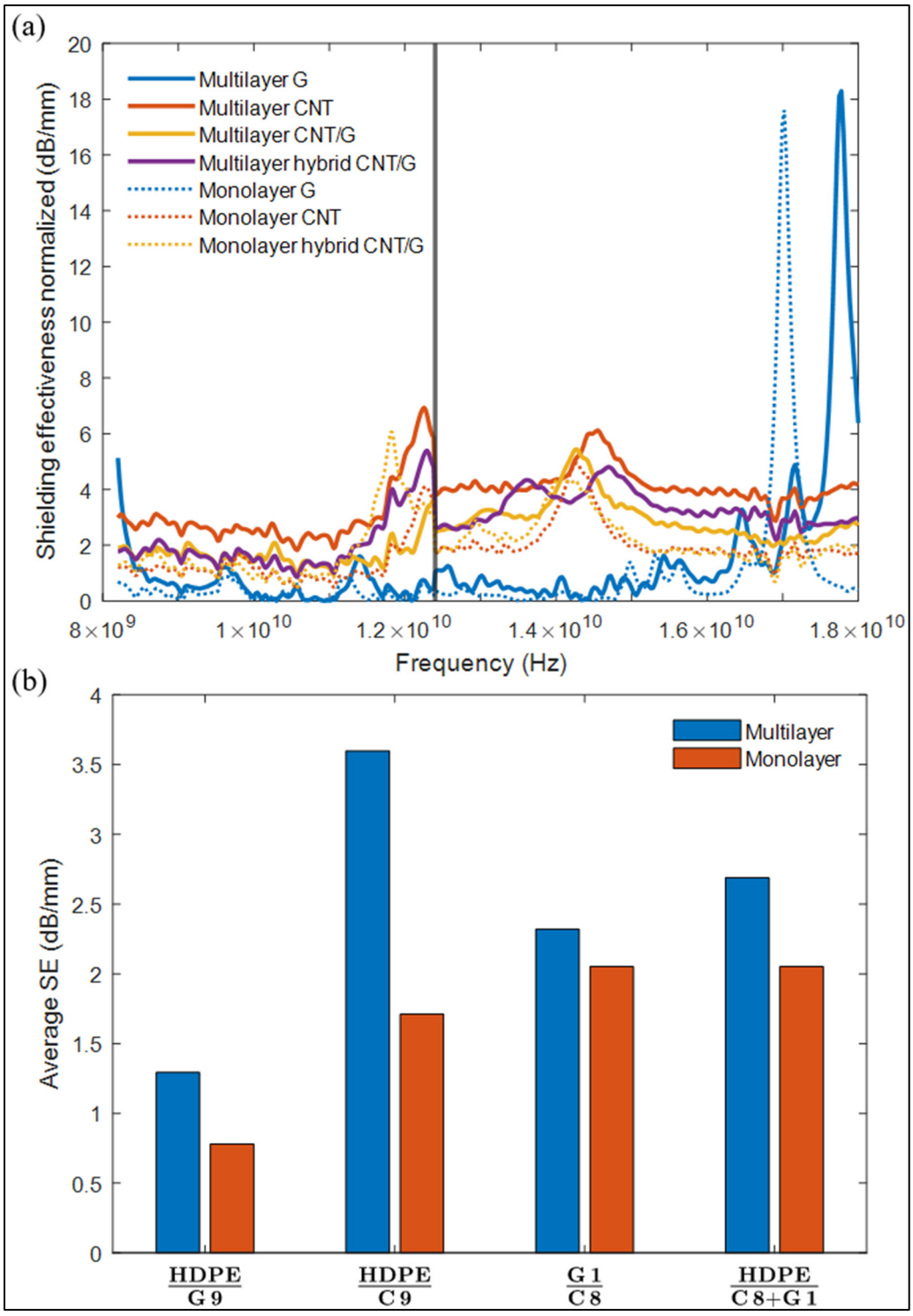

Figure 5.5 Multilayered and monolayered flexible films a) shielding effectiveness normalized and b) average shielding effectiveness normalized

Multilayered structures resulted in improved SE for all the investigated structures compared to monolayered samples with the same amount of filler. CNT composites exhibited the highest performance, followed by hybrid and alternating G/CNT structures and G-only samples. Figure 5.5 b) illustrates the overall positive effect of multilayered structures on shielding property, with an increase ranging from 13% to 110% depending on the structure type. The highest value was achieved with HDPE/CNT composites. These differences can be attributed to the increased electrical conductivity of CNT- containing composites and their dielectric properties, as later discussed. However, as permeability results showed, HDPE/CNT had the highest permeation rate compared to the others, which was effectively improved using a hybrid composite that also exhibited the second largest SE result. Interestingly, compared to the frequency response, higher peaks were observed for samples containing G only. This has been reported as frequency-selective shielding (Song et al., 2017) and recently attributed to the graphene particle size and the composite microstructure, where the particle-particle distance could create preferential attenuation (B. Lee et al., 2023). It should be noted that the effect was only investigated in 2-mm-thick composites and hasn't been reported so far for flexible films. Also, the type of structure influenced the peak location of these samples, with a shift towards higher frequencies for multilayered films, indicating that the technique type and layer arrangement could allow for frequency-selection. But additional investigation is required to optimize this property.

To further investigate the observed responses for the multilayered and monolayered films, their dielectric properties were investigated, as there is a dependence between SE performance and dielectric properties. Figure 5.6 presents the dielectric properties of the composite films, including the real part of permittivity (ε') and the imaginary part permittivity (ε'') and loss tangent (tan δ) of a) multilayered and b) monolayered films.

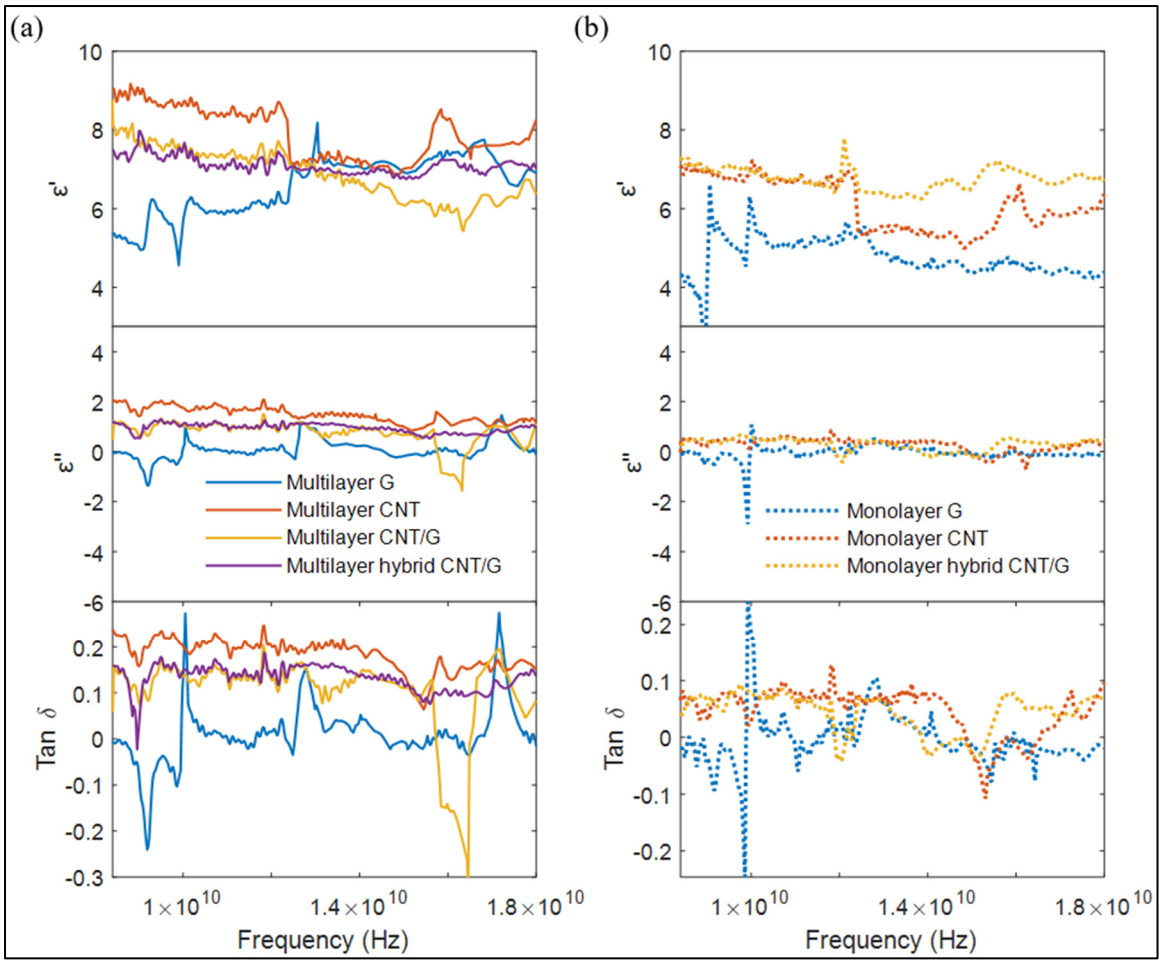

Figure 5.6 Real part of permittivity, imaginary part of permittivity, and loss tangent properties of (a) multilayered and (b) monolayered flexible films

Multilayered composites shown increased ε' and ε'' compared to monolayered films. The selective distribution of layers achieved with the coextrusion process has been shown to increase the storage permittivity of PP/carbon black composites linked to the charges accumulated at the interfaces (W. Gao et al., 2015). And the increase in the ε'' may also indicate improved electrical conductivity and increased SE of HDPE/CNT films. Both providing higher SE performance in multilayered films. The higher peaks mainly observed with can be assigned to the uncertainty of the VNA measurements at certain frequencies depending on the sample thickness (Vicente, Dip, & Junqueira, 2011).

5.4.6 Effect of thickness of the shielding performance

The shielding performance of the multilayered structures as function of the thickness was also investigated. Figure 5.7 presents the shielding performance expressed as shielding effectiveness for the different produced structures.

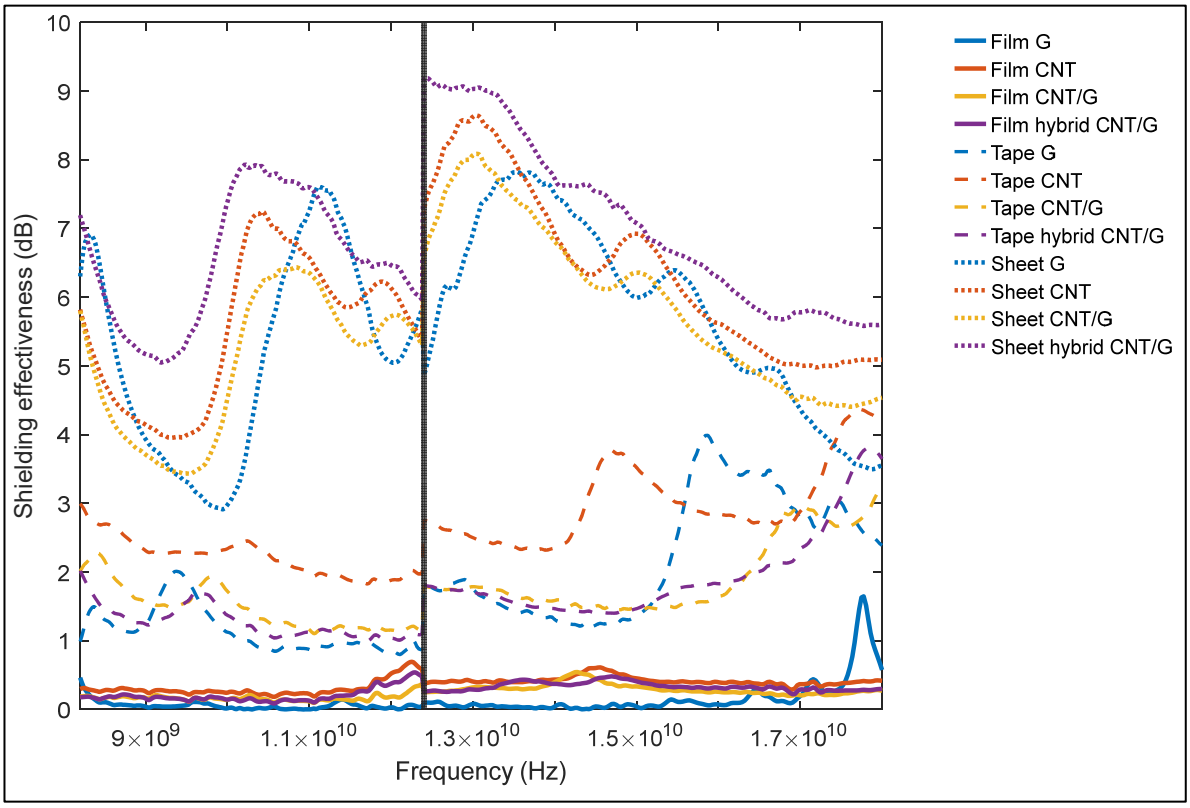

Figure 5.7 Shielding effectiveness of flexible films, tapes, and sheet samples

A clear correlation between shielding effectiveness and sample thickness can be seen in the Figure 5.7. From the highest to the lowest performance was obtained with sheet, tapes, and films samples. Regrettably, the flexible films are below the recommended SE to protect sensitive electronic devices as packing material, of at least 10 dB, even the maximum shielding of the sheet hybrid CNT/G sample was below that recommended value. Interestingly, even after normalizing the shielding performance of sheet materials a different trend was noticed, a synergistic effect for hybrid composite. This could be related to the fact that with a reduction

of the thickness an increase in electrical conductivity can be obtained, but for sheet materials G could be acting in synergism with CNT and providing improved properties. Indeed, a reduction in both storage and loss modulus was observed for the HDPE/CNT sheet samples compared to the hybrid material. And once again, with G it was observed a shielding selectiveness at certain frequencies.

To better understand the effect of sample thickness and the effect in shielding for a thin sample the Equation 5.5 can be used:

$$SE(dB) = -20log_{10}\left[1 + \frac{Z_0 t \sigma_T}{2}\right] \quad (5.5)$$

Where, Z_0 is the free space impedance and is equal to 377 Ω, t is the material thickness and is σ_T the total electrical conductivity of the composite (Saini & Aror, 2012). Figure 5.7 shows the experimental SE obtained for each of the different samples as a function of its thickness and the theoretical SE based on the previous equation, compared to the mono and multilayered experimental shielding performance.

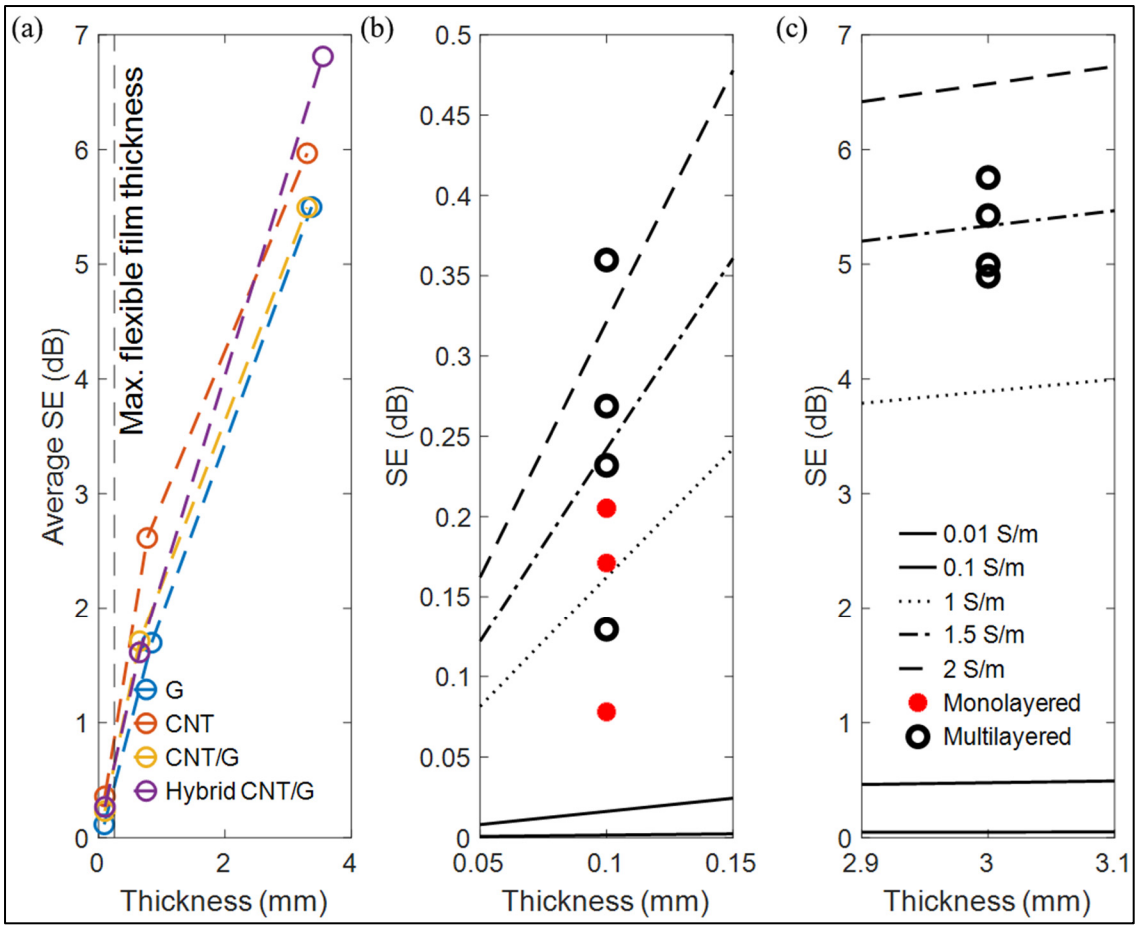

Figure 5.8 (a) Experimental average SE as function of thickness, and compared to theoretical shielding effectiveness of (b) flexible films (c) sheet samples for specific electrical conductivities

Here, the effect of thickness on shielding is more apparent; with increasing thickness, a higher average SE was obtained. Figures 5.7 b) and c) show the expected SE based on the total conductivity. Monolayered samples were less conductive than the multilayered ones, as indicated by the lower ε'' values as a function of frequency. However, total conductivity is given by $2\pi f\varepsilon_0\varepsilon''$ (Saini & Aror, 2012), and considering the experimental data, a lower SE would be expected considering only Equation 5.5. This difference could be associated with the fact that the main shielding mechanism in the previous equation is reflection. Even though thin samples were used, usually shielding in carbon-based materials has also a contribution of absorption mechanism rather only reflection. Therefore, Equations 1.12 and 1.13 were used to

determine the shielding mechanisms of the composites. Figure 5.9 presents the main shielding mechanisms for the a) multilayered flexible films and the b) sheet samples.

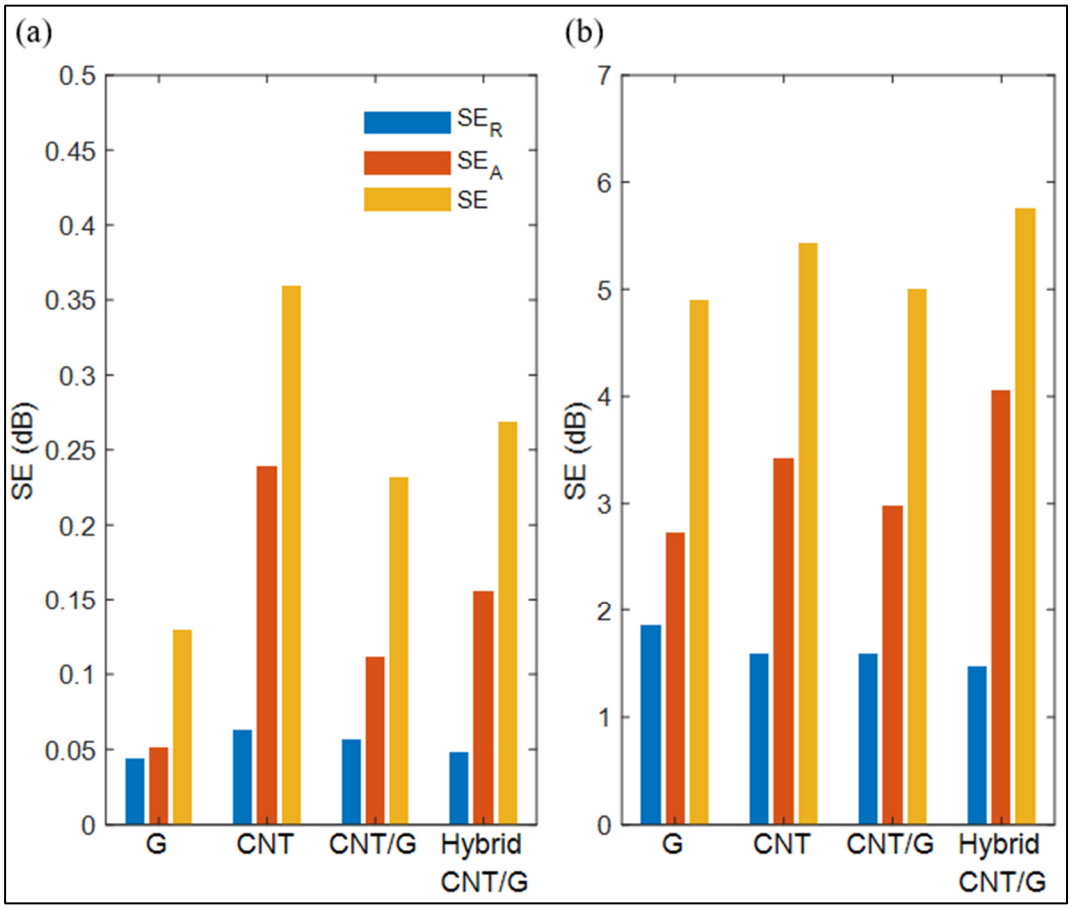

Figure 5.9 Shielding by reflection and absorption and shielding effectiveness for multilayered (a) flexible films and (b) sheet samples

The main contributing mechanism for shielding in all the investigated composites is the absorption mechanism, even for flexible films. A similar result for PP/CNT has also been reported for thinner films and thicker samples, where shielding by reflection was the secondary mechanism (Al-Saleh & Sundararaj, 2009). In general, the proportion of shielding by each mechanism remained practically the same for each composition and thickness.

Based on these results, a flexible film of 100 μm thick with an average SE of 0.35 dB would have a shielding efficiency of only around 8% of the incident field. To achieve a SE of 10 dB with a flexible film, considering Equation 5.5, a total electrical conductivity of around 115 S/m should be attained. However, this conductivity is higher than that obtained with the produced HDPE/CNT masterbatch. Such greater conductivity is more frequently found in segregated structures (Jia et al., 2018).

5.4.7 Reflection loss of multilayered structures

Multilayered structures have been investigated as a way to improve microwave absorption of carbon-based materials in the GHz range, reducing electromagnetic pollution. Its performance is expressed in terms of reflection loss (RL), with a minimum RL value indicating increased absorption. The absorption ability of multilayered structures was evaluated as a function of thickness. Figure 5.10 presents the RL for the multilayered structures, grouped either by a) thickness or b) group type.

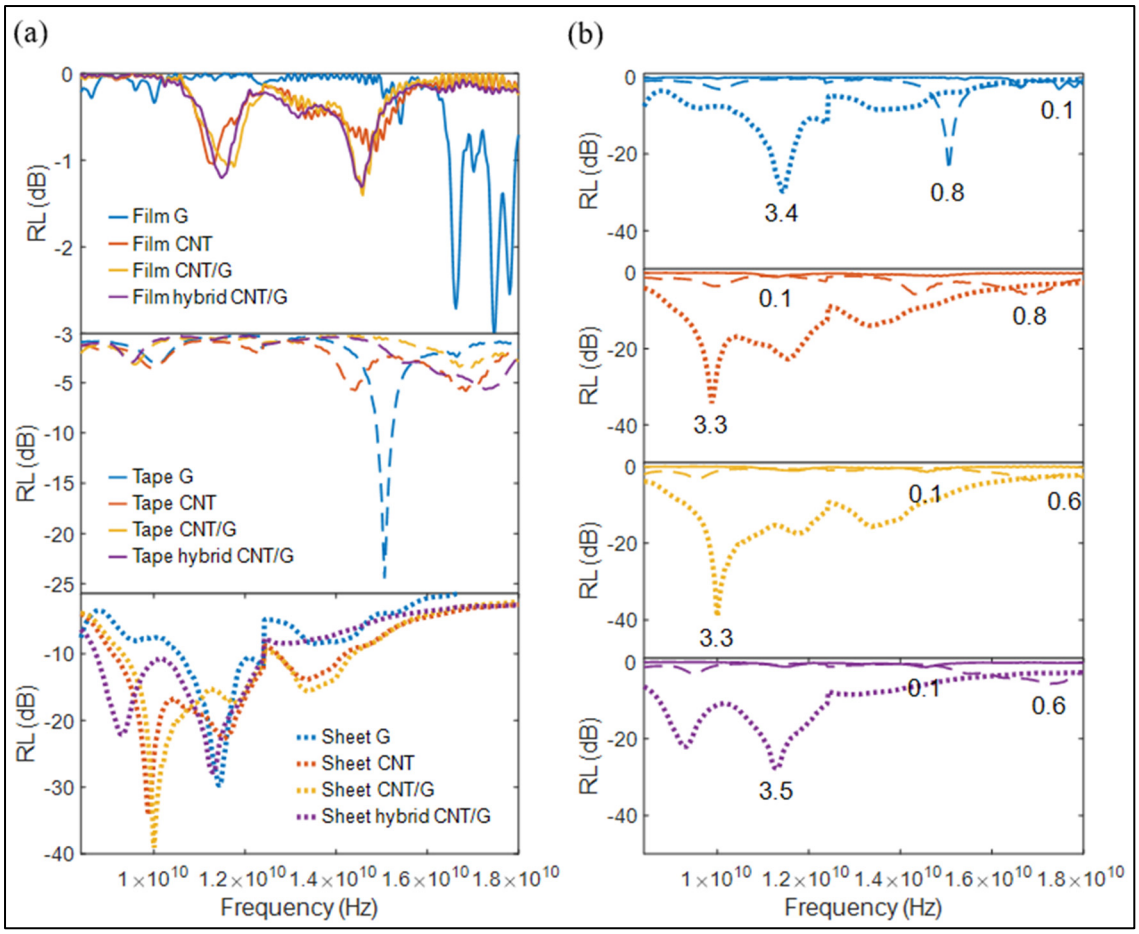

Figure 5.10 RL for grouped by similar (a) thickness, namely, films, tape or sheet and (b) group type based on composition with the minimum peak of RL highlighted with the material thickness in mm

For flexible films, G samples showed the lowest values of RL, with 3 peaks of around 3 dB, almost 3 times the values obtained with the other composites, allowing for a reduction of 50%. Also, the addition of G resulted in a higher peak for CNT-containing samples. This demonstrates that RL is not as dependent on electrical conductivity for shielding; instead, there is a dependency on dielectric and magnetic losses. As thickness increases, so does RL. Tape G achieved the highest reduction once again, but towards lower frequencies, at approximately -25 dB, or a 99.7% reduction. This is higher than the minimum of -6 dB achieved with CNT with a 0.8 mm thick sample. To the best of our knowledge, such a high value has not been reported in the literature under similar conditions. For thicker samples, a broader RL is

obtained for all samples, with an increase in the number of peaks. For G, the RL peak shifted towards lower frequencies. Adding G to CNT samples had different effects depending on the sample design. For the hybrid composite with alternating layers of G and CNT, the peak changed from -34 dB to -39 dB, achieving a reduction from 99.96% to 99.99%. With G 0.5 wt. % combined with CNT, the sample behaviour resembled more the G-only sample, and the CNT peak shifted towards lower frequencies. Using G at the surface may have led to increased match impedances (X. Gao et al., 2016).

5.5 Conclusions

The main goal of the current study was to explore a simpler multilayered flexible packaging composite with both barrier and shielding properties based on HDPE and CNT/G fillers. This study appears to be one of the first attempts to examine those combined properties in flexible films. Overall, the results showed that with coextrusion, layer design, and selective filler distribution, improved permeability and shielding properties could be obtained compared to single-layered films. For instance, the alternating layers of HDPE and CNT/G achieved improved barrier properties superior to single-layer HDPE films with the addition of conductive and shielding properties. These findings could be used to develop flexible packaging for commercial applications with improved recyclability by adjusting the filler type, its content, and distribution. This work also highlights the potential usefulness of packaging with microwave absorption ability. Future research could be undertaken to explore the effects of the number of layers on the permeability and shielding properties.

CHAPTER 6

SUMMARY OF THE MAIN RESULTS

The main aim of this thesis was to investigate the potential use of polymeric composites with carbon-based materials for flexible packaging to protect sensitive electronic devices with barrier and shielding properties. To that end, high-density polyethylene (HDPE), one of the most common packaging materials, was chosen as the polymeric matrix with which a layered filler, industrial-grade graphene (G), was combined to improve the barrier properties at low filler contents. Electrical properties were improved by combining multiwalled carbon nanotubes (CNT) with HDPE, and hybrid composites of CNT and G were also investigated for improved electrical conductivity and consequently higher shielding properties. By combining those materials, we aimed to develop a simpler, multilayered structure for a more recycle-friendly solution in flexible packaging. This study was conducted in three parts, with mixed methodological approaches to investigate in a separate manner barrier properties, increased electrical conductivity and combining both of those properties in multilayered structures. Each of the previous topics are detailed below, where each title states the main fabrication technique used and the main investigated properties.

6.1 Chapter 3 – Cast film coextrusion and barrier properties

The first study focused on the investigation of barrier properties using an industrially compatible technique, cast film coextrusion, to obtain flexible films. The effect of G on the barrier properties varied depending on its concentration in the HDPE composites and the surface finishing. At concentrations lower than 0.5 wt.%, G improved the barrier effect to oxygen and water. However, creating a smoother surface through the industrial nipping process increased light transmission by reducing film surface roughness but also induced some defects with G at the surface, affecting permeability. Nonetheless, with layer design, the detrimental effect of surface finishing was avoided. At the maximum concentration of 1 wt.% G, the barrier

effect remained practically unchanged and was not enough to cause a significant difference in terms of the electrical conductivity. Morphological analysis using TEM and optical microscopy allowed for comparison with theoretical models for permeability and mechanical properties. Leading to the conclusion that a reduction in the filler aspect ratio resulted in decreased barrier efficiency and low mechanical reinforcement effects due to reduced dispersion efficiency.

6.2 Chapter 4 – Extrusion and compression molding, and electrical properties

The main goal of the second study was to achieve sufficient electrical conductivity for shielding and investigate further improvements using hybrid composites with G as a secondary filler. To this end, the extrusion process of HDPE/CNT was performed with increasing filler concentrations, resulting in a percolation threshold of 6.49 wt.%. This higher value was attributed to the high viscosity of the polymeric matrix and its semicrystalline nature, which reduce filler availability in the conduction process through heterogeneous nucleation. The effect of the secondary filler, G, was investigated in terms of permeability and hybrid composites. Synergism was preliminary found for hybrid composites with 99:1 CNT:G ratios at a fixed concentration of 9 wt.%, which was already in the recommended conductivity range for shielding. However, further investigations at that ratio did not yield significant improvements in permeability, and synergism was not found. Two heat treatment protocols were established to investigate the lack of synergism, either in the solid or molten state. The results indicated that thermal history and cooling conditions are crucial in influencing the final electrical conductivity of the composite and possibly induced synergistic effects on hybrid composites.

6.3 Chapter 5 – Coextrusion and compression molding, barrier and shielding properties

In this last study, we made use of the insights gained from our previous research, particularly the significance of layer design in multilayered structures for achieving combined properties.

Using a comparative approach, we evaluated the barrier and shielding properties of multilayered composite films based on HDPE and CNT/G fillers against single-layer films with the same filler compositions. The multilayered structures were obtained with a coextrusion technique with a multiplying element, resulting in a total of 129 layers, which were then compression molded to the same thickness as single-layer films. Overall, the multilayered films exhibited improved barrier properties when G was added, mitigating the detrimental effects of the higher content of CNT required for increased electrical properties. Enhanced shielding was obtained for all the tested conditions within the investigated frequency range, attributed to increased electrical conductivity and dielectric properties of the multilayered structures. Finally, for flexible films containing only G, a higher microwave absorption was observed. And with increased sample thicknesses, high reflection losses were obtained for other structures, with the hybrid sheet composite displaying the highest reduction. It is unfortunate that in this study we were unable to achieve the commercial values for shielding using concentrations as high as 4.5 wt.% of filler. Nonetheless, future research could focus on developing flexible packaging in the commercial application range by adjusting the filler type, its content, and distribution.

CONCLUSION

In this investigation, the aim was to obtain a simpler and more recycling-friendly multilayered film based on carbon-based polyolefin composites for packaging applications. The materials and techniques used were compatible with industrial settings, aiming to protect sensitive electronic devices using flexible packaging with barrier and shielding properties. The properties of the composites were highly dependent on the processing method, with layer design playing a crucial role in achieving combined properties such as barrier and shielding. These properties were successfully obtained using multilayered structures and hybrid composites and were superior to single-layer films. However, the film properties were unable to meet the necessary requirements for protecting sensitive electronics devices at the maximum filler content investigated suitable for commercial use due to a lower shielding ability. Despite these constraints, the investigation demonstrates the potential to achieve combined properties in a composite flexible film for packaging applications. To improve performance, future work should focus on reducing the negative impact of higher filler amounts on dispersion efficacy and the strong influence of a semicrystalline polymeric matrix under processing conditions on the desired properties.

RECOMMENDATIONS

Further research should be undertaken to investigate the following topics:

1. Evaluate the impact of the type of HDPE used, in terms of flow index and whether it is a homopolymer or copolymer, on the barrier and electrical properties of single-layer composites.

2. Investigate the performance of polypropylene-based multilayered composites as a barrier and shielding matrix for flexible packaging.

3. Investigate the barrier and shielding properties of multilayered films produced using only the coextrusion technique with a multiplying element and the optimum number of layers.

4. Assess the effect of flexing on the barrier properties of multilayered films.

5. Investigate the impact of solid-state annealing on the permeability and shielding properties of multilayered films.

6. Explore the effect of incorporating G or CNT papers or segregated structures into flexible films on their shielding and barrier properties.

7. Investigate the barrier and shielding performance of conductive polymer in-situ polymerization with clay materials.

APPENDIX I

CHAPTER 3 - SUPPORTING INFORMATION

Thermogravimetric analysis (TGA) – The average weight content of graphene was determined by subtracting the weight residue of the neat HDPE from the composite films obtained through TGA tests. The tests were carried out in a Diamond TG/DTA PerkinElmer in a temperature ranging from 50°C to 575 °C and a heating rate of 10 °C/min in nitrogen atmosphere (flow rate of 100 ml/min), Figure AI -1. Table A I-1 summarizes the average G content found in the composite films by TGA analysis. The amounts found correspond well to the nominal amount of graphene that was added to the polymer 0.1, 0.5 and 1 wt. %. Additionally, the respective contents for both groups of samples, nipped (N) and non-nipped (NN) are similar. Hence, a comparison between both types of samples can be conducted.

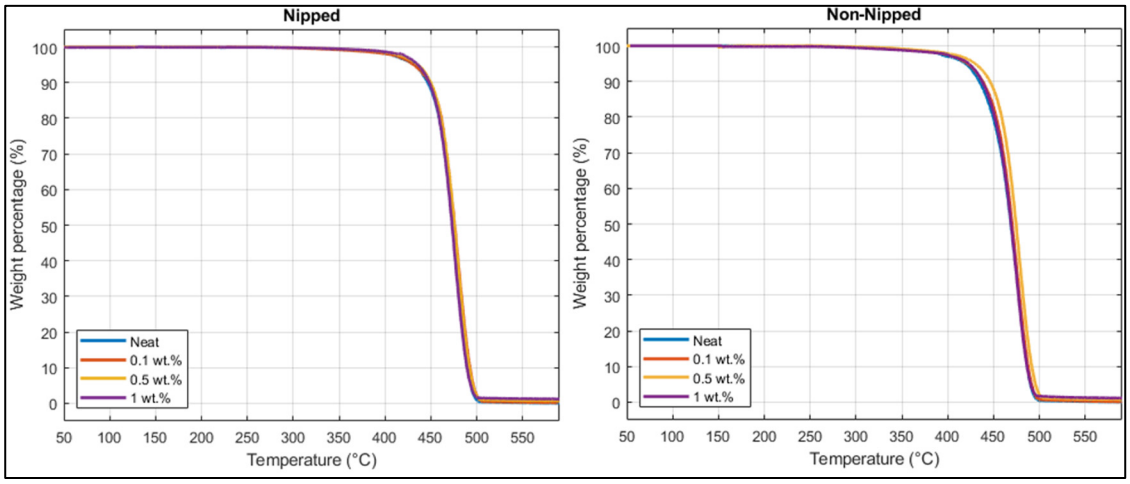

Figure A I-1 Thermogravimetric of neat and composite films nipped and non-nipped

Table A I-1 Expected and measured G concentration by TGA

Expected G concentration (wt. %)	G concentration (wt. %)	
	Nipped (N)	Non-nipped (NN)
0.1	0.1±0.0	0.1±0.0
0.5	0.6±0.2	0.7±0.1
1.0	1.0±0.1	1.1±0.0

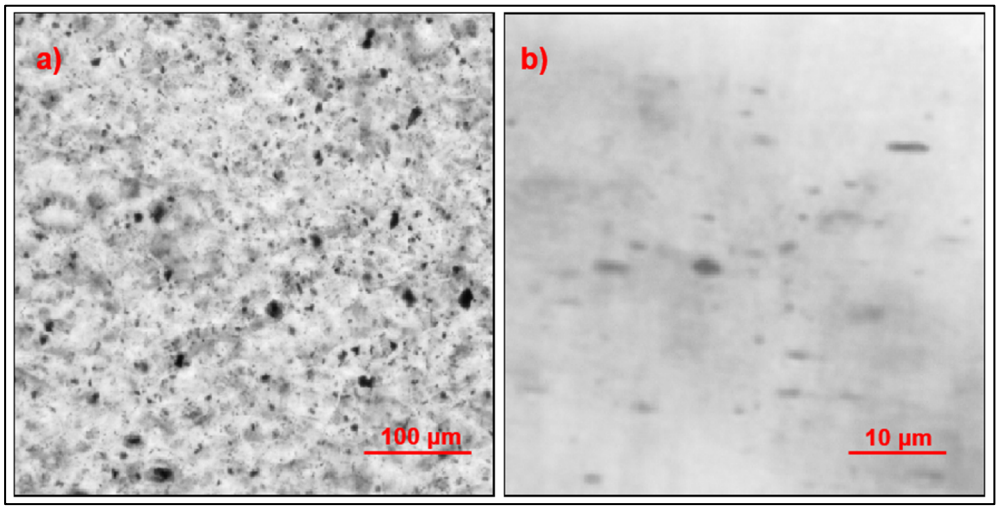

Figure A I-2 Original OM pictures of NN 0.1 wt.% G a) top view and b) cross section view, respectively

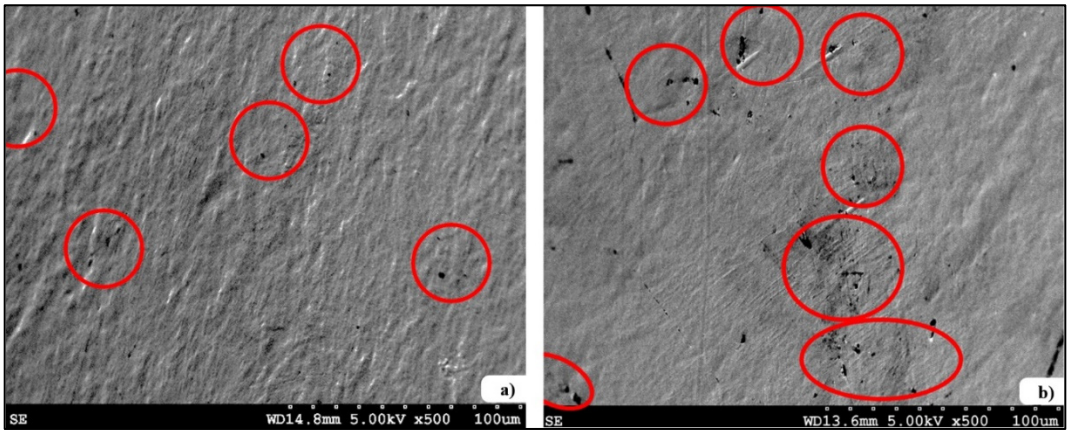

Figure A I-3 SEM surface pictures of a) Neat film and b) 1 wt.% composite both with surface finishing

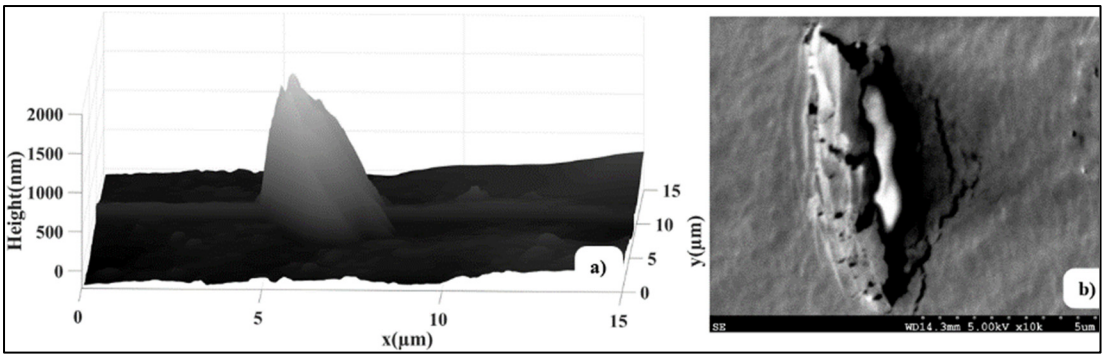

Figure A I-4 a) AFM mapping in height mode and b) SEM picture where both shows filler defects at the surface of the 1 wt.% composite films induced by surface finishing

Polarized FTIR – The spectres of the neat films in the MD and TD were obtained with a Nicolet 170SX FTIR, resolution of 2 cm^{-1} and accumulation of 128 scans. Beam polarization was performed using a SpectraTech zinc selenide wire grid polarizer (Ajji, Zhang, & Elkoun, 2005). The Herman's orientation function (f_i) was calculated by the dichroic ratio (D) with the absorption ratio in the MD and TD directions, as follows (Yadegari, Morshedian, Khonakdar, & Wagenknecht, 2016b):

$$D = \frac{A_{MD}}{A_{TD}}$$
$$f_i = \frac{(D-1)}{(D+2)} \quad \text{(A I-1)}$$

The chosen absorbance wavenumber to obtain f_a and f_b was 730 and 720 cm^{-1} (Read & Stein, 1968), respectively by their spectra deconvolution. And the f_c was obtained with Equation A I-2 (Read & Stein, 1968).

$$f_a + f_b + f_c = 0 \quad \text{(A I-2)}$$

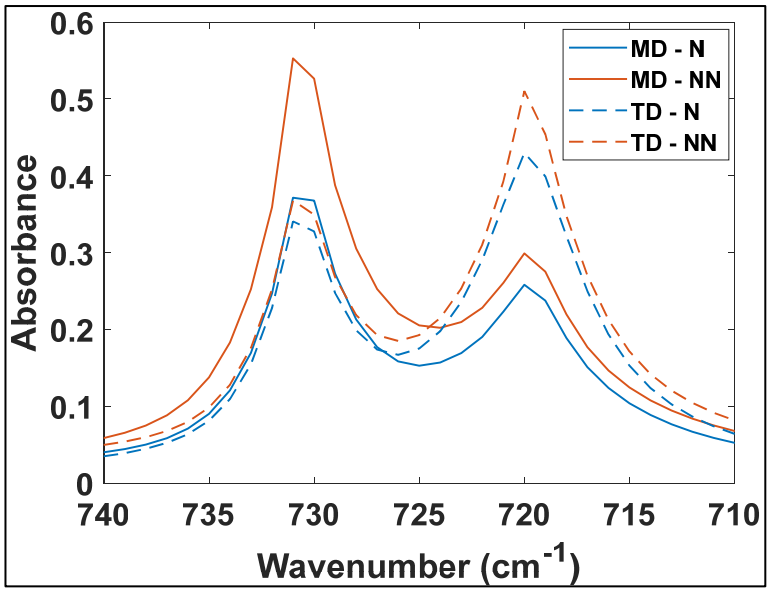

Figure A I-5 Polarized FTIR spectra in MD and TD for nipped (N) and non-nipped (NN) composites

Table A I-2 Calculated Herman's Orientation functions of nipped and non-nipped films

Herman's Orientation functions	Nipped (N)	Non-nipped (NN)
f_a	0.04	0.14
f_b	-0.15	-0.16
f_c	0.11	0.02

APPENDIX II

CHAPTER 4 - SUPPORTING INFORMATION

The crystallization behaviour was determined by DSC (PerkinElmer model Pyris 1) to evaluate the annealing in the solid state closer to the peak crystallization of the samples. Amounts varying between 10 and 20 mg of material were taken from the samples as pressed. The samples were encapsulated in an aluminum pan and tested in the range of 180°C to 50 °C at a coaling heating rate of 10 °C/min. Figure A II-1 shows the obtained result.

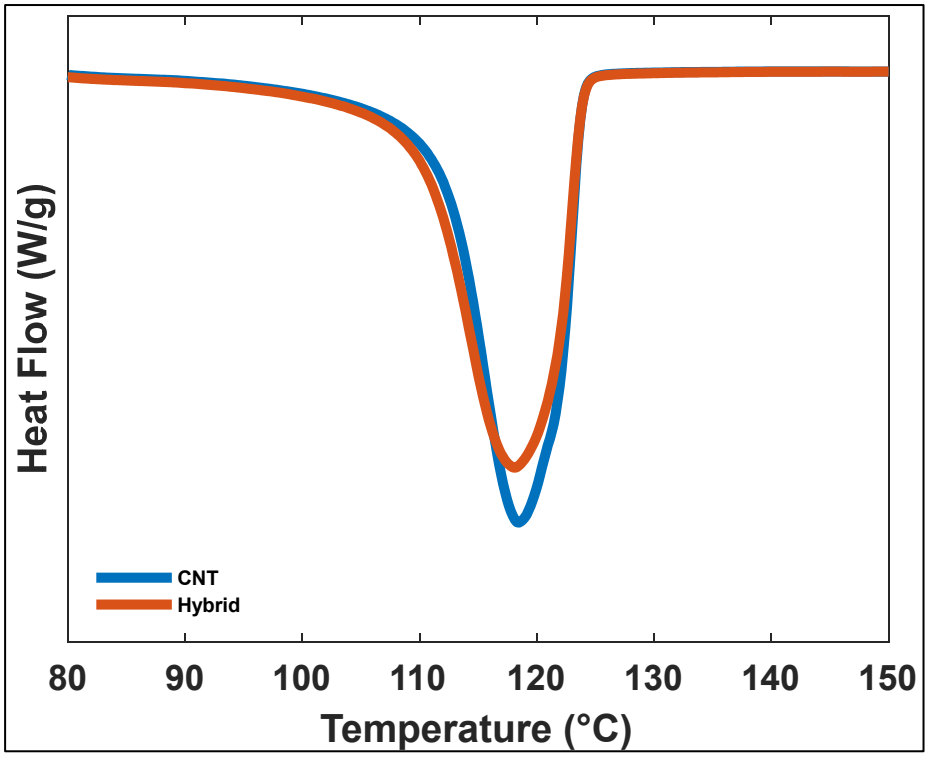

Figure A II-1 Crystallization behaviour of HDPE/CNT and HDPE/Hybrid composites

APPENDIX III

CHAPTER 5 - SUPPORTING INFORMATION

Figure A III-1 show the measured complex viscosity of different concentrations of filler at 0.3% strain and 240 ºC. At higher angular frequencies viscosity ratios are lower than 2.

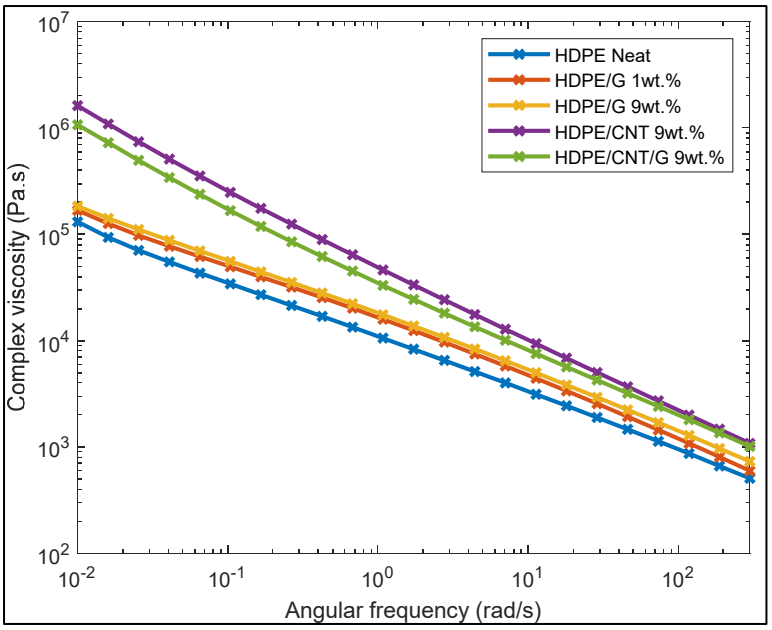

Figure A III-1 Complex viscosity data as function of angular frequency

LIST OF BIBLIOGRAPHICAL REFERENCES

Abdallah, W., Mirzadeh, A., Tan, V., & Kamal, M. (2018). Influence of Nanoparticle Pretreatment on the Thermal, Rheological and Mechanical Properties of PLA-PBSA Nanocomposites Incorporating Cellulose Nanocrystals or Montmorillonite. *Nanomaterials*, *9*(1), 29. DOI: 10.3390/nano9010029

Ajji, A., Zhang, X., & Elkoun, S. (2005). Biaxial orientation in HDPE films: comparison of infrared spectroscopy, X-ray pole figures and birefringence techniques. *Polymer*, *46*(11), 3838–3846. DOI: 10.1016/j.polymer.2005.03.002

Akkachai, P., Kittipong, H., Darunee, A., & Duanghathai, P. (2014). Oxygen-Plasma Treated Graphene Nanoplatelet/Multi-Walled Carbon Nanotube/Polycarbonate Hybrid Nanocomposites for Anti-Electrostatic Discharge Applications: Preparation and Properties. *Applied Mechanics and Materials*, *510*, 63–72. DOI: 10.4028/www.scientific.net/AMM.510.63

Alig, I., Lellinger, D., Engel, M., Skipa, T., & Pötschke, P. (2008). Destruction and formation of a conductive carbon nanotube network in polymer melts: In-line experiments. *Polymer*, *49*(7), 1902–1909. DOI: 10.1016/j.polymer.2008.01.073

Alig, I., Pötschke, P., Lellinger, D., Skipa, T., Pegel, S., Kasaliwal, G. R., & Villmow, T. (2012). Establishment, morphology and properties of carbon nanotube networks in polymer melts. *Polymer*, *53*(1), 4–28. DOI: 10.1016/j.polymer.2011.10.063

Al-Saleh, M. H. (2016a). Carbon nanotube-filled polypropylene/polyethylene blends: compatibilization and electrical properties. *Polymer Bulletin*, *73*(4), 975–987. DOI: 10.1007/s00289-015-1530-1

Al-Saleh, M. H. (2016b). Electrical, EMI shielding and tensile properties of PP/PE blends filled with GNP:CNT hybrid nanofiller. *Synthetic Metals*, *217*, 322–330. DOI: 10.1016/j.synthmet.2016.04.023

Al-Saleh, M. H., & Sundararaj, U. (2009). Electromagnetic interference shielding mechanisms of CNT/polymer composites. *Carbon*, *47*(7), 1738–1746. DOI: 10.1016/j.carbon.2009.02.030

APR. (2022). *PE Film Standard Laboratory Processing Practices*. Retrieved from https://plasticsrecycling.org/images/Design-Guidance-Tests/APR-pe-film-practices-fpe-p-00.pdf

Bajpai, P. (2019). Chapter 4 - Packaging types. In P. Bajpai (Ed.), *Biobased Polymers* (pp. 113–127). Elsevier. DOI: 10.1016/B978-0-12-818404-2.00004-7

Balazs, A. C., Emrick, T., & Russell, T. P. (2006). Nanoparticle Polymer Composites: Where Two Small Worlds Meet. *Science*, *314*(5802), 1107–1110. DOI: 10.1126/science.1130557

Bashmakov, I. A., Nilsson, L. J., Acquaye, A., Bataille, C., Cullen, J. M., de la Rue du Can, S., … Tanaka, K. (2022). Industry (P. R. Shukla, J. Skea, R. Slade, A. A. Khourdajie, R. van Diemen, D. McCollum, … J. Malley, Eds.). Cambridge, UK and New York, NY, USA: Cambridge University Press. DOI: 10.1017/9781009157926.013

Batista, N. L., Helal, E., Kurusu, R. S., Moghimian, N., David, E., Demarquette, N. R., & Hubert, P. (2019). Mass-produced graphene—HDPE nanocomposites: Thermal, rheological, electrical, and mechanical properties. *Polymer Engineering & Science*, *59*(4), 675–682. DOI: 10.1002/pen.24981

Beswick, R., & Dunn, D. J. (2002). *Plastics in Packaging: Western Europe and North America*. iSmithers Rapra Publishing. Retrieved from https://books.google.ca/books?id=0RW6ne-xYmMC

Boldt, R., Leuteritz, A., Schob, D., Ziegenhorn, M., & Wagenknecht, U. (2020). Barrier Properties of GnP–PA-Extruded Films. *Polymers*, *12*(3), 669. DOI: 10.3390/polym12030669

Bouakaz, B. S., Habi, A., Grohens, Y., & Pillin, I. (2018). Effect of combinations of nanofillers on rheology-structure relations in biodegradable poly(ε-caprolactone) nanocomposites. *Applied Clay Science*, *161*, 35–47. DOI: 10.1016/j.clay.2018.04.006

Boufarguine, M., Guinault, A., Miquelard-Garnier, G., & Sollogoub, C. (2013). PLA/PHBV Films with Improved Mechanical and Gas Barrier Properties. *Macromolecular Materials and Engineering*, *298*(10), 1065–1073. DOI: 10.1002/mame.201200285

Canopoli, L., Fidalgo, B., Coulon, F., & Wagland, S. T. (2018). Physico-chemical properties of excavated plastic from landfill mining and current recycling routes. *Waste Management*, *76*, 55–67. DOI: 10.1016/j.wasman.2018.03.043

Cao, M.-S., Cai, Y.-Z., He, P., Shu, J.-C., Cao, W.-Q., & Yuan, J. (2019). 2D MXenes: Electromagnetic property for microwave absorption and electromagnetic interference shielding. *Chemical Engineering Journal*, *359*, 1265–1302. DOI: 10.1016/j.cej.2018.11.051

Cervantes-Reyes, A., Núñez-Pineda, A., Barrera-Díaz, C., Varela-Guerrero, V., Martínez-Barrera, G., & Cuevas-Yañez, E. (2015). Solvent effect in the polyethylene recovery from multilayer postconsumer aseptic packaging. *Waste Management*, *38*, 61–64. DOI: 10.1016/j.wasman.2015.01.034

Chen, J., Wei, S., & Xie, H. (2021). A Brief Introduction of Carbon Nanotubes: History, Synthesis, and Properties. *Journal of Physics: Conference Series*, *1948*(1), 012184. DOI: 10.1088/1742-6596/1948/1/012184

Chen, J.-T., Fu, Y.-J., An, Q.-F., Lo, S.-C., Zhong, Y.-Z., Hu, C.-C., … Lai, J.-Y. (2014). Enhancing polymer/graphene oxide gas barrier film properties by introducing new crystals. *Carbon*, *75*, 443–451. DOI: 10.1016/j.carbon.2014.04.024

Cui, Y., Kundalwal, S. I., & Kumar, S. (2016). Gas barrier performance of graphene/polymer nanocomposites. *Carbon*, *98*, 313–333. DOI: 10.1016/j.carbon.2015.11.018

Cussler, E. L., Hughes, S. E., Ward, W. J., & Aris, R. (1988). Barrier membranes. *Journal of Membrane Science*, *38*(2), 161–174. DOI: 10.1016/S0376-7388(00)80877-7

Danlée, Y., Huynen, I., & Bailly, C. (2012). Thin smart multilayer microwave absorber based on hybrid structure of polymer and carbon nanotubes. *Applied Physics Letters*, *100*(21), 213105. DOI: 10.1063/1.4717993

David, D. A., Jabeen Fatima, M. J., Khan, A., Joy, R., Thakur, V. K., Ruiz-Rosas, R. R., … Raghavan, P. (2023). Porous Carbon Materials and Their Composites for Electromagnetic Interference (EMI) Shielding: The State-of-the-Art of Technologies. In A. N. Grace, P. Sonar, P. Bhardwaj, & A. Chakravorty (Eds.), *Handbook of Porous Carbon Materials* (pp. 669–702). Singapore: Springer Nature Singapore. DOI: 10.1007/978-981-19-7188-4_25

Decker, W., & Henry, B. (2002). *Basic principles of thin film barrier coatings*. 492–502.

Demirci, A., & Ngadi, M. O. (2012). 22.4.4 Plastics. In *Microbial Decontamination in the Food Industry - Novel Methods and Applications* (p. 708). Elsevier. Retrieved from https://app.knovel.com/hotlink/pdf/id:kt010XOJ41/microbial-decontamination/plastics

Dhakal, S., Minx, J. C., Toth, F. L., Abdel-Aziz, A., Figueroa Meza, M. J., Hubacek, K., … Wiedmann, T. (2022). Emissions Trends and Drivers (P. R. Shukla, J. Skea, R. Slade, A. A. Khourdajie, R. van Diemen, D. McCollum, … J. Malley, Eds.). Cambridge, UK and New York, NY, USA: Cambridge University Press. DOI: 10.1017/9781009157926.004

Dhinakaran, V., Lavanya, M., Vigneswari, K., Ravichandran, M., & Vijayakumar, M. D. (2020). Review on exploration of graphene in diverse applications and its future horizon. *Materials Today: Proceedings*, *27*, 824–828. DOI: 10.1016/j.matpr.2019.12.369

Doyon, G., Arch, J., Doyon, G., Twede, D., Drasner, B., Baylis, A. M., … Henningsen, P. (2009). B. In K. L. Yam (Ed.), *The Wiley Encyclopedia of Packaging Technology* (pp. 71–180). Hoboken, NJ, USA: John Wiley & Sons, Inc. DOI: 10.1002/9780470541395.ch2

Duan, Z., & Thomas, N. L. (2014). Water vapour permeability of poly(lactic acid): Crystallinity and the tortuous path model. *Journal of Applied Physics*, *115*(6), 064903. DOI: 10.1063/1.4865168

Duffo, P., Monasse, B., & Haudin, J. M. (1990). Influence of Stretching and Cooling Conditions in Cast Film Extrusion of PP Films. *International Polymer Processing*, *5*(4), 272–283. DOI: 10.3139/217.900272

Dul, S., Fambri, L., Merlini, C., Barra, G. M. O., Bersani, M., Vanzetti, L., & Pegoretti, A. (2019). Effect of graphene nanoplatelets structure on the properties of acrylonitrile–butadiene–styrene composites. *Polymer Composites*, *40*(S1). DOI: 10.1002/pc.24645

Ehrenstein, G. W., Riedel, G., & Trawiel, P. (2004). Differential Scanning Calorimetry (DSC). In *Thermal Analysis of Plastics - Theory and Practice* (p. 15). Hanser Publishers.

Fatahi, S., Ajji, A., & Lafleur, P. G. (2005). Correlation between Structural Parameters and Property of PE Blown Films. *Journal of Plastic Film & Sheeting*, *21*(4), 281–305. DOI: 10.1177/8756087905059979

Ferreira Junior, J. C., Moghimian, N., Gutiérrez, G., Helal, E., Ajji, A., Barra, G. M. de O., & Demarquette, N. R. (2022). Effects of an industrial graphene grade and surface finishing on water and oxygen permeability, electrical conductivity, and mechanical properties of high-density polyethylene (HDPE) multilayered cast films. *Materials Today Communications*, *31*, 103470. DOI: 10.1016/j.mtcomm.2022.103470

Fredrickson, G. H., & Bicerano, J. (1999). Barrier properties of oriented disk composites. *The Journal of Chemical Physics*, *110*(4), 2181–2188. DOI: 10.1063/1.477829

Gao, W., Shen, J., & Guo, S. (2014). Effects of layer-multiplying process on conducting properties of multilayer composites consisting of alternating layers of carbon black/polypropylene and polyamide 6/polypropylene. *Polymer Engineering & Science*, *54*(6), 1471–1476. DOI: 10.1002/pen.23663

Gao, W., Zheng, Y., Shen, J., & Guo, S. (2015). Electrical Properties of Polypropylene-Based Composites Controlled by Multilayered Distribution of Conductive Particles. *ACS Applied Materials & Interfaces*, *7*(3), 1541–1549. DOI: 10.1021/am506773c

Gao, X., Li, J., Gao, Y., Guo, S., Wu, H., & Chen, R. (2016). Microwave absorbing properties of alternating multilayer composites consisting of poly (vinyl chloride) and multi-walled carbon nanotube filled poly (vinyl chloride) layers. *Composites Science and Technology*, *130*, 10–19. DOI: 10.1016/j.compscitech.2016.03.004

Gao, Y., Picot, O. T., Zhang, H., Bilotti, E., Peijs, T., Gao, Y., … Peijs, T. (2017). Synergistic effects of filler size on thermal annealing-induced percolation in polylactic acid (PLA)/ graphite nanoplatelet (GNP) nanocomposites. *Nanocomposites*, *0324*, 0. DOI: 10.1080/20550324.2017.1333780

Garzón, C., & Palza, H. (2014). Electrical behavior of polypropylene composites melt mixed with carbon-based particles: Effect of the kind of particle and annealing process. *Composites Science and Technology*, *99*, 117–123. DOI: 10.1016/j.compscitech.2014.05.018

Gbaguidi, A., Namilae, S., & Kim, D. (2020). Synergy effect in hybrid nanocomposites based on carbon nanotubes and graphene nanoplatelets. *Nanotechnology*, *31*(25), 255704. DOI: 10.1088/1361-6528/ab7fcc

Geim, A. K., & Novoselov, K. S. (2007). The rise of graphene. *Nature Materials*, *6*(3), 183–191. DOI: 10.1038/nmat1849

Geyer, R., Jambeck, J. R., & Law, K. L. (2017). Production, use, and fate of all plastics ever made. *Science Advances*, *3*(7), e1700782. DOI: 10.1126/sciadv.1700782

Ghisellini, P., Cialani, C., & Ulgiati, S. (2016). A review on circular economy: the expected transition to a balanced interplay of environmental and economic systems. *Journal of Cleaner Production*, *114*, 11–32. DOI: 10.1016/j.jclepro.2015.09.007

Gómez, E. F., & Michel, F. C. (2013). Biodegradability of conventional and bio-based plastics and natural fiber composites during composting, anaerobic digestion and long-term soil incubation. *Polymer Degradation and Stability*, *98*(12), 2583–2591. DOI: 10.1016/j.polymdegradstab.2013.09.018

Govindan, K., & Hasanagic, M. (2018). A systematic review on drivers, barriers, and practices towards circular economy: a supply chain perspective. *International Journal of Production Research*, *56*(1–2), 278–311. DOI: 10.1080/00207543.2017.1402141

G. Papageorgiou, D., Li, Z., Liu, M., A. Kinloch, I., & J. Young, R. (2020). Mechanisms of mechanical reinforcement by graphene and carbon nanotubes in polymer nanocomposites. *Nanoscale*, *12*(4), 2228–2267. DOI: 10.1039/C9NR06952F

Greenhouse, H., Lowry, R., & Romenesko, B. (2012). 9 - Water in Sealed Packages. In H. Greenhouse, R. Lowry, & B. Romenesko (Eds.), *Hermeticity of Electronic Packages (Second Edition)* (pp. 243–288). Oxford: William Andrew Publishing. DOI: 10.1016/B978-1-4377-7877-9.00009-X

Ha, H., Kim, S. C., & Ha, K. (2010). Effect of molecular weight of polymer matrix on the dispersion of MWNTs in HDPE/MWNT and PC/MWNT composites. *Macromolecular Research*, *18*(5), 512–518. DOI: 10.1007/s13233-010-0510-4

Haley, J. C., & Borke, J. S. (2009). The Interplay between Polymer Polydispersity and Film Gauge in HDPE Barrier Films: How Polydispersity Controls the Gauge Dependence of Film Barrier Properties. In *ANTEC 2009 Plastics: Annual Technical Conference Proceedings*. Society of Plastics Engineers (SPE). Retrieved from https://app.knovel.com/hotlink/pdf/id:kt006PTNF1/antec-2009-plastics-annual/interplay-between-polymer

He, L., Shi, Y., Wang, Q., Chen, D., Shen, J., & Guo, S. (2020). Strategy for constructing electromagnetic interference shielding and flame retarding synergistic network in poly (butylene succinate) and thermoplastic polyurethane multilayered composites. *Composites Science and Technology*, *199*, 108324. DOI: 10.1016/j.compscitech.2020.108324

He, P., Cao, M.-S., Cao, W.-Q., & Yuan, J. (2021). Developing MXenes from Wireless Communication to Electromagnetic Attenuation. *Nano-Micro Letters*, *13*(1), 115. DOI: 10.1007/s40820-021-00645-z

Hedesiu, C., Demco, D. E., Kleppinger, R., Buda, A. A., Blümich, B., Remerie, K., & Litvinov, V. M. (2007). The effect of temperature and annealing on the phase composition, molecular mobility and the thickness of domains in high-density polyethylene. *Polymer*, *48*(3), 763–777. DOI: 10.1016/j.polymer.2006.12.019

Helal, E., Kurusu, R. S., Moghimian, N., Gutierrez, G., David, E., & Demarquette, N. R. (2019). Correlation between morphology, rheological behavior, and electrical behavior of conductive cocontinuous LLDPE/EVA blends containing commercial graphene nanoplatelets. *Journal of Rheology*, *63*(6), 961–976. DOI: 10.1122/1.5108919

Horodytska, O., Valdés, F. J., & Fullana, A. (2018). Plastic flexible films waste management – A state of art review. *Waste Management*, *77*, 413–425. DOI: 10.1016/j.wasman.2018.04.023

Huang, H.-D., Ren, P.-G., Chen, J., Zhang, W.-Q., Ji, X., & Li, Z.-M. (2012). High barrier graphene oxide nanosheet/poly(vinyl alcohol) nanocomposite films. *Journal of Membrane Science*, *409–410*, 156–163. DOI: 10.1016/j.memsci.2012.03.051

Iijima, S., & Ichihashi, T. (1993). Single-shell carbon nanotubes of 1-nm diameter. *Nature*, *363*(6430), 603–605. DOI: 10.1038/363603a0

IPCC. (2022). Summary for Policymakers (P. R. Shukla, J. Skea, R. Slade, A. A. Khourdajie, R. van Diemen, D. McCollum, … J. Malley, Eds.). Cambridge, UK and New York, NY, USA: Cambridge University Press. DOI: 10.1017/9781009157926.001

ISO Nanotechnologies — Vocabulary — Part 13: Graphene and related two-dimensional (2D) materials. (2017). Retrieved from https://www.iso.org/obp/ui/en/#iso:std:iso:ts:80004:-13:ed-1:v1:en

Jalali Dil, E., Ben Dhieb, F., & Ajji, A. (2019). Modeling the effect of nanoplatelets orientation on gas permeability of polymer nanocomposites. *Polymer*, *168*, 126–130. DOI: 10.1016/j.polymer.2019.02.024

Jambeck, J. R., Geyer, R., Wilcox, C., Siegler, T. R., Perryman, M., Andrady, A., … Law, K. L. (2015). Plastic waste inputs from land into the ocean. *Science*, *347*(6223), 768–771. DOI: 10.1126/science.1260352

Jia, L.-C., Yan, D.-X., Jiang, X., Pang, H., Gao, J.-F., Ren, P.-G., & Li, Z.-M. (2018). Synergistic Effect of Graphite and Carbon Nanotubes on Improved Electromagnetic Interference Shielding Performance in Segregated Composites. *Industrial & Engineering Chemistry Research*, *57*(35), 11929–11938. DOI: 10.1021/acs.iecr.8b03238

Jiang, X., & Drzal, L. T. (2011). Improving electrical conductivity and mechanical properties of high density polyethylene through incorporation of paraffin wax coated exfoliated graphene nanoplatelets and multi-wall carbon nano-tubes. *Composites Part A: Applied Science and Manufacturing*, *42*(11), 1840–1849. DOI: 10.1016/j.compositesa.2011.08.011

Jin, J., Rafiq, R., Gill, Y. Q., & Song, M. (2013). Preparation and characterization of high performance of graphene/nylon nanocomposites. *European Polymer Journal*, *49*(9), 2617–2626. DOI: 10.1016/j.eurpolymj.2013.06.004

Jones, H., Saffar, F., Koutsos, V., & Ray, D. (2021). Polyolefins and Polyethylene Terephthalate Package Wastes: Recycling and Use in Composites. *Energies*, *14*(21), 7306. DOI: 10.3390/en14217306

Jouni, M., Faure-Vincent, J., Fedorko, P., Djurado, D., Boiteux, G., & Massardier, V. (2014). Charge carrier transport and low electrical percolation threshold in multiwalled carbon nanotube polymer nanocomposites. *Carbon*, *76*, 10–18. DOI: 10.1016/j.carbon.2014.04.031

Kaiser, K., Schmid, M., & Schlummer, M. (2017). Recycling of Polymer-Based Multilayer Packaging: A Review. *Recycling*, *3*(1), 1. DOI: 10.3390/recycling3010001

Kalaitzidou, K., Fukushima, H., & Drzal, L. T. (2007). Multifunctional polypropylene composites produced by incorporation of exfoliated graphite nanoplatelets. *Carbon*, *45*(7), 1446–1452. DOI: 10.1016/j.carbon.2007.03.029

Kanai, T., & Campbell, G., A,. (1999a). 5.3 Monolayer Blown Film Extrusion. In *Film Processing*. Hanser Publishers. Retrieved from https://app.knovel.com/hotlink/pdf/id:kt003J7FH8/film-processing/monolayer-blown-film

Kanai, T., & Campbell, G., A,. (1999b). 5.5 Coextrusion Feedblock and Multimanifold Dies. In *Film Processing*. Hanser Publishers. Retrieved from https://app.knovel.com/hotlink/pdf/id:kt003J7FJ1/film-processing/coextrusion-feedblock

Kauling, A. P., Seefeldt, A. T., Pisoni, D. P., Pradeep, R. C., Bentini, R., Oliveira, R. V. B., … Castro Neto, A. H. (2018). The Worldwide Graphene Flake Production. *Advanced Materials*, *30*(44), 1803784. DOI: 10.1002/adma.201803784

Kausar, A. (2020). A review of high performance polymer nanocomposites for packaging applications in electronics and food industries. *Journal of Plastic Film & Sheeting*, *36*(1), 94–112. DOI: 10.1177/8756087919849459

Kazemi, Y., Kakroodi, A. R., Wang, S., Ameli, A., Filleter, T., Pötschke, P., & Park, C. B. (2017). Conductive network formation and destruction in polypropylene/carbon nanotube composites via crystal control using supercritical carbon dioxide. *Polymer*, *129*, 179–188. DOI: 10.1016/j.polymer.2017.09.056

Keles, O., & Dundar, M. (2007). Aluminum foil: Its typical quality problems and their causes. *Journal of Materials Processing Technology*, *186*(1), 125–137. DOI: 10.1016/j.jmatprotec.2006.12.027

Kim, H., & Macosko, C. W. (2009). Processing-property relationships of polycarbonate/graphene composites. *Polymer*, *50*(15), 3797–3809. DOI: 10.1016/j.polymer.2009.05.038

King, J. A., Klimek, D. R., Miskioglu, I., & Odegard, G. M. (2015). Mechanical properties of graphene nanoplatelet/epoxy composites. *Journal of Composite Materials*, *49*(6), 659–668. DOI: 10.1177/0021998314522674

Kirchherr, J., Reike, D., & Hekkert, M. (2017). Conceptualizing the circular economy: An analysis of 114 definitions. *Resources, Conservation and Recycling*, *127*, 221–232. DOI: 10.1016/j.resconrec.2017.09.005

Kirkpatrick, S. (1973). Percolation and Conduction. *Reviews of Modern Physics*, *45*(4), 574–588. DOI: 10.1103/RevModPhys.45.574

Kovtun, A., Treossi, E., Mirotta, N., Scidà, A., Liscio, A., Christian, M., … Palermo, V. (2019). Benchmarking of graphene-based materials: real commercial products versus ideal graphene. *2D Materials*, *6*(2), 025006. DOI: 10.1088/2053-1583/aafc6e

Kranauskaitė, I., Macutkevič, J., Borisova, A., Martone, A., Zarrelli, M., Selskis, A., … Banys, J. (2018). Enhancing electrical conductivity of multiwalled carbon nanotube/epoxy composites by graphene nanoplatelets. *Lithuanian Journal of Physics*, *57*(4), 232–242. DOI: 10.3952/physics.v57i4.3602

Kreyling, W. G., Semmler-Behnke, M., & Chaudhry, Q. (2010). A complementary definition of nanomaterial. *Nano Today*, *5*(3), 165–168. DOI: 10.1016/j.nantod.2010.03.004

Kuester, S., Demarquette, N. R., Ferreira, J. C., Soares, B. G., & Barra, G. M. O. (2017). Hybrid nanocomposites of thermoplastic elastomer and carbon nanoadditives for electromagnetic shielding. *European Polymer Journal*, *88*, 328–339. DOI: 10.1016/j.eurpolymj.2017.01.023

Langhe, D., & Ponting, M. (2016). Introduction to Multilayered Films. In *Manufacturing and Novel Applications of Multilayer Polymer Films* (pp. 1–15). Elsevier. DOI: 10.1016/B978-0-323-37125-4.00001-0

Lee, B., Hwang, U., Kim, J., Kim, S.-H., Choi, K., Park, I.-K., … Nam, J.-D. (2023). Highly dispersed graphene nanoplatelets in polypropylene composites by employing high-shear stress for enhanced dielectric properties and frequency-selective electromagnetic interference shielding capability. *Composites Communications*, *37*, 101409. DOI: 10.1016/j.coco.2022.101409

Lee, P. C., Dooley, J., Robacki, J., Jenkins, S., & Wrisley, R. (2014). Improvements in flex oxygen barrier properties of polymeric films by microlayer coextrusion. *Journal of Plastic Film & Sheeting*, *30*(3), 234–247. DOI: 10.1177/8756087913506728

Lei, F., Du, Q., Li, T., Li, J., & Guo, S. (2013). Effect of phase morphology and interfacial strength on barrier properties of high density polyethylene/polyamide 6 membranes. *Polymer Engineering & Science*, *53*(9), 1996–2003. DOI: 10.1002/pen.23448

Li, H., Lu, X., Yuan, D., Sun, J., Erden, F., Wang, F., & He, C. (2017). Lightweight flexible carbon nanotube/polyaniline films with outstanding EMI shielding properties. *Journal of Materials Chemistry C*, *5*(34), 8694–8698. DOI: 10.1039/C7TC02394D

Lim, G.-O., Min, K.-T., & Kim, G.-H. (2010). Effect of cooling rate on the surface resistivity of polymer/multi-walled carbon nanotube nanocomposites. *Polymer Engineering & Science*, *50*(2), 290–294. DOI: 10.1002/pen.21537

Linares, A., Canalda, J. C., Cagiao, M. E., García-Gutiérrez, M. C., Nogales, A., Martín-Gullón, I., … Ezquerra, T. A. (2008). Broad-Band Electrical Conductivity of High Density Polyethylene Nanocomposites with Carbon Nanoadditives: Multiwall Carbon Nanotubes and Carbon Nanofibers. *Macromolecules*, *41*(19), 7090–7097. DOI: 10.1021/ma801410j

Liu, M., Papageorgiou, D. G., Li, S., Lin, K., Kinloch, I. A., & Young, R. J. (2018). Micromechanics of reinforcement of a graphene-based thermoplastic elastomer nanocomposite. *Composites Part A: Applied Science and Manufacturing*, *110*, 84–92. DOI: 10.1016/j.compositesa.2018.04.014

Liu, Z., Bai, G., Huang, Y., Li, F., Ma, Y., Guo, T., … Chen, Y. (2007). Microwave Absorption of Single-Walled Carbon Nanotubes/Soluble Cross-Linked Polyurethane Composites. *The Journal of Physical Chemistry C*, *111*(37), 13696–13700. DOI: 10.1021/jp0731396

Logakis, E., Pandis, Ch., Peoglos, V., Pissis, P., Pionteck, J., Pötschke, P., … Omastová, M. (2009). Electrical/dielectric properties and conduction mechanism in melt processed polyamide/multi-walled carbon nanotubes composites. *Polymer*, *50*(21), 5103–5111. DOI: 10.1016/j.polymer.2009.08.038

Lux, F. (1993). Models proposed to explain the electrical conductivity of mixtures made of conductive and insulating materials. *Journal of Materials Science*, *28*(2), 285–301. DOI: 10.1007/BF00357799

Madinehei, M., Kuester, S., Kaydanova, T., Moghimian, N., & David, É. (2021). Influence of Graphene Nanoplatelet Lateral Size on the Electrical Conductivity and Electromagnetic Interference Shielding Performance of Polyester Nanocomposites. *Polymers*, *13*(15), 2567. DOI: 10.3390/polym13152567

Mangaraj, S., Goswami, T. K., & Panda, D. K. (2015). Modeling of gas transmission properties of polymeric films used for MA packaging of fruits. *Journal of Food Science and Technology*, *52*(9), 5456–5469. DOI: 10.1007/s13197-014-1682-2

Marinho, B., Ghislandi, M., Tkalya, E., Koning, C. E., & de With, G. (2012). Electrical conductivity of compacts of graphene, multi-wall carbon nanotubes, carbon black, and graphite powder. *Powder Technology*, *221*, 351–358. DOI: 10.1016/j.powtec.2012.01.024

Marini, J., & Bretas, R. E. S. (2017). Optical Properties of Blown Films of PA6/MMT Nanocomposites. *Materials Research*, *20*(suppl 1), 53–60. DOI: 10.1590/1980-5373-mr-2017-0280

Markarian, J. (2008). New developments in antistatic and conductive additives. *Plastics, Additives and Compounding*, *10*(5), 22–25. DOI: 10.1016/S1464-391X(08)70172-7

Marsden, A. J., Papageorgiou, D. G., Vallés, C., Liscio, A., Palermo, V., Bissett, M. A., … Kinloch, I. A. (2018). Electrical percolation in graphene–polymer composites. *2D Materials*, *5*(3), 032003. DOI: 10.1088/2053-1583/aac055

McNally, G. M., Small, C. M., Murphy, W. R., & Garrett, G. (2005). The Effect of Polymer Properties on the Mechanical Behavior and Morphological Characteristics of Cast Polyethylene Film for Stretch and Cling Film Applications. *Journal of Plastic Film & Sheeting*, *21*(1), 39–54. DOI: 10.1177/8756087905052804

McNally, T., Pötschke, P., Halley, P., Murphy, M., Martin, D., Bell, S. E. J., … Quinn, J. P. (2005). Polyethylene multiwalled carbon nanotube composites. *Polymer*, *46*(19), 8222–8232. DOI: 10.1016/j.polymer.2005.06.094

Méndez, R., Constant, B., Garzon, C., Nisar, M., Nachtigall, S. M. B., & Quijada, R. (2017). Barrier, mechanical and conductive properties of polycaprolactam nanocomposites containing carbon-based particles: Effect of the kind of particle. *Polymer*, *130*, 10–16. DOI: 10.1016/j.polymer.2017.09.063

Messin, T., Follain, N., Guinault, A., Sollogoub, C., Gaucher, V., Delpouve, N., & Marais, S. (2017). Structure and Barrier Properties of Multinanolayered Biodegradable PLA/PBSA Films: Confinement Effect via Forced Assembly Coextrusion. *ACS Applied Materials & Interfaces*, *9*(34), 29101–29112. DOI: 10.1021/acsami.7b08404

MIL-PRF-81705 - Performance specification: barrier materials, flexible, electrostatic protective, heat- sealable. (2009). Retrieved from http://everyspec.com/MIL-PRF/MIL-PRF-080000-99999/MIL-PRF-81705E_21254/

Mirzadeh, A., Ghasemi, H., Mahrous, F., & Kamal, M. R. (2015). Reactive extrusion effects on rheological and mechanical properties of poly(lactic acid)/poly[(butylene succinate)-co-adipate]/epoxy chain extender blends and clay nanocomposites. *Journal of Applied Polymer Science*, *132*(48), n/a-n/a. DOI: 10.1002/app.42664

Moghimian, N., & Nazarpour, S. (2020). The Future of Carbon: An Update on Graphene's Dermal, Inhalation, and Gene Toxicity. *Crystals*, *10*(9), 718. DOI: 10.3390/cryst10090718

Mohan, V. B., Lau, K., Hui, D., & Bhattacharyya, D. (2018). Graphene-based materials and their composites: A review on production, applications and product limitations. *Composites Part B: Engineering*, *142*, 200–220. DOI: 10.1016/j.compositesb.2018.01.013

Morris, B. A. (2017a). 1 - Introduction. In B. A. Morris (Ed.), *The Science and Technology of Flexible Packaging* (pp. 3–21). Oxford: William Andrew Publishing. DOI: 10.1016/B978-0-323-24273-8.00001-0

Morris, B. A. (2017b). 2 - Converting Processes. In B. A. Morris (Ed.), *The Science and Technology of Flexible Packaging* (pp. 25–49). Oxford: William Andrew Publishing. DOI: 10.1016/B978-0-323-24273-8.00002-2

Morris, B. A. (2017c). 8 - Barrier. In B. A. Morris (Ed.), *The Science and Technology of Flexible Packaging* (pp. 259–308). Oxford: William Andrew Publishing. DOI: 10.1016/B978-0-323-24273-8.00008-3

Morris, B. A. (2017d). 9 - Strength, Stiffness, and Abuse Resistance. In B. A. Morris (Ed.), *The Science and Technology of Flexible Packaging* (pp. 309–350). Oxford: William Andrew Publishing. DOI: 10.1016/B978-0-323-24273-8.00009-5

Müller, M., Hilarius, K., Liebscher, M., Lellinger, D., Alig, I., & Pötschke, P. (2017). Effect of Graphite Nanoplate Morphology on the Dispersion and Physical Properties of Polycarbonate Based Composites. *Materials*, *10*(5), 545. DOI: 10.3390/ma10050545

Murray, L. J. (2005). *The Impact of Foil PInholes and Flex Cracks on the Moisture and Oxygen Barrier of Flexible Packaging*. Presented at the Place conference. Retrieved from https://imisrise.tappi.org/TAPPI/Products/05/PLA/05PLA76.aspx

N, M., V.p, S. K., S, S. M., G, R., K, V. S., & T.k, S. (2021). Carbon nanotubes and their properties-The review. *Materials Today: Proceedings*, *47*, 4682–4685. DOI: 10.1016/j.matpr.2021.05.543

Nan, C.-W., Shen, Y., & Ma, J. (2010). Physical Properties of Composites Near Percolation. *Annual Review of Materials Research*, *40*(1), 131–151. DOI: 10.1146/annurev-matsci-070909-104529

Nanocyl. (2016). *NC7000 - Material datasheet*. Retrieved from https://www.nanocyl.com/product/nc7000/

NanoXplore. (2021). *GrapheneBlack 3X Technical Data Sheet*. Retrieved from https://nanoxplore.ca/wp-content/uploads/2021/09/TDS-GB3X-210816.pdf

Nielsen, L. E. (1967). Models for the Permeability of Filled Polymer Systems. *Journal of Macromolecular Science: Part A - Chemistry*, *1*(5), 929–942. DOI: 10.1080/10601326708053745

Novoselov, K. S., Geim, A. K., Morozov, S. V., Jiang, D., Zhang, Y., Dubonos, S. V., … Firsov, A. A. (2004). Electric Field Effect in Atomically Thin Carbon Films. *Science*, *306*(5696), 666–669. DOI: 10.1126/science.1102896

Okunola A., A. (2019). Public and Environmental Health Effects of Plastic Wastes Disposal: A Review. *Journal of Toxicology and Risk Assessment*, *5*(021), 1–13. DOI: 10.23937/2572-4061.1510021

Oyarzabal, A., Cristiano-Tassi, A., Laredo, E., Newman, D., Bello, A., Etxeberría, A., … Müller, A. J. (2017). Dielectric, mechanical and transport properties of bisphenol A polycarbonate/graphene nanocomposites prepared by melt blending. *Journal of Applied Polymer Science*, *134*(13). DOI: 10.1002/app.44654

Paasi, J., Nurmi, S., Vuorinen, R., Strengell, S., & Maijala, P. (2001). Performance of ESD protective materials at low relative humidity. *Journal of Electrostatics*, *51–52*, 429–434. DOI: 10.1016/S0304-3886(01)00038-9

Palomba, M., Longo, A., Carotenuto, G., Coscia, U., Ambrosone, G., Rusciano, G., … Longobardo, L. (2018). Optical and electrical characterizations of graphene nanoplatelet coatings on low density polyethylene. *Journal of Vacuum Science & Technology B, Nanotechnology and Microelectronics: Materials, Processing, Measurement, and Phenomena*, *36*(1), 01A104. DOI: 10.1116/1.4998570

Parkar, A. (2005). Effect of Flexing on the Barrier Properties of Metallized Films. *Theses*. Retrieved from https://scholarworks.rit.edu/theses/8196

Paszkiewicz, S., Szymczyk, A., Pawlikowska, D., Subocz, J., Zenker, M., & Masztak, R. (2018). Electrically and Thermally Conductive Low Density Polyethylene-Based Nanocomposites Reinforced by MWCNT or Hybrid MWCNT/Graphene Nanoplatelets with Improved Thermo-Oxidative Stability. *Nanomaterials*, *8*(4), 264. DOI: 10.3390/nano8040264

Paszkiewicz, S., Szymczyk, A., Zubkiewicz, A., Subocz, J., Stanik, R., & Szczepaniak, J. (2020). Enhanced Functional Properties of Low-Density Polyethylene Nanocomposites Containing Hybrid Fillers of Multi-Walled Carbon Nanotubes and Nano Carbon Black. *Polymers*, *12*(6), 1356. DOI: 10.3390/polym12061356

Peng, M., & Qin, F. (2021). Clarification of basic concepts for electromagnetic interference shielding effectiveness. *Journal of Applied Physics*, *130*(22), 225108. DOI: 10.1063/5.0075019

Pötschke, P., Mothes, F., Krause, B., & Voit, B. (2019). Melt-Mixed PP/MWCNT Composites: Influence of CNT Incorporation Strategy and Matrix Viscosity on Filler Dispersion and Electrical Resistivity. *Polymers*, *11*(2), 189. DOI: 10.3390/polym11020189

Qu, M., Nilsson, F., & Schubert, D. W. (2019). Novel definition of the synergistic effect between carbon nanotubes and carbon black for electrical conductivity. *Nanotechnology*, *30*(24), 245703. DOI: 10.1088/1361-6528/ab0bec

Rahaman, M., Aldalbahi, A., Govindasami, P., Khanam, N. P., Bhandari, S., Feng, P., & Altalhi, T. (2017). A New Insight in Determining the Percolation Threshold of Electrical Conductivity for Extrinsically Conducting Polymer Composites through Different Sigmoidal Models. *Polymers*, *9*(10), 527. DOI: 10.3390/polym9100527

Rathinavel, S., Priyadharshini, K., & Panda, D. (2021). A review on carbon nanotube: An overview of synthesis, properties, functionalization, characterization, and the application. *Materials Science and Engineering: B*, *268*, 115095. DOI: 10.1016/j.mseb.2021.115095

Ravindren, R., Mondal, S., Nath, K., & Das, N. Ch. (2019). Synergistic effect of double percolated co-supportive MWCNT-CB conductive network for high-performance EMI shielding application. *Polymers for Advanced Technologies*, *30*(6), 1506–1517. DOI: 10.1002/pat.4582

Rawshan Ara Begum, R., Lempert, R., E. Ali, T. A. B., Bernauer, T., Cramer, W., Cui, X., … Wester, P. (2022). Point of Departure and Key Concepts (H. O. Pörtner, D. C. Roberts, M. Tignor, E. S. Poloczanska, K. Mintenbeck, A. Alegría, … B. Rama, Eds.). Cambridge, UK and New York, USA: Cambridge University Press. DOI: 10.1017/9781009325844.003

Read, B. E., & Stein, R. S. (1968). Polarized Infrared Studies of Amorphous Orientation in Polyethylene and Some Ethylene Copolymers. *Macromolecules*, *1*(2), 116–126. DOI: 10.1021/ma60002a004

Rostami, A., & Moosavi, M. I. (2020). High-performance thermoplastic polyurethane nanocomposites induced by hybrid application of functionalized graphene and carbon nanotubes. *Journal of Applied Polymer Science*, *137*(14), 48520. DOI: 10.1002/app.48520

Rousseaux, D., Lhost, O., & Lodefier, P. (2013). Industrial advanced carbon nanotubes-based materials for electrostatic discharge packaging. *2013 14th International Conference on Electronic Packaging Technology*, 386–388. Dalian, China: IEEE. DOI: 10.1109/ICEPT.2013.6756495

Russo, P., Acierno, D., Capezzuto, F., Buonocore, G. G., Di Maio, L., & Lavorgna, M. (2015). Thermoplastic polyurethane/graphene nanocomposites: The effect of graphene oxide on physical properties. *AIP Conference Proceedings*, *1695*(1), 020030. DOI: 10.1063/1.4937308

Sabet, M., & Soleimani, H. (2014). Mechanical and electrical properties of low density polyethylene filled with carbon nanotubes. *IOP Conference Series: Materials Science and Engineering*, *64*, 012001. DOI: 10.1088/1757-899X/64/1/012001

Saini, P., & Aror, M. (2012). Microwave Absorption and EMI Shielding Behavior of Nanocomposites Based on Intrinsically Conducting Polymers, Graphene and Carbon Nanotubes. In A. De Souza Gomes (Ed.), *New Polymers for Special Applications*. InTech. DOI: 10.5772/48779

Samtec. (2017, September 6). Microelectronics Group Provides Support For Advanced Microelectronics Applications. Retrieved November 26, 2018, from The Samtec Blog website: https://blog.samtec.com/post/microelectronics-group-provides-support-advanced-microelectronics-applications/

Sankaran, S., Deshmukh, K., Ahamed, M. B., & Khadheer Pasha, S. K. (2018). Recent advances in electromagnetic interference shielding properties of metal and carbon filler reinforced flexible polymer composites: A review. *Composites Part A: Applied Science and Manufacturing*, *114*, 49–71. DOI: 10.1016/j.compositesa.2018.08.006

Schmitz, D. P., Soares, B. G., Barra, G. M. O., & Santana, L. (2023). Sandwich structures based on fused filament fabrication 3D-printed polylactic acid honeycomb and poly(vinylidene fluoride) nanocomposites for microwave absorbing applications. *Polymer Composites*, *44*(4), 2250–2261. DOI: 10.1002/pc.27240

Seethamraju, S., Kumar, S., B, K. B., Madras, G., Raghavan, S., & Ramamurthy, P. C. (2016). Million-Fold Decrease in Polymer Moisture Permeability by a Graphene Monolayer. *ACS Nano*, *10*(7), 6501–6509. DOI: 10.1021/acsnano.6b02588

Selke, S. E. M., & Culter, J. D. (2015). Introduction. In *Plastics Packaging* (pp. 1–7). Carl Hanser Verlag GmbH & Co. KG. DOI: 10.3139/9783446437197.001

Shokrieh, M. M., & Moshrefzadeh-Sani, H. (2016). On the constant parameters of Halpin-Tsai equation. *Polymer*, *106*, 14–20. DOI: 10.1016/j.polymer.2016.10.049

Silva, L. N., dos Anjos, E. G. R., Morgado, G. F. de M., Marini, J., Backes, E. H., Montagna, L. S., & Passador, F. R. (2020). Development of antistatic packaging of polyamide 6/linear low-density polyethylene blends-based carbon black composites. *Polymer Bulletin*, *77*(7), 3389–3409. DOI: 10.1007/s00289-019-02928-3

Simon, D. A., Bischoff, E., Buonocore, G. G., Cerruti, P., Raucci, M. G., Xia, H., … Mauler, R. S. (2017). Graphene-based masterbatch obtained via modified polyvinyl alcohol liquid-shear exfoliation and its application in enhanced polymer composites. *Materials & Design*, *134*, 103–110. DOI: 10.1016/j.matdes.2017.08.032

Singh, Y. T., Patra, P. K., Obodo, K. O., & Rai, D. P. (2022). Electronic and mechanical properties of (6,1) single-walled carbon nanotubes with different tube diameters: a theoretical study. *Carbon Letters*, *32*(2), 451–460. DOI: 10.1007/s42823-021-00274-x

Smart ecofilms. (2023). Retrieved July 18, 2023, from smart ecofilms website: https://www.smart-ecofilms.com/en/technology

Soares, B. G., Barra, G. M. O., & Indrusiak, T. (2021). Conducting Polymeric Composites Based on Intrinsically Conducting Polymers as Electromagnetic Interference Shielding/Microwave Absorbing Materials—A Review. *Journal of Composites Science*, *5*(7), 173. DOI: 10.3390/jcs5070173

Soares, C. T. de M., Ek, M., Östmark, E., Gällstedt, M., & Karlsson, S. (2022). Recycling of multi-material multilayer plastic packaging: Current trends and future scenarios. *Resources, Conservation and Recycling*, *176*, 105905. DOI: 10.1016/j.resconrec.2021.105905

Socher, R., Krause, B., Hermasch, S., Wursche, R., & Pötschke, P. (2011). Electrical and thermal properties of polyamide 12 composites with hybrid fillers systems of multiwalled carbon nanotubes and carbon black. *Composites Science and Technology*, *71*(8), 1053–1059. DOI: 10.1016/j.compscitech.2011.03.004

Socher, R., Krause, B., Müller, M. T., Boldt, R., & Pötschke, P. (2012). The influence of matrix viscosity on MWCNT dispersion and electrical properties in different thermoplastic nanocomposites. *Polymer*, *53*(2), 495–504. DOI: 10.1016/j.polymer.2011.12.019

Song, W.-L., Gong, C., Li, H., Cheng, X.-D., Chen, M., Yuan, X., … Fang, D. (2017). Graphene-Based Sandwich Structures for Frequency Selectable Electromagnetic Shielding. *ACS Applied Materials & Interfaces*, *9*(41), 36119–36129. DOI: 10.1021/acsami.7b08229

Strugova, D., David, É., & Demarquette, N. R. (2022). Linear viscoelasticity of PP/PS/MWCNT composites with co-continuous morphology. *Journal of Rheology*, *66*(4), 671–681. DOI: 10.1122/8.0000441

Strugova, D., Ferreira Junior, J. C., David, É., & Demarquette, N. R. (2021). Ultra-low percolation threshold induced by thermal treatments in co-continuous blend-based pp/ps/mwcnts nanocomposites. *Nanomaterials*, *11*(6). DOI: 10.3390/nano11061620

Sudha, J. D., Sivakala, S., Patel, K., & Radhakrishnan Nair, P. (2010). Development of electromagnetic shielding materials from the conductive blends of polystyrene polyaniline-clay nanocomposite. *Composites Part A: Applied Science and Manufacturing*, *41*(11), 1647–1652. DOI: 10.1016/j.compositesa.2010.07.015

Sundramoorthy, A. K., & Gunasekaran, S. (2014). Applications of graphene in quality assurance and safety of food. *TrAC Trends in Analytical Chemistry*, *60*, 36–53. DOI: 10.1016/j.trac.2014.04.015

Taherian, R. (2016). Experimental and analytical model for the electrical conductivity of polymer-based nanocomposites. *Composites Science and Technology*, *123*, 17–31. DOI: 10.1016/j.compscitech.2015.11.029

Tan, B., & Thomas, N. L. (2016). A review of the water barrier properties of polymer/clay and polymer/graphene nanocomposites. *Journal of Membrane Science*, *514*, 595–612. DOI: 10.1016/j.memsci.2016.05.026

Tarani, E., Wurm, A., Schick, C., Bikiaris, D. N., Chrissafis, K., & Vourlias, G. (2016). Effect of graphene nanoplatelets diameter on non-isothermal crystallization kinetics and melting behavior of high density polyethylene nanocomposites. *Thermochimica Acta*, *643*, 94–103. DOI: 10.1016/j.tca.2016.09.018

Tolinski, M. (2015a). 6.1.3 Conductive Fillers as Antistatic/ESD Additives. In *Additives for Polyolefins - Getting the Most Out of Polypropylene, Polyethylene and TPO* (2nd ed., p. 62). Elsevier. Retrieved from https://app.knovel.com/hotlink/pdf/id:kt010QHFLC/additives-polyolefins/conductive-fillers-antistatic BT - Additives for Polyolefins - Getting the Most Out of Polypropylene, Polyethylene and TPO (2nd Edition)

Tolinski, M. (2015b). Additives for Modifying Electrical Properties. In *Additives for Polyolefins* (pp. 57–67). Elsevier. DOI: 10.1016/B978-0-323-35884-2.00006-5

Tong, X. C. (2016). *Advanced Materials and Design for Electromagnetic Interference Shielding* (1st ed.). CRC Press. DOI: 10.1201/9781420073591

Trinh, B. M., Chang, B. P., & Mekonnen, T. H. (2023). The barrier properties of sustainable multiphase and multicomponent packaging materials: A review. *Progress in Materials Science*, *133*, 101071. DOI: 10.1016/j.pmatsci.2023.101071

Trost, T. (1995a). Electrostatic discharge (ESD)–Facts and faults–A review. *Packaging Technology and Science*, *8*(6), 303–313. DOI: 10.1002/pts.2770080604

Trost, T. (1995b). Electrostatic discharge (ESD)—Facts and faults—A review. *Packaging Technology and Science*, *8*(5), 231–247. DOI: 10.1002/pts.2770080502

Tseng, I.-H., Tsai, M.-H., & Chung, C.-W. (2014). Flexible and Transparent Polyimide Films Containing Two-Dimensional Alumina Nanosheets Templated by Graphene Oxide for Improved Barrier Property. *ACS Applied Materials & Interfaces*, *6*(15), 13098–13105. DOI: 10.1021/am502962b

Twede, D., Fowler, S., Havens, M., Raymond, M., Selke, S., Cascio, J., … Alsdorf, M. G. (2009). E. In *The Wiley Encyclopedia of Packaging Technology* (pp. 383–444). DOI: https://doi.org/10.1002/9780470541395.ch5

Van Buren, N., Demmers, M., Van der Heijden, R., & Witlox, F. (2016). Towards a Circular Economy: The Role of Dutch Logistics Industries and Governments. *Sustainability*, *8*(7), 647. DOI: 10.3390/su8070647

Verma, M., Verma, P., Dhawan, S. K., & Choudhary, V. (2015). Tailored graphene based polyurethane composites for efficient electrostatic dissipation and electromagnetic interference shielding applications. *RSC Advances*, *5*(118), 97349–97358. DOI: 10.1039/C5RA17276D

Vicente, A. N., Dip, G. M., & Junqueira, C. (2011). The step by step development of NRW method. *2011 SBMO/IEEE MTT-S International Microwave and Optoelectronics Conference (IMOC 2011)*, 738–742. DOI: 10.1109/IMOC.2011.6169318

Wagner, J. R., & Marks, S. B. (2016). Introduction. In *Multilayer Flexible Packaging* (pp. 3–13). Elsevier. DOI: 10.1016/B978-0-323-37100-1.00001-6

Wang, J., Kazemi, Y., Wang, S., Hamidinejad, M., Mahmud, M. B., Pötschke, P., & Park, C. B. (2020). Enhancing the electrical conductivity of PP/CNT nanocomposites through crystal-induced volume exclusion effect with a slow cooling rate. *Composites Part B: Engineering*, *183*(December 2019). DOI: 10.1016/j.compositesb.2019.107663

Wang, Q., Wang, T., Wang, J., Guo, W., Qian, Z., & Wei, T. (2018). Preparation of antistatic high-density polyethylene composites based on synergistic effect of graphene nanoplatelets and multi-walled carbon nanotubes. *Polymers for Advanced Technologies*, *29*(1), 407–416. DOI: 10.1002/pat.4129

Watt, M. R., & Gerhardt, R. A. (2020). Factors that Affect Network Formation in Carbon Nanotube Composites and their Resultant Electrical Properties. *Journal of Composites Science*, *4*(3), 100. DOI: 10.3390/jcs4030100

Weiss, J. (1991). Parameters that influence the barrier properties of metallized polyester and polypropylene films. *Thin Solid Films*, *204*(1), 203–216. DOI: 10.1016/0040-6090(91)90506-S

Wick, P., Louw-Gaume, A. E., Kucki, M., Krug, H. F., Kostarelos, K., Fadeel, B., … Bianco, A. (2014). Classification Framework for Graphene-Based Materials. *Angewandte Chemie International Edition*, *53*(30), 7714–7718. DOI: 10.1002/anie.201403335

Winotapun, C., Phattarateera, S., Aontee, A., Junsook, N., Daud, W., Kerddonfag, N., & Chinsirikul, W. (2019). Development of multilayer films with improved aroma barrier properties for durian packaging application. *Packaging Technology and Science*, *32*(8), 405–418. DOI: 10.1002/pts.2452

Wolf, C., Angellier-Coussy, H., Gontard, N., Doghieri, F., & Guillard, V. (2018). How the shape of fillers affects the barrier properties of polymer/non-porous particles nanocomposites: A review. *Journal of Membrane Science*, *556*, 393–418. DOI: 10.1016/j.memsci.2018.03.085

Wurm, A., Lellinger, D., Minakov, A. A., Skipa, T., Pötschke, P., Nicula, R., … Schick, C. (2014). Crystallization of poly(ε-caprolactone)/MWCNT composites: A combined SAXS/WAXS, electrical and thermal conductivity study. *Polymer*, *55*(9), 2220–2232. DOI: 10.1016/j.polymer.2014.02.069

Xiang, D., Harkin-Jones, E., & Linton, D. (2014). Processability, structural evolution and properties of melt processed biaxially stretched HDPE/MWCNT nanocomposites. *RSC Advances*, *4*(83), 44130–44140. DOI: 10.1039/C4RA07166B

Xiang, D., Harkin-Jones, E., & Linton, D. (2015). Characterization and structure–property relationship of melt-mixed high density polyethylene/multi-walled carbon nanotube composites under extensional deformation. *RSC Advances*, *5*(59), 47555–47568. DOI: 10.1039/C5RA06075C

Xiang, D., Harkin-Jones FREng, E., & Linton, D. (2014). *Effect of cooling rate on the properties of high density polyethylene/multi-walled carbon nanotube composites*. *1664*. DOI: 10.1063/1.4918440

Yadav, S. K., Jung, Y. C., Kim, J. H., Ko, Y.-I., Ryu, H. J., Yadav, M. K., … Cho, J. W. (2013). Mechanically Robust, Electrically Conductive Biocomposite Films Using Antimicrobial Chitosan-Functionalized Graphenes. *Particle & Particle Systems Characterization*, *30*(8), 721–727. DOI: 10.1002/ppsc.201300044

Yadegari, A., Morshedian, J., Khonakdar, H.-A., & Wagenknecht, U. (2016a). Influence of annealing on anisotropic crystalline structure of HDPE cast films. *Polyolefins Journal*, *3*(1). DOI: 10.22063/poj.2016.1269

Yadegari, A., Morshedian, J., Khonakdar, H.-A., & Wagenknecht, U. (2016b). Influence of annealing on anisotropic crystalline structure of HDPE cast films. *Polyolefins Journal*, *3*(1), 1–9.

Yam, K. L., Yam, K. L., & Davis, M. W. (2009). G. In *The Wiley Encyclopedia of Packaging Technology* (pp. 547–565). DOI: https://doi.org/10.1002/9780470541395.ch7

Yilmaz, S. (2015). The geometric resistivity correction factor for several geometrical samples. *Journal of Semiconductors*, *36*(8), 082001. DOI: 10.1088/1674-4926/36/8/082001

Zeng, X., Cheng, X., Yu, R., & Stucky, G. D. (2020). Electromagnetic microwave absorption theory and recent achievements in microwave absorbers. *Carbon*, *168*, 606–623. DOI: 10.1016/j.carbon.2020.07.028

Zhang, G., Lee, P. C., Jenkins, S., Dooley, J., & Baer, E. (2014). The effect of confined spherulite morphology of high-density polyethylene and polypropylene on their gas barrier properties in multilayered film systems. *Polymer*, *55*(17), 4521–4530. DOI: 10.1016/j.polymer.2014.07.009